A&A 613, A70 (2018)
https://doi.org/10.1051/0004-6361/201629243

Astronomy & Astrophysics

Study of a sample of faint Be stars in the exofield of CoRoT

II. Pulsation and outburst events: Time series analysis of photometric variations⋆

T. Semaan[1,2], A. M. Hubert[3], J. Zorec[4,5], J. Gutiérrez-Soto[6], Y. Frémat[4,5,7], C. Martayan[8], J. Fabregat[9], and P. Eggenberger[1]

[1] Observatoire de Genève, Université de Genève, Chemin des Maillettes 51, 1290 Versoix, Switzerland
e-mail: thierry.semaan@unige.ch
[2] Institut d'Astrophysique et de Géophysique, Université de Liège, Allée du 6 Août, Bât. B5c, 4000 Liège, Belgium
[3] GEPI, Observatoire de Paris, PSL Research University, CNRS, Place Jules Janssen, 92190 Meudon, France
[4] Sorbonne Universités, UPMC Université Paris 06, UMR 7095 Institut d'Astrophysique de Paris, 75014 Paris, France
[5] CNRS, UMR 7095, Institut d'Astrophysique de Paris, 98bis Bd. Arago, 75014 Paris, France
[6] Departamento de Didáctica de la Matemática, Universidad de Valencia, Edificio Magisterio, Avda. Tarongers, 4, 46022 Valencia, Spain
[7] Royal Observatory of Belgium, 3 Avenue Circulaire, 1180 Brussels, Belgium
[8] European Organization for Astronomical Research in the Southern Hemisphere, Alonso de Cordova 3107, Vitacura, Santiago de Chile, Chile
[9] Observatorio Astronómico de la Universidad de Valencia, Calle Catedrático Agustín Escardino 7, 46980 Paterna, Valencia, Spain

Received 4 July 2016 / Accepted 28 November 2017

ABSTRACT

Context. The class of Be stars are the epitome of rapid rotators in the main sequence. These stars are privileged candidates for studying the incidence of rotation on the stellar internal structure and on non-radial pulsations. Pulsations are considered possible mechanisms to trigger mass-ejection phenomena required to build up the circumstellar disks of Be stars.
Aims. Time series analyses of the light curves of 15 faint Be stars observed with the CoRoT satellite were performed to obtain the distribution of non-radial pulsation (NRP) frequencies in their power spectra at epochs with and without light outbursts and to discriminate pulsations from rotation-related photometric variations.
Methods. Standard Fourier techniques were employed to analyze the CoRoT light curves. Fundamental parameters corrected for rapid-rotation effects were used to study the power spectrum as a function of the stellar location in the instability domains of the Hertzsprung–Russell (H-R) diagram.
Results. Frequencies are concentrated in separate groups as predicted for g-modes in rapid B-type rotators, except for the two stars that are outside the H-R instability domain. In five objects the variations in the power spectrum are correlated with the time-dependent outbursts characteristics. Time-frequency analysis showed that during the outbursts the amplitudes of stable main frequencies within 0.03 c d^{-1} intervals strongly change, while transients and/or frequencies of low amplitude appear separated or not separated from the stellar frequencies. The frequency patterns and activities depend on evolution phases: (i) the average separations between groups of frequencies are larger in the zero-age main sequence (ZAMS) than in the terminal age main sequence (TAMS) and are the largest in the middle of the MS phase; (ii) a poor frequency spectrum with $f \lesssim 1$ cd^{-1} of low amplitude characterizes the stars beyond the TAMS; and (iii) outbursts are seen in stars hotter than B4 spectral type and in the second half of the MS.
Conclusions. The two main frequency groups are separated by $\delta f = (1.24 \pm 0.28) \times f_{\rm rot}$ in agreement with models of prograde sectoral g-modes ($m = -1, -2$) of intermediate-mass rapid rotators. The changes of amplitudes of individual frequencies and the presence of transients correlated with the outburst events deserve further studies of physical conditions in the subatmospheric layers to establish the relationship between pulsations and sporadic mass-ejection events.

Key words. stars: early-type – stars: emission-line, Be – stars: rotation – stars: oscillations

1. Introduction

Be stars are main sequence (MS) or slightly evolved B-type stars. Their main characteristics are very fast rotation and a circumstellar environment that is anisotropic in density, velocity, and shape, where emission lines and the thermal IR continuum flux excess are formed. Although very rapid, rotation of Be stars remains subcritical (Cranmer 2005; Zorec et al. 2016), which requires that some additional energy sources or mechanisms must help to produce material ejections and place the ejecta into orbits to form short- or long-lasting circumstellar disks. In short, the phenomena that trigger these ejections and the dynamics of disk formation in Be stars remain poorly understood (e.g., Rivinius et al. 2013).

Spectroscopic and photometric outbursts of different amplitudes are considered as evidence of episodic mass ejection that builds up the circumstellar disks. Since the years 1920–1940,

⋆ Tables 7 to 22 are only available at the CDS via anonymous ftp to cdsarc.u-strasbg.fr (130.79.128.5) or via http://cdsarc.u-strasbg.fr/viz-bin/qcat?J/A+A/613/A70

spectroscopic long-lived outbursts of high intensity have been known in many bright Be stars, which most often are of early B-type. The first examples of spectacular outbursts are those of γ Cas (Underhill & Doazan 1982; Doazan et al. 1983), 59 Cyg (Hubert-Delplace & Hubert 1979), and 11 Cam (Schild 1973). Changes of equivalent widths of emission-line components and sometimes Doppler displaced spectroscopic signatures were put forward as spectroscopic evidence in support of discrete mass ejections in the Be star μ Cen (Smith et al. 1996; Hanuschik et al. 1993). Long- and short-lived photometric outbursts attaining $\Delta V \simeq -0.3$ mag of Galactic and Magellanic Be stars have been observed since the mid-1990s (Cook et al. 1995; Hubert & Floquet 1998; Keller et al. 2002; Mennickent et al. 2002).

In the last decade, modulations of line emission intensity produced by the circumstellar disks were found to be associated with non-radial pulsations (NRP; Rivinius et al. 1998b, 2003; Floquet et al. 2000; Levenhagen et al. 2003; Hubert 2007). Thus, stellar pulsations that deserved some attention since the eighties are more and more studied in detail in Be stars in the context of mechanisms able to provide additional energy needed to unleash discrete mass ejections (Osaki 1986; Baade 1987; Lee & Saio 1993; Walker et al. 2005; Hubert 2007; Huat et al. 2009); (Cranmer 2009; Kee et al. 2016). While Rivinius et al. (1998a) have found that the times of maximal amplitude composition of frequencies correlate with increases of line emission intensities, the study of the light outburst observed with CoRoT in the very early spectral-type Be star HD 49330 has revealed for the first time the correlation between pulsation modes and outburst: acoustic modes are dominant in the quiet phase, but gravity modes mainly appear during the outburst phase (Huat et al. 2009). Moreover, these authors have also shown that some g-mode frequency groups, which are almost unseen during the quiescent phases of HD 49330, appear during the precursor phase of the outburst and synchronize just before the onset of the outburst (see their Fig. 5).

Thanks to spatial photometric missions (MOST, CoRoT, *Kepler*, and BRITE), studies of variable stars have greatly increased during the last decade. A significant number of light curves of Be stars are now available. In particular, the CoRoT (Convection, Rotation and planetary Transits; Baglin et al. 2006) mission made it possible to considerably extend the samples through the observation of faint Be stars in the fields dedicated to the search of exoplanets (Weiss et al. 2004).

For our part, we focused on Be stars that share the instability domain of classic B pulsators (β Cephei and SPB variables) in the Hertzsprung–Russell (H-R) diagram, with the aim of better specifying the relation between rapid rotation, pulsations, outbursts, and mass loss events. In Semaan et al. (2013, hereafter Paper I) the goals were to set up a faint Be-star sample observed in the first exofields of CoRoT (IR1, LRA1, LRC1), characterize the stars spectroscopically, and determine their fundamental parameters by taking into account the effects of fast rotation and veiling induced by their circumstellar environment. The present study is devoted to the analysis of the CoRoT light curves of a subsample of the Be stars studied in Paper I. This sample contains 15 faint Be stars including a late Oe, 10 early B1-B3e, 3 late Be, and a multiple system with a Be star component.

The subsample of Be stars studied in the present work is presented in Sect. 2. In Sect. 3 we briefly describe the light curve treatment. The methods used to determine the frequencies are given in Sect. 4. Section 5 presents a short overview of common properties of the light curves studied and of their frequency spectra. In Sect. 6, we investigate the characteristics of the frequencies detected in all Be stars studied according to their position in the H-R diagram. Section 7 focuses on the behavior of frequencies in those Be stars of the sample whose CoRoT data showed light outbursts. For these stars we present a time-frequency analysis undertaken in the same way as Huat et al. (2009) made for the bright Be star HD 49330 observed in the seismology field of CoRoT. In Sect. 8 we study some characteristic patterns in the discrete Fourier transform (DFT). Finally, the conclusions and a discussion on the results obtained are given in Sect. 9. Complementary notes on the description of light curves and oscillation frequencies are presented in Appendix B. The data obtained on frequencies are listed in Tables 7 to 22 (available at the CDS).

2. The stellar sample

The Be stars studied in the present paper are a subsample of the group established in Paper I. This subsample is listed in Table 1 and encompasses 15 stars, of which 14 have fundamental parameters determined from the spectroscopic data that we could obtain for them, even though they are not simultaneous with the CoRoT observations. The fundamental parameters were corrected for rotational effects, which have then enabled us to study some characteristics of the detected frequencies as a function of the stellar evolutionary phase. Table A.1 reproduces the fundamental parameters of the studied stars for which it was assumed that they rotate at the angular velocity ratio $\Omega/\Omega_c = 0.95$.

Among 38 Be stars identified in the exofields observed by CoRoT and reported in Paper I, we collected spectroscopic data for 22 of these stars, only some of which have spectra in the blue spectral range which makes it possible to determine reliable fundamental parameters. Also excluding the spectra that are strongly affected by variable line emission or shell absorptions, we were finally left with 14 Be stars that have reliable fundamental parameters. The light curves of the remaining B-type stars in Paper I are currently analyzed to complete the statistical inferences presented in the present work.

The above-mentioned spectroscopic data also contain the Hα line profiles of the program stars (see Paper I) that we use in Sect. 9.3 to discuss the characteristics of outbursts as a function of the inclination angle.

3. Treatment of the entire light curve

We used CoRoT data provided at N2 level (Baudin et al. 2006) through the CoRoT Science archive[1] for faint Be stars observed in the first exofields IR1 (Initial run; anticenter direction), LRC1 (First long run; center direction), and LRA1 (First long run; anticenter direction). Lately, we also analyzed the data obtained for star No 9 in the LRA6 run (see Table 1), whose light curve seems to be a little less rugged. Faint stars in the exofields are observed as light curves.

The observations were made in the IR1 from February 2 to March 31, 2007, in the LRC1 from May 9 to October 15, 2007, the LRA1 from October 18, 2007 to March 3, 2008, and in the LRA6 the data were obtained from December 12, 2012 to February 24, 2013 (star No 9). The visual magnitudes of the stars roughly range from 12 to 15.5 mag. The data at N0 level are raw data and are not available. Those at N1 level are corrected from instrumental effects, but only at the first order (sky background, electronic offset, cosmic rays, and jitter effects). The N2 data are corrected at higher order and are ready to use for the study of intrinsic photometric variations. These data are sampled with

[1] hhtp://idoc-corot.ias.u-psud.fr

Table 1. Some basic characteristics of the CoRoT data.

CoRoT ID	No	V mag	Run	t_o	Pts.	Sampl.	ΔT d	Δf c d^{-1}	N_f	A_{min} ppm	Cross references to sections, figures and tables
CoRoT 101486436	1	12.33	LRC1	2691.75311	25596	S1	152.007	0.0016	74	39	Sect. 8.1.1; Sect. B.1; Fig. 2; Fig. 31; Table 7
CoRoT 102595654	2	13.82	LRA1	2852.43938	21415	S1	131.463	0.0019	10	81	Sect. B.2; Fig. 10; Table 8
CoRoT 102656190	4	13.89	LRA1	2852.43932	22034	S1	131.463	0.0019	95	71	Sect. 8.1.2; Sect. B.3; Fig. 13; Table 9
CoRoT 102672979	5	11.47	LRA1	2852.43930	22034	S1	131.463	0.0019	48	94	Sect. 7.1; Sect. B.4; Fig. 4; Fig. 21; Fig. 22; Table 10
CoRoT 102686433	6	13.48	LRA1	2852.43929	22034	S1	131.463	0.0019	84	153	Sect. 8.2.1; Sect. 8.2.1; Sect. 7.2; Sect. B.5; Fig. 3; Fig. 23; Fig. 24; Fig. 32; Table 11
CoRoT 102719279	9	14.07	IR1	2590.05584	86563	S1, S2	57.446	0.0044	24	1769	Sect. B.6; Fig. 6; Fig. 25; Table 12
			LRA1	2852.43929	22034	S1	131.463	0.0019	64	941	Sect. 8.2.2; Sect. 7.3; Sect. B.6; Fig. 6; Fig. 25; Fig. 26; Fig. 27; Table 12
			LRA6	4394.27693	206592	S2	76.618	0.0032	42	805	Fig. 7; Fig. B.1, Fig. B.2, Fig. B.3, Table 13
CoRoT 102725623	11	15.17	IR1	2590.05583	9662	S1	57.441	0.0044	2	273	Sect. B.7; Fig. 11; Table 14
			LRA1	2852.43927	22034	S1	131.463	0.0019	8	186	Sect. B.7; Fig. 11; Table 14
CoRoT 102728404	12	11.93	LRA1	2852.43930	338782	S2	131.462	0.0019	62	112	Sect. B.8; Fig. B.4; Table 15
CoRoT 102766835	14	13.20	IR1	2590.05585	9662	S1	57.441	0.0044	23	710	Sect. B.9; Fig. 8; Table 16
			LRA1	2853.94531	348702	S2	131.462	0.0019	68	411	Sect. 8.3.1; Sect. B.9; Fig. 8; Table 16
CoRoT 102785204	16	12.06	LRA1	2853.94533	338782	S2	131.462	0.0019	30	622	Sect. B.10; Fig. B.5; Table 17
CoRoT 102785480	17	12.90	LRA1	2853.94534	338782	S2	131.462	0.0019	114	199	Sect. 8.2.3; Sect. B.11;Fig. 9; Fig.28; Fig. 29; Table 18
CoRoT 102825808	18	14.42	IR1	2590.05587	9662	S1	57.441	0.0044	44	135	Sect. B.12; Fig. 12; Table 19
CoRoT 102829773	19	15.21	IR1	2593.07642	9178	S1	54.421	0.0046	26	194	Sect. B.13; Fig. B.6; Table 20
CoRoT 102847615	20	13.87	IR1	2593.18500	147021	S1	54.315	0.0046	7	99	Sect. B.14; Fig. B.7; Table 21
CoRoT 102904910	22	14.02	IR1	2590.05590	9662	S1	57.441	0.0044	32	181	Sect. B.15; Fig. 5; Fig. 30; Table 22

Notes. No = sequence number in Table 1 of Paper I; t_o = CoRoT time of phase 0 (heliocentric JD with origin on 01/01/2000 at 12h00 UT); Pts. = number of data points; Sampl. = sampling: S1 = 512 sec., S2 = 32 sec.; ΔT = total duration of CoRoT observations; $\Delta f = 1/4\Delta T$ frequency accuracy; N_f = number of identified frequencies; A_{min} is the lower amplitude detected in ppm units; d = days.

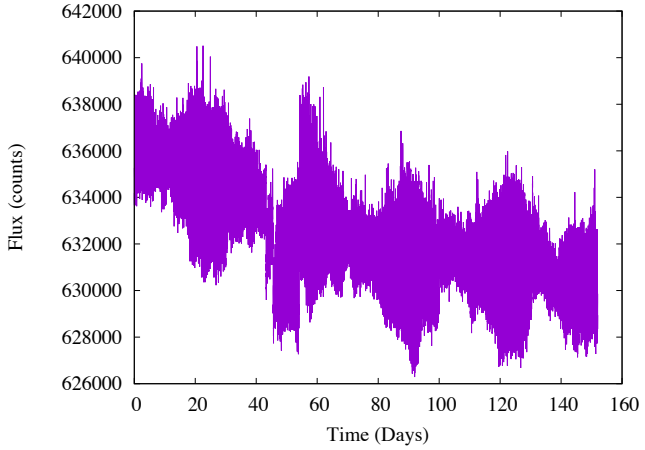

Fig. 1. Original light curve of the Be star CoRoT 101486436 (star No 1) observed in the LRC1 run, which is shown as an example of nominal N2 data with a linear interpolation filling the gaps.

constant steps; hot pixels are identified (see versions 1 to 3 p. 91, The CoRoT Legacy Book, edp Science). The steps represent either data elements of 32 s of integration or elements of 512 s formed by 16 successive summed up elementary integrations (see also Boisnard & Auvergne 2006). Each flux measurement has a quality flag, which indicates whether the value is correct or perturbed by hot pixels, South Atlantic Anomaly, and other effects.

The first step of the treatment was to keep only the nominal data points. Therefore, missing points were replaced by interpolated values to avoid having gaps in the data and adding spurious signals. The interpolated curves often show a long-term trend due to instrumental effects (Auvergne et al. 2009) superposed on the signature produced by the stellar variability proper. In some light curves we found one or several jumps that look like steps, as can be seen in Fig. 1. If there was no step, the data were detrended using slopes determined by a linear fit of the original light curves. The light curve in Fig. 1 treated in this way is shown in Fig. 2(a), where the flux is transcribed in ppm units. When several steps were present in the light curve, the parts broken by steps were joined up by translation, which then made it possible to rectify the light curve in its totality, as done when there is no step.

Several Be stars of the sample suddenly showed a steep increase or, on the contrary, a decrease of brightness in their CoRoT light curve. We call these light outbursts brightenings and fadings, respectively. In those cases in which the outbursts lasted during a large portion of the CoRoT run, we carried out additional treatment of data similar to that performed by Huat et al. (2009) for HD 49330. This treatment consists of removing the general trend induced by the outburst in the light curve with polynomials. In fact, the long-duration outbursts introduce slow, non-sinusoidal variations into the light curve, which convey a large number of frequencies that highly pollute the low frequency spectrum.

Every determination of frequencies carried out in this work uses only the rectified light curves.

4. Determination of frequencies

The frequencies from the light curves were extracted iteratively using several methods based on the DFT. A preliminary determination was made with the PASPER code (Diago et al. 2009). Afterward, the frequencies were identified with the FREQFIND code (Leroy 2012). This code is similar to PASPER, but faster and more appropriate for the study of large data samples. The process is interrupted each time a new frequency is detected in the DFT that has a signal-to-noise ratio $S/N < 3$. The S/N value is computed in the vicinity of the frequency detected over a $\Delta f \sim 5\ \mathrm{c\,d^{-1}}$ interval. In this study we considered as significant only the frequencies that had $S/N \geq 4.0$ (Breger et al. 1993; Kuschnig et al. 1997; Lenz & Breger 2005). The origin of time for the determination of phases is determined by the initial JD of the CoRoT run. The Rayleigh frequency resolution and the lower frequency limit is $f_l = 1/\Delta T$, where ΔT is the total time span of observations. In accordance with Kallinger et al. (2008), the criterion for frequency accuracy that we have adopted is $\Delta f = 1/(4\Delta T)$.

A number of tests were performed with several methods described by Gutiérrez-Soto et al. (2009) such as PERIOD04 (Lenz & Breger 2005) and CLEAN-NG written by B. Leroy (unpublished). Generally, these tests showed that there is no difference between the frequencies provided by different methods. However, there can be small differences in the order of detection of frequencies and in the values of those frequencies that have low S/N, i.e., ranging from 3.5 to 4. The frequencies, amplitudes, and phases of our program stars reported in the present paper were all obtained with the FREQFIND code and the frequencies are in very good agreement with those provided by PASPER. The frequencies with low S/N were not included in this work. The list of targets whose CoRoT light curves were analyzed, as well as some basic observation characteristics, are given in Table 1. In this table "No" is the sequence number attributed to each Be star in Paper I (see their Table 2), N_f is the number of frequencies detected, and A_min is the lowest amplitude detected for a $S/N \geq 4.0$. Several objects toward the anticenter of the Galaxy were first observed in the IR1 initial run and then in the LRA1 long run.

5. Analysis of the complete light curves

We studied the rectified light curves and corresponding DFT of 15 Be stars. The light curves are shown in Figs. 2–13 and Figs. B.4–B.7, and a short description of their properties is given in Appendix B. The light curve observed during the LRC1 run is shown in pink, while those of LRA1 are in blue and of IR1 in green. This color coding of light curves is useful when the results obtained for the same star in different runs are compared in the same figure. The lists of the frequencies found, their amplitudes and phases that describe the entire rectified light curves, and the respective signal-to-noise ratios are presented in ascending order in Tables 7 to 22 (at the CDS). These tables also give the sequence order of frequency detection by the FREQFIND code. For a given star in stable stages, the number of frequencies detected depends on the resolution, and the lower the resolution, the lower the number of frequencies found, i.e., $N_\mathrm{f}(\mathrm{IR1}) < N_\mathrm{f}(\mathrm{LRA6}) < N_\mathrm{f}(\mathrm{LRA1})$. Some frequencies from the shorter runs can appear as blends of apparently individual frequencies obtained in longer runs. Other frequencies may appear as new frequencies. It is frequently found that the IR1 blends imply two frequencies in the LRA1 run, but only an individual IR1 frequency may also appear either near or in between two close individual LRA1 frequencies.

For the majority of targets, the frequencies are distributed in several groups, which are more or less equally spaced. A large number of low frequencies are concentrated in intervals

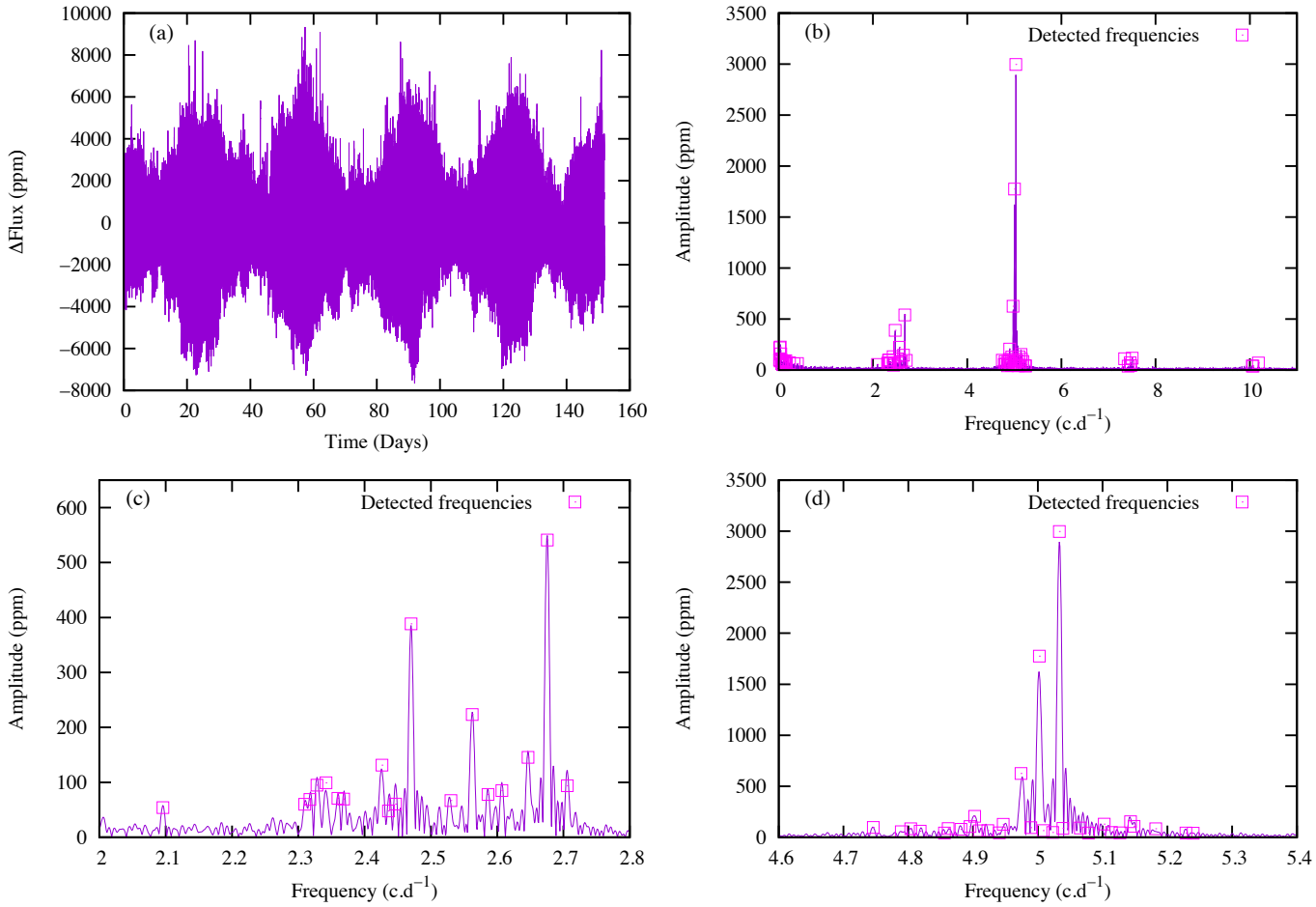

Fig. 2. Frequency analysis of the Be star CoRoT 101486436 (star No 1) observed in the LRC1 run. *Panel a*: rectified light curve; *panel b*: discrete Fourier transform (DFT) of the rectified light curve; *panel c*: DFT zoomed on the second frequency group located at 2.5 c d^{-1}; and *panel d*: DFT zoomed on the third frequency group located at 5.0 c d^{-1}.

ranging from 0 to 0.2 c d^{-1}. Some frequencies come from light beatings and a large number of these frequencies appear as (fx–fy) combinations between dominant g-mode frequencies. They can also be r-modes (Saio 2013). We do not exclude the possibility that some frequencies could be either the consequence of residual long-term trends left in the light curves in spite of our detailed treatment, or signatures produced by stellar activities and/or circumstellar disk-related cycles. There are frequencies with no stellar origin such as $f_{\rm orbital}$ = 13.970 c d^{-1}, which is due to the orbital frequency of the satellite. There are also harmonics, and $f_{\rm d/n}$ = 2.004 c d^{-1}, the day/night alternation.

We searched for harmonics and simple combinations (addition or subtraction) between the first 20 dominant frequencies. According to the adopted accuracy $1/(4\Delta T)$ for the frequency determination, most frequencies beyond the first 20 dominant frequencies could simply be combinations. It is worth noting that sometimes there are frequencies that can be reproduced through combinations within $\Delta f \lesssim 1/(10\Delta T)$. Harmonics, possible combinations of frequencies, and the very low frequencies (< $6/\Delta$T c d^{-1}) are also indicated in these Tables.

The light curves of our Be stars are very complex and show large flux variations characterized by fairly different timescales. However, these curves, and the frequencies we found, have several common behaviors:

5.1. Light curve trends

Three types of long-term flux variations are observed: beatings, slow oscillations, irregular in amplitude and duration (QPO), and outbursts that are characterized by sudden increase or decrease of the light brightness that hereinafter we call *brightening* or *fading*, respectively. One, two or three types of flux variations can be found in a same star, but weak beatings are difficult to distinguish from low amplitude variations (see Table 2, col. 9).

– Large amplitude short-term oscillations of flux (≤1 day) are detected, except for three stars: Nos. 2, 11, and 20. At the epochs of outbursts (brightenings and fadings), these variations are more prominent.

– Light beatings are observed with timescales ranging from several days (stars No 4, 6, 8, and 22) to several tens of days (stars No 1 and 12), independent of the spectral type. The amplitude and duration of the beatings are not strictly constant, which may imply that several frequencies are involved. The maximal peak-to-peak amplitude of beatings is at about 12 000, 25 000, and 32 000 ppm in stars No 1, 4, and 12, respectively, where the strong beatings are the main characteristics of their light curve.

– Slow and rather irregular amplitude variations (QPO) with timescales ranging from 7 to 40 days are observed in several stars: Nos 2, 5, 9 (LRA6), 17, 18, and 19.

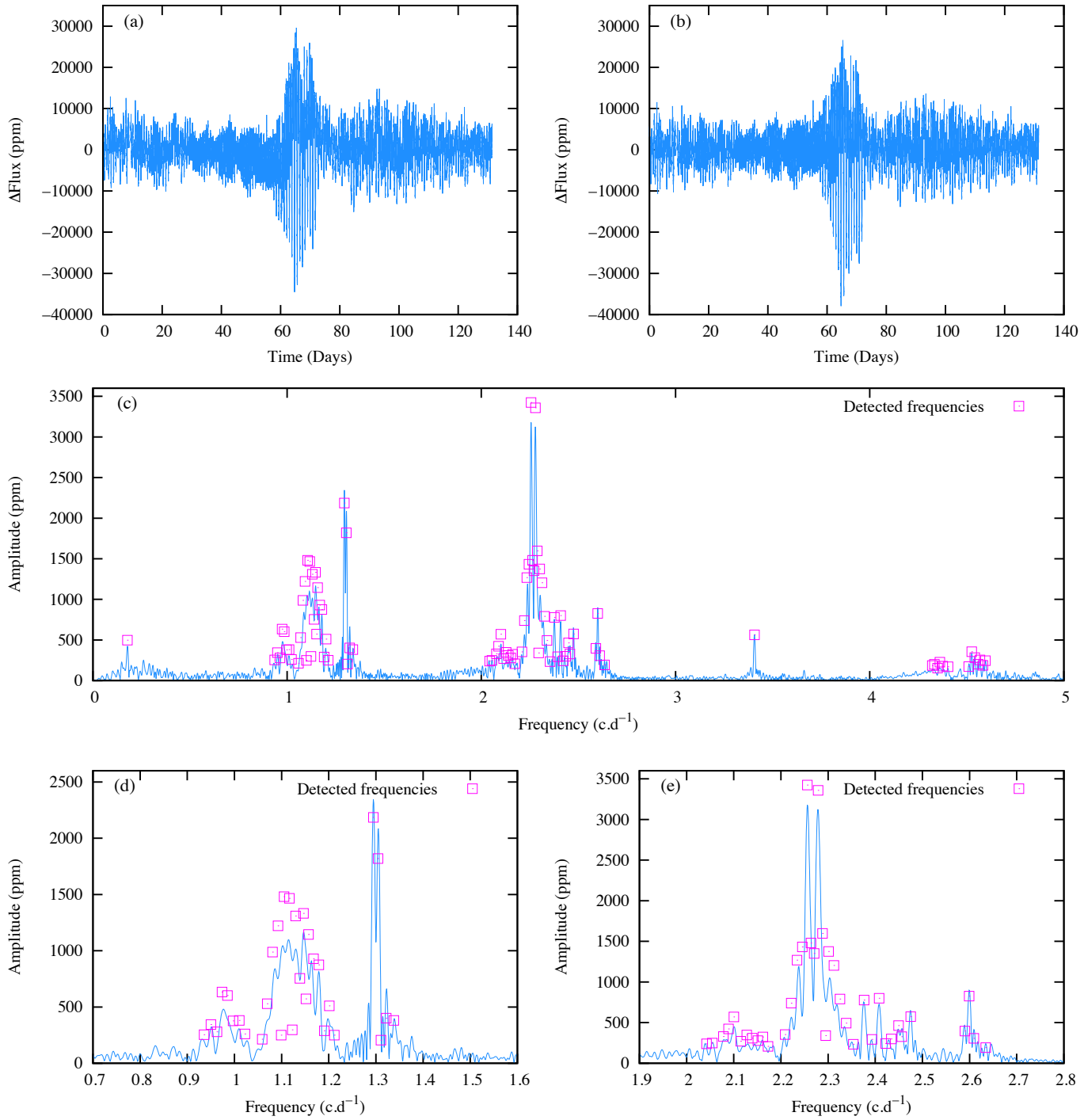

Fig. 3. Frequency analysis of the Be star CoRoT 102686433 (star No 6) observed in the LRA1. *Panel a*: rectified light curve. *Panel b*: rectified light curve corrected from the shape of the outburst. *Panel c*: DFT of the corrected light curve depicted in (b); we note the low number of frequencies in group 1 ~ 0 c d^{-1}; *panel d*: DFT zoomed on the second frequency group located at 1.1 c d^{-1}; and *panel e*: DFT zoomed on the third frequency group located at 2.3 c d^{-1}.

– Outbursts are detected or suspected in six objects. Their intensity, timescale, and number vary from one star to another.

5.1.1. Outbursts as brightenings

Outbursts as light brightenings are detected in stars No 5, 6, and 22. Their behaviors are summed up for each star as follows:

– A noticeable light brightening that lasts over 20 days (50 000 ppm) is detected in star No 6 (Fig. 3a), which is similar to that reported for HD 49330 by Huat et al. (2009).
– A short time prior to the start of observations, a light brightening (15 000 ppm) may have occurred in star No 5 (Fig. 4a).
– A weak and short (≤10 days) brightening, superposed on conspicuous beatings, seems to occur in star No 22 in the middle of the IR1 run (Fig. 5a).

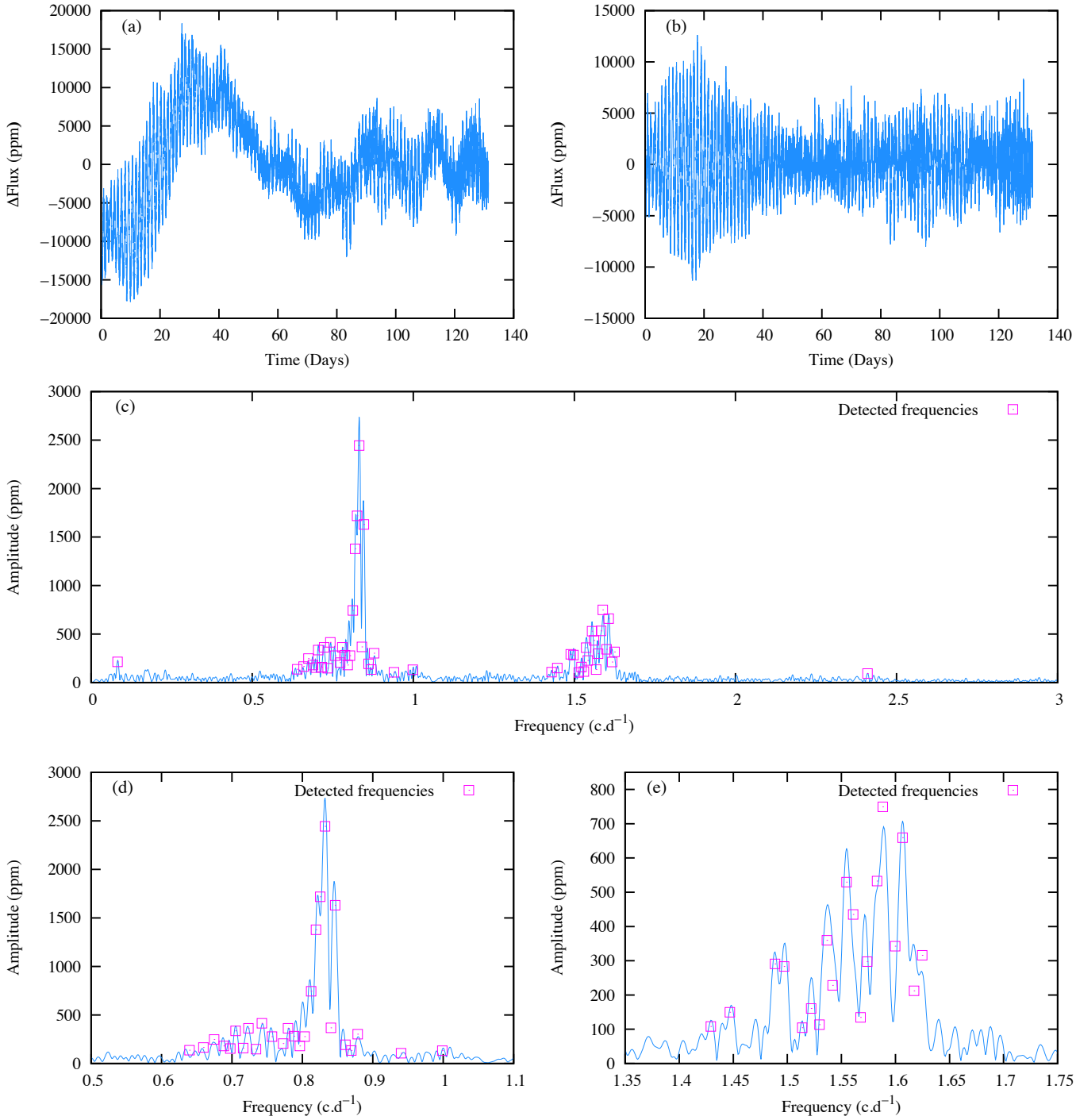

Fig. 4. Frequency analysis of the Be star CoRoT 102672979 (star No 5) observed in the LRA1 run. *Panel a*: rectified light curve; *panel b*: rectified light curve corrected from the shape of the outburst. *Panel c*: DFT of the corrected light curve shown in (b); we note the low number of frequencies in group 1 ~ 0 c d^{-1}; *panel d*: DFT zoomed on the second frequency group located at 0.8 c d^{-1}; and *panel e*: DFT zoomed on the third frequency group located at 1.6 c d^{-1}.

– Brightenings are detected in those sample stars that are observed under $i \leq 60°$.

5.1.2. Outbursts as fadings

Outbursts seen as fadings are detected in stars No 9, 14, and 22. Their behaviors are shortly reported, as follows:
– In star No 9 a strong fading (0.02 mag) lasting about 30 days was first observed in the IR1 and then in the LRA1 run (see Fig. 6a and c). The latter was preceded and followed by several weak and irregular fadings (0.005 mag). Between the two runs the stellar flux increased by about 0.06 mag. The recurrence of fadings in the LRA1 run is about 15–20 days.
– Star No 14 is peculiar. The flux behavior is similar to a periodic sawtooth-shaped curve that can be considered as recurrent 18-d fadings of varying peak-to-peak amplitude that attain up to 80 000 ppm (Fig. 8a and b).

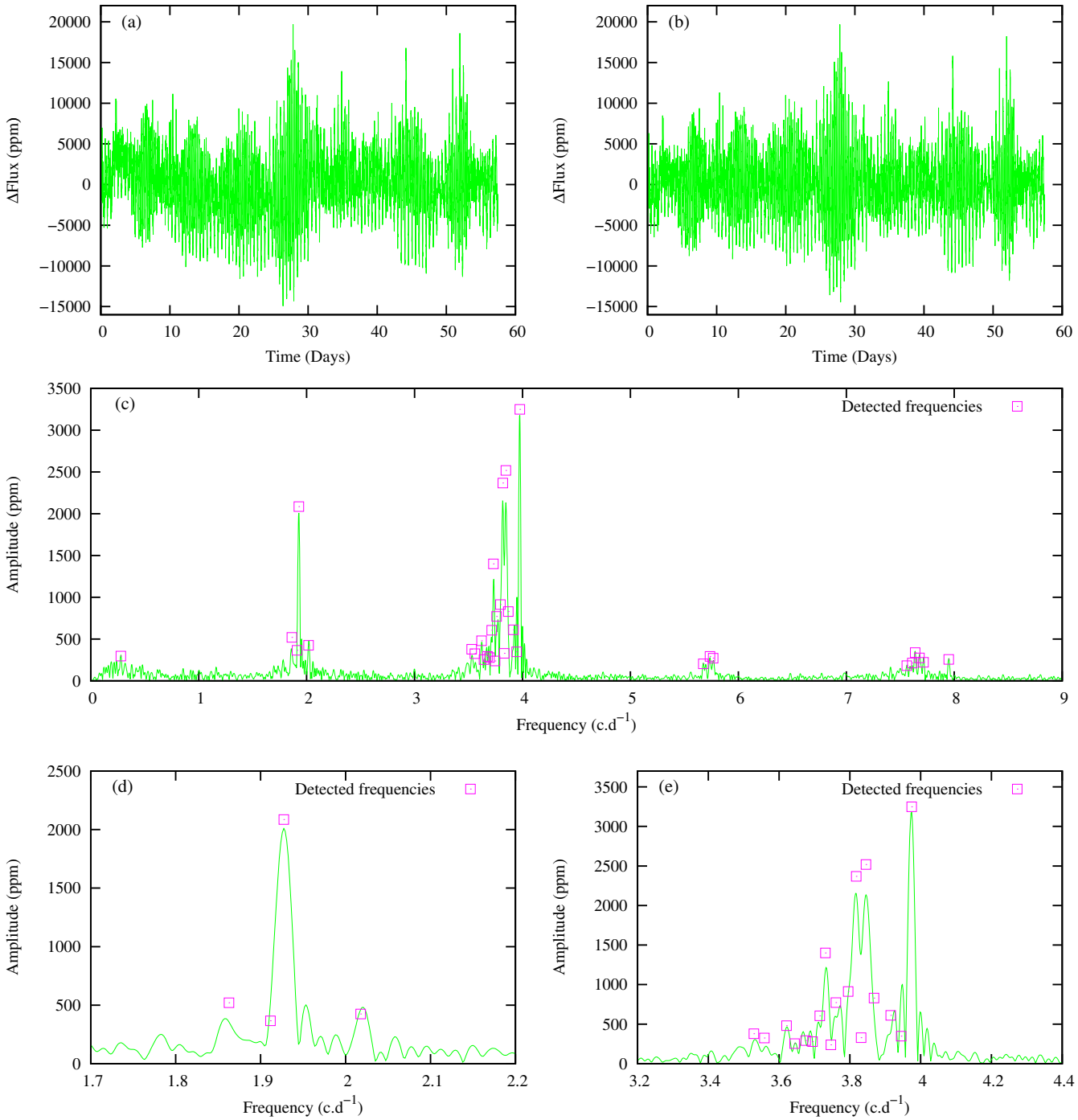

Fig. 5. Frequency analysis of the Be star CoRoT 102904910 (star No 22) observed in the IR1. *Panel a*: rectified light curve; *panel b*: rectified light curve corrected for the shape of the outburst; *panel c*: DFT of the corrected light curve shown in (b); *panel d*: DFT zoomed on the second frequency group located at 1.9 c d^{-1}; and *panel e*: DFT zoomed on the third frequency group located at 3.8 c d^{-1}.

– A very short fading of low intensity was observed over 4 days in star No 17. It repeated 109 days later (Fig. 9a).
– Fadings were observed in two stars with strong shells: No 9 (H-shell) and 14 (He-shell). A fading can be the consequence of ejected material whose optical depth toward the observer is high enough to partly absorb the stellar light. Both objects are particularly complex. In particular, for star No 14 we estimated $i \sim 30°$, but the object is likely a binary. This and other objects showing fadings are discussed in Sects. 7.5 and 9.3.

5.1.3. Outbursts versus inclination angle i[2] and the shape of the Hα line profile

It is of some interest to study the outbursts phenomenon as a function of the stellar inclination angle. Thus, we can note the following findings:
– According to Table A.1, brightenings occur in stars with $220 \lesssim V \sin i \lesssim 300$ km s^{-1}(stars No 5, 6, and 22), while fadings appear

[2] Regarding the large uncertainties that may affect the estimate of inclination angles as a function of Ω/Ω_c see Appendix A.

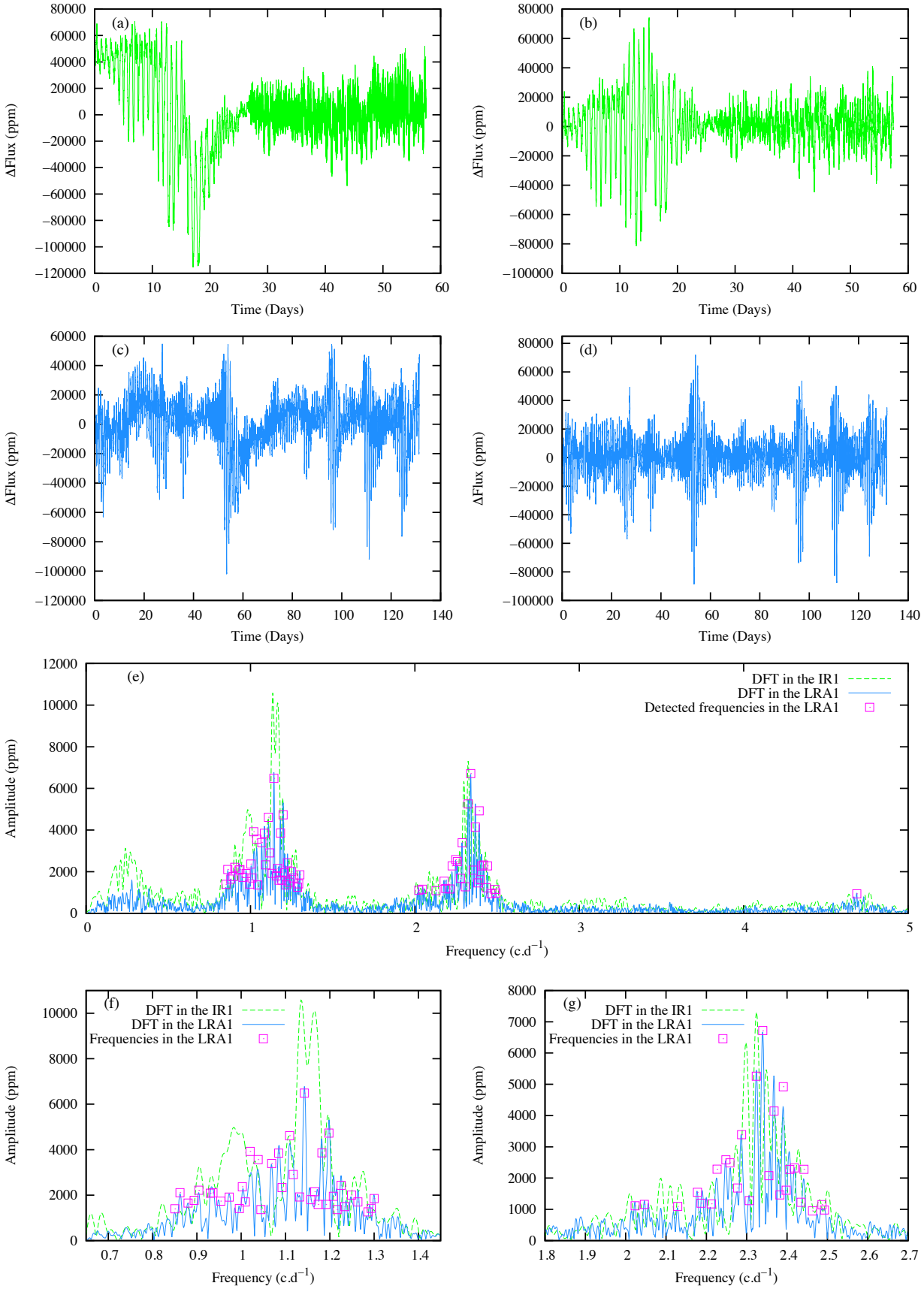

Fig. 6. Frequency analysis of the Be star CoRoT 102719279 (star No 9) observed first in the IR1 (in green), then in the LRA1 (in blue). *Panel a*: rectified light curve (IR1); *panel b*: rectified light curve (IR1) corrected from the shape of the outburst; *panel c*: rectified light curve (LRA1); *panel d*: rectified light curve (LRA1) corrected from the shape of the strong outburst; *panel e*: DFT is shown of the corrected light curves shown in *(b)* and *(d)* for the IR1 (green dashed line) and the LRA1 (blue full line), respectively; *panel f*: DFT zoomed in each run on the second frequency group located at 1.1 c d^{-1}; and *panel g*: DFT zoomed in each run on the third frequency group located at 2.3 c d^{-1}.

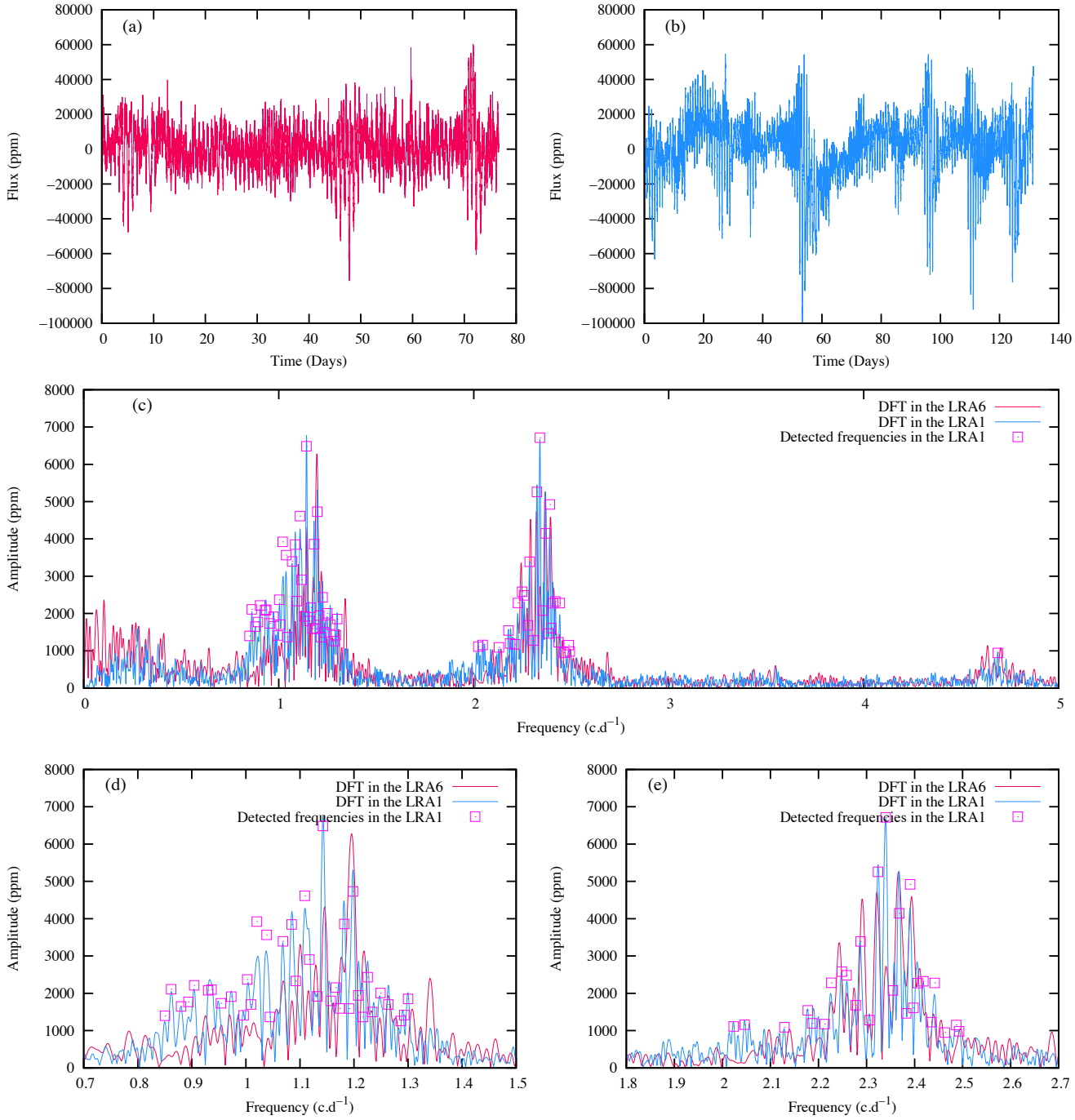

Fig. 7. Comparison of the frequency analysis carried out on the Be star CoRoT 102719279 (star No 9) observed in the LRA6 (in red) and in the LRA1 (in blue). *Panel a*: rectified light curve (LRA6); *panel b*: rectified light curve (LRA1) without correction for the shape of the outburst; *panel c*: DFT is shown of the corrected light curves shown in *(a)* and *(b)* corrected for the shape of the outburst LRA6 (red line); LRA1 (blue full line), respectively; *panel d*: DFT zoomed in each run on the second frequency group located at 1.1 c d^{-1}; and *panel e*: DFT zoomed in each run on the third frequency group located at 2.3 c d^{-1}.

in stars with $260 \lesssim V \sin i \lesssim 330$ km s^{-1} (stars No 9, 14, and 17);
– Brightenings and fadings were observed in stars with inclination angles $40° \lesssim i \lesssim 60°$ and $30° \lesssim i \lesssim 60°$, respectively, but it was not possible to establish a well-defined correlation (see Sect. 9.3);
– Stars No 5 ($i \simeq 50°$) and 22 ($i \simeq 40°$) with brightenings have Hα emission line profiles of pole-on type similar to those of stars without brightening No 20 ($i \simeq 30°$) and 4 ($i \simeq 40°$), respectively. The brightening star No 6 ($i \simeq 60°$) has a double peaked Hα emission-line profile, which is normally expected for intermediate inclination angles. Fadings appear in star No 9 ($i \simeq 50°$) whose asymmetric Hα emission-line profile presents a shell-like structure and in star No 14 ($i \simeq 30°$), where the Hα emission-line profile is of the type seen in brightening low inclination stars No 4 and 22. Nevertheless, star No 14 has a strong He-shell and many metallic lines. Star No 17 ($i \simeq 60°$) presents a fading of low intensity, but we have no Hα line profile.

A more detailed analysis of stars showing outbursts is presented in Sect. 7.

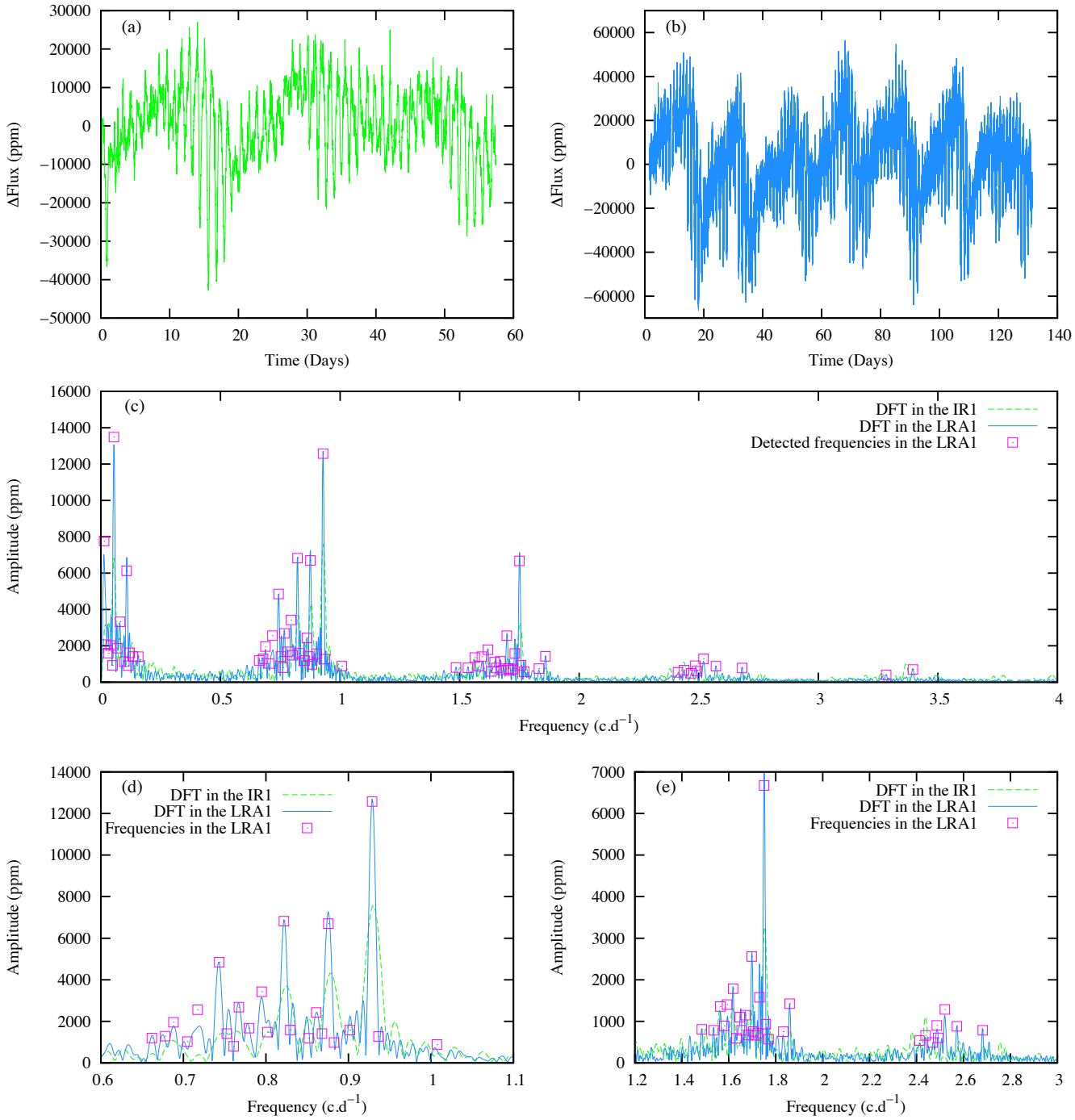

Fig. 8. Frequency analysis of the Be star CoRoT 102766835 (star No 14) observed first in the IR1 (in green), then in the LRA1 (in blue). *Panel a*: rectified light curve (IR1); *panel b*: rectified light curve (LRA1); *panel c*: DFT of the rectified light curve in each run (green dashed line for the IR1 and blue full line for the LRA1); *panel d*: DFT zoomed in each run on the second frequency group located at 0.85 c d^{-1}; and *panel e*: DFT zoomed in each run on the third and fourth frequency groups located at 1.7 c d^{-1} and 2.5 c d^{-1}.

5.2. Frequencies

5.2.1. Frequency groups

Frequencies are generally concentrated in rather well-separated groups, except for two stars No 2 and 11. The characteristics of these frequency groups can be summed up as follows:

– The number of groups varies from two to five, including a group near $f \sim 0$ c d^{-1} (Figs. 10 and 11). In this work, the groups are named as follows: frequencies $f \sim 0$ c d^{-1} are said to form "group 0", but it is referred to as the "first group". The subsequent "group 1", "group 2", ... are referred as the "second group", "third group", ... respectively. The dominant frequencies belong to one or two groups, but their amplitudes differ from star to star. The second and the third group always have the largest number of frequencies and their amplitudes are also the highest.

– In some stars, the two main groups consist of substructures as seen in stars No 6 (Fig. 3d and e) and No 18 (Fig. 12c and

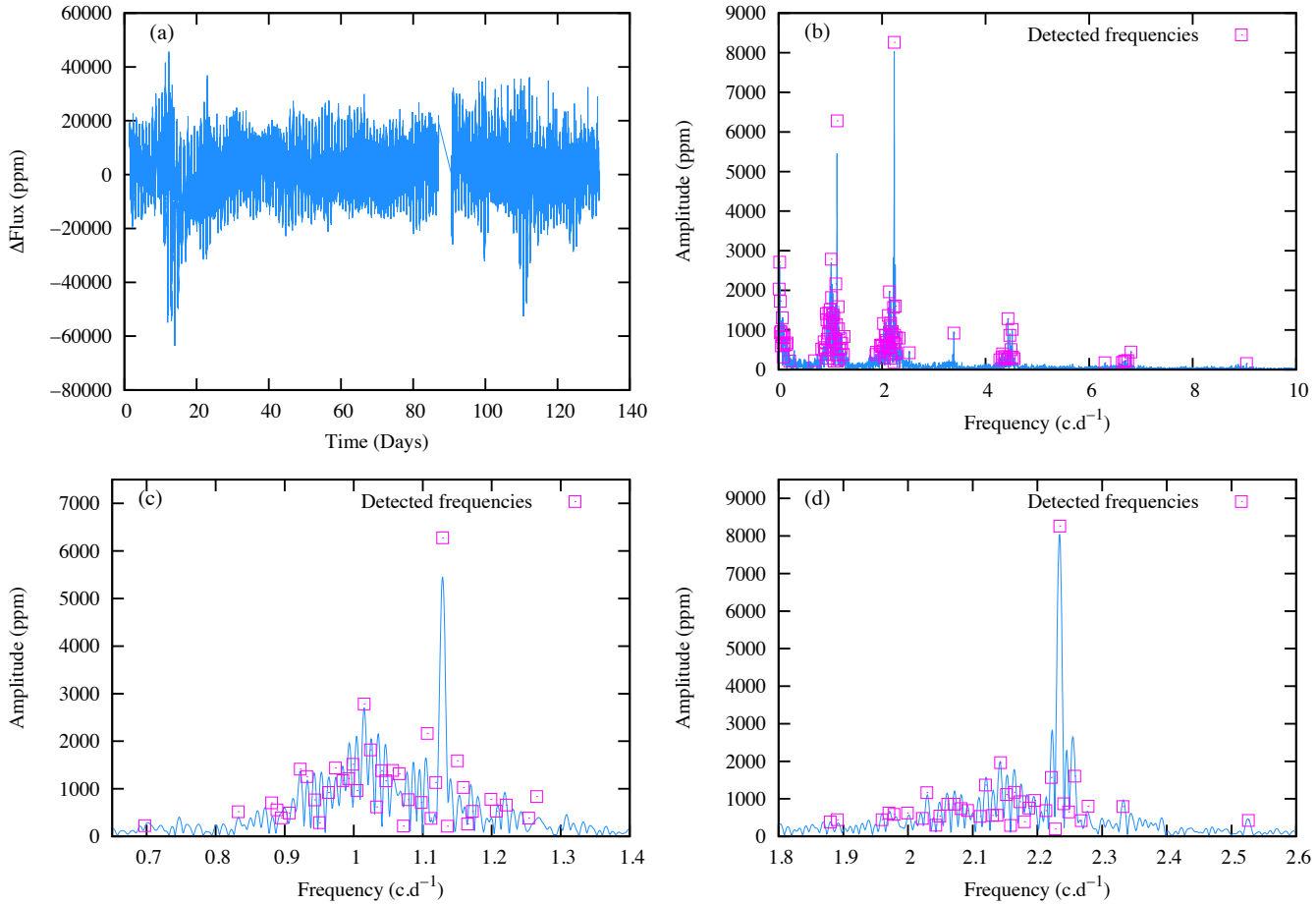

Fig. 9. Frequency analysis of the Be star CoRoT 102785480 (star No 17) observed in the LRA1 (in blue). *Panel a*: rectified light curve; *panel b*: DFT of the rectified light curve; *panel c*: DFT zoomed on the second frequency group located at 1.1 c d^{-1}; and *panel d*: DFT zoomed on the third frequency group located at 2.2 c d^{-1}.

d). In the first star, these subfeatures are related to the outburst (see Sect. B.5 and Fig. 24). Since no outburst has been detected in the second star, another explanation related to the possible multiplicity of the object may be proposed.
– The number of intrinsic frequencies detected with $S/N \geq 4.0$ varies from one star to another (Table 1). For stars No 9, 11, and 14, which were observed several times, the frequencies are listed in multiple tables (Tables 12, 13, 14, and 16). The first six frequencies and amplitudes found for each star by FREQFIND are listed in Table 2. The amplitudes of these frequencies differ strongly from one star to another and are not the same from one run to another. In the DFT of stars No 2, 11, and 20, we detected only low frequencies that also have low amplitudes. It is worth noting that some high frequencies identified in the DFTs may be combinations and therefore they may not be independent (see Tables 7 to 22). Finally, in star No 14, the frequencies detected in several groups in the LRA1 are very compact, but the resolution in the IR1 is not high enough to separate them.

5.2.2. Harmonics and combinations

Two main comments can be put forward regarding harmonics and combinations of frequencies:
– Generally, the first harmonic of some dominant frequencies is detected. For instance, this concerns up to six main frequencies in star No 6, which displays an outburst. Second and third harmonics of a very small number of frequencies are also identified in stars No 14 and No 17 (Figs. 8 and 9) (Tables 16 and 18, respectively). In some stars, several frequencies of moderate amplitude are detected with their first harmonic. In the same object, the first harmonic may have lower, similar or higher amplitude than the fundamental, as is also reported for stars No 4 and 5 (see Tables 7 to 22) and also for classic pulsators like SPB (e.g., Degroote et al. 2012, Table A.2). For stars showing outbursts, which were observed both in long and short runs, the first harmonics detected in the long run for several frequencies are not found or seen clearly enough to be distinguished in the short run, probably because the frequency resolution is not sufficiently high in the latter (see Fig. 8d and e, for instance).
– Combinations of frequencies can be explained as couplings between several modes (Degroote et al. 2009, and references therein). In this work we searched only for combinations $f_x \pm f_y$, where the differences with the frequencies tested are smaller than $\Delta f = 1/(4\Delta T)$. The rate of these combinations is relatively high in stars showing a high number of frequencies. It may vary from 20 to 50% among the first 20 dominant frequencies. However, combinations implying the sum or difference of frequencies are rarely identified together; at most only three or four cases were confirmed in stars No 1, 6, 14, and 17. The most obvious combinations involving the first 20 dominant frequencies are given in Tables 7 to 22. Most often, frequencies with a lower amplitude than that of the first detected frequencies

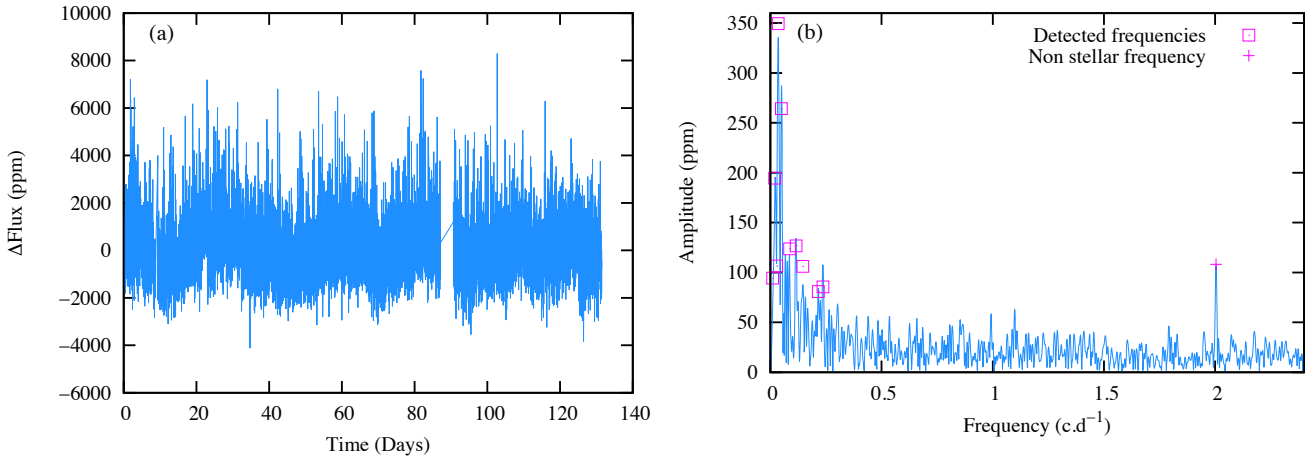

Fig. 10. Frequency analysis of the Be star CoRoT 102595654 (star No 2) observed in the LRA1 run: (a) rectified light curve, (b) DFT of the rectified light curve.

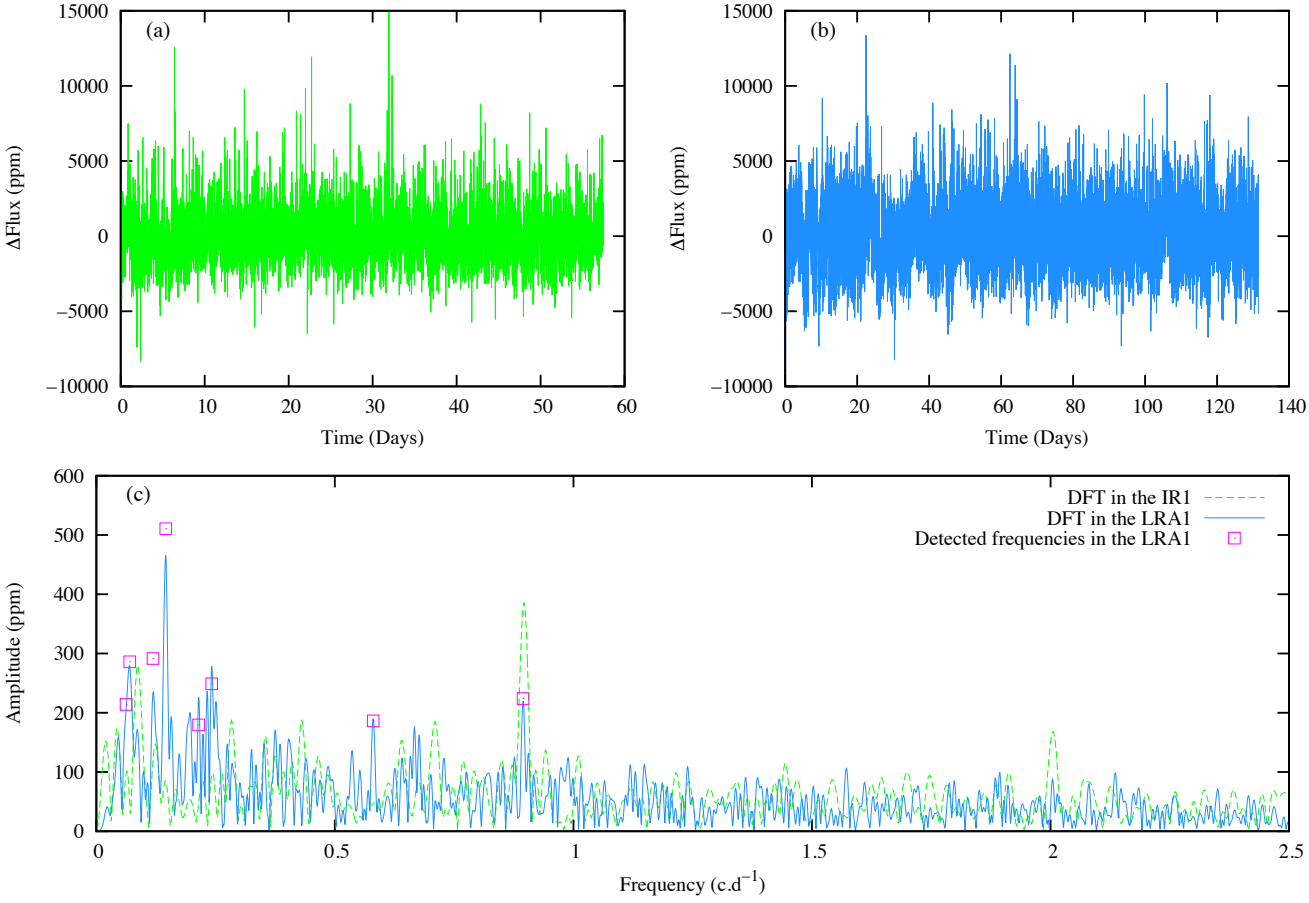

Fig. 11. Frequency analysis of the Be star CoRoT 102725623 (star No 11) observed first in the IR1 (in green), then in the LRA1 (in blue). *Panel a*: rectified light curve (IR1), *panel b*: rectified light curve (LRA1) and *panel c*: DFT of the rectified light curve in each run (green dashed line for the IR1 and blue full line for the LRA1).

could be the result of combinations. The amplitudes of combinations of frequencies are lower than the amplitudes of the parent frequencies.

5.2.3. Frequency spacings and beatings

Common frequency spacings are detected in several stars: In No 4, two common spacings (0.1978 and 0.1658 c d^{-1}) are detected between dominant frequency couples that belong to the same group (Fig. 13e). Both spacings are compatible with the occurrence of beatings in the light curve, which is not strictly regular. In No 12, a first spacing (0.0586 c d^{-1}) is found between f_{30}, f_{36}, and f_{42}, and another (0.0373 c d^{-1}) between f_{36}, f_{39}, and f_{43}. Again, both spacings are compatible with beating frequencies. In star No 14, the common spacing 0.0546 c d^{-1} found between f_{23}, f_{27}, f_{32}, and f_{35}

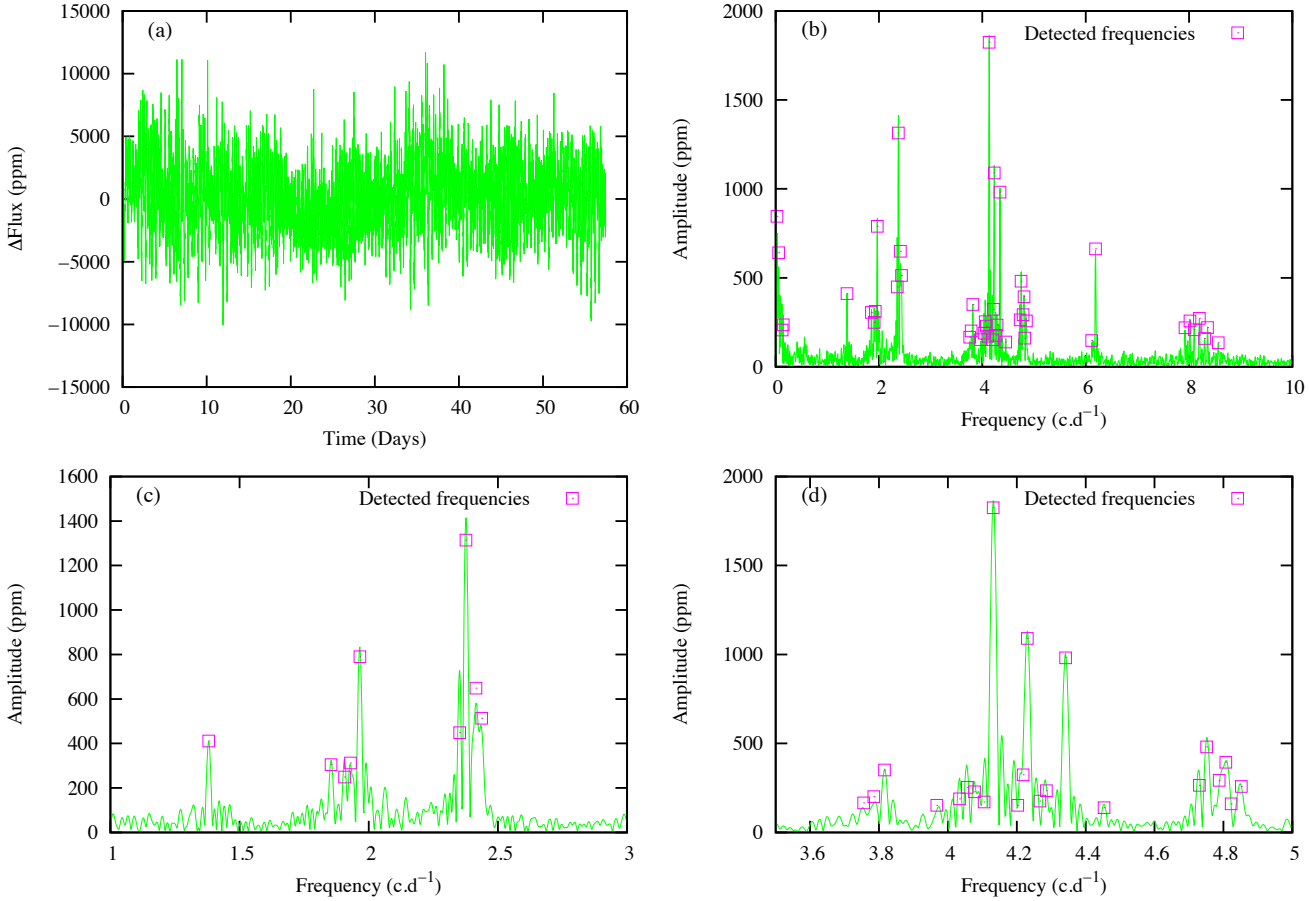

Fig. 12. Frequency analysis of the Be star CoRoT 102825808 (star No 18) in the IR1. *Panel a*: rectified light curve, *panel b*: DFT of the rectified light curve, *panel c*: DFT zoomed on the second frequency group formed by subgroups located at 1.9 and 2.4 c d^{-1}. and *panel d*: DFT zoomed on the third frequency group formed by subgroups located at 3.8, 4.2, and 4.8 c d^{-1}.

corresponds to the frequency of occurrence of fadings (sawtooth variation).

5.2.4. Frequencies from IR1, LRA1, and LRA6

Two stars of the sample, stars No 11 and 14, were observed in two runs, first in the IR1 and then in the LRA1, while star No 9 was observed in three runs, IR1, LRA1, and five years later in the LRA6. Stars No 9 and 14 showed outbursts in the IR1 and LRA1 runs with various amplitudes and durations. During the LRA6 run the light curve of star No 9 was less disturbed than in the two previous runs, but showing mainly QPO, several beatings and perhaps a short-duration outburst at the end of the run.

For a given star, the number of frequencies detected in the IR1 is roughly three times lower than in the LRA1. The temporal resolution in the IR1 and LRA6 does not allow separation of close frequencies detected in the LRA1. So, most of those detected in the IR1, and to a lesser degree in the LRA6, may be blends of frequencies detected in the LRA1. They can be easily recognized in Tables 12, 13, 14, and 16 of stars No 9, 11, and 14, respectively. The value of these frequencies, compared with those in the LRA1 run, differ by $\lesssim$0.011 c d^{-1} (|LRA1-LRA6|, star No 9; |LRA1-IR1|) and $\lesssim$0.008 c d^{-1} (|LRA6-IR1|, star No 9), which is close to or less than the respective resolutions $1/\Delta T$: 0.008 c d^{-1} (LRA1), 0.013 c d^{-1} (LRA6) and 0.017 c d^{-1} (IR1). These results show that most of frequencies identified in the observed groupings have the same origin.

Unfortunately, the original light curves of star No 11 presented several instrumental defects, so that even after correction they remained very noisy. Moreover, the number of frequencies detected in the DFT of each light curve is very small and most of them are low frequencies of low amplitude, which made their comparison unavailing.

For stars No 9 and 14, the behavior of the DFTs of the complete light curves in the IR1, LRA1 and LRA6 runs of star No 9, and in the IR1 and LRA1 runs of star No 14 are very similar, but the amplitude of frequency groups are often different. This confirms the change of mode amplitudes that occurs when passing from quiescent to non-quiescent states, as has been revealed in HD 49330 (Huat et al. 2009).

5.2.5. Stability of frequencies in stars showing outbursts

The dominant frequencies across the different photometric phases are always present, even during the outbursts. They are stable within 0.03 c d^{-1}, but their amplitudes can change significantly as it is confirmed by the time-frequency analysis in the LRA1 using a 40d-window moving with a 1d-constant step across the complete light curve. From one run to another, the frequencies of higher amplitudes form very similar and recognizable patterns of groups of frequencies, which is particularly true for star No 9, where three different runs were analyzed.

The case of star No 9 deserves to be outlined. The frequencies detected in the three IR1, LRA1, and LRA6 light

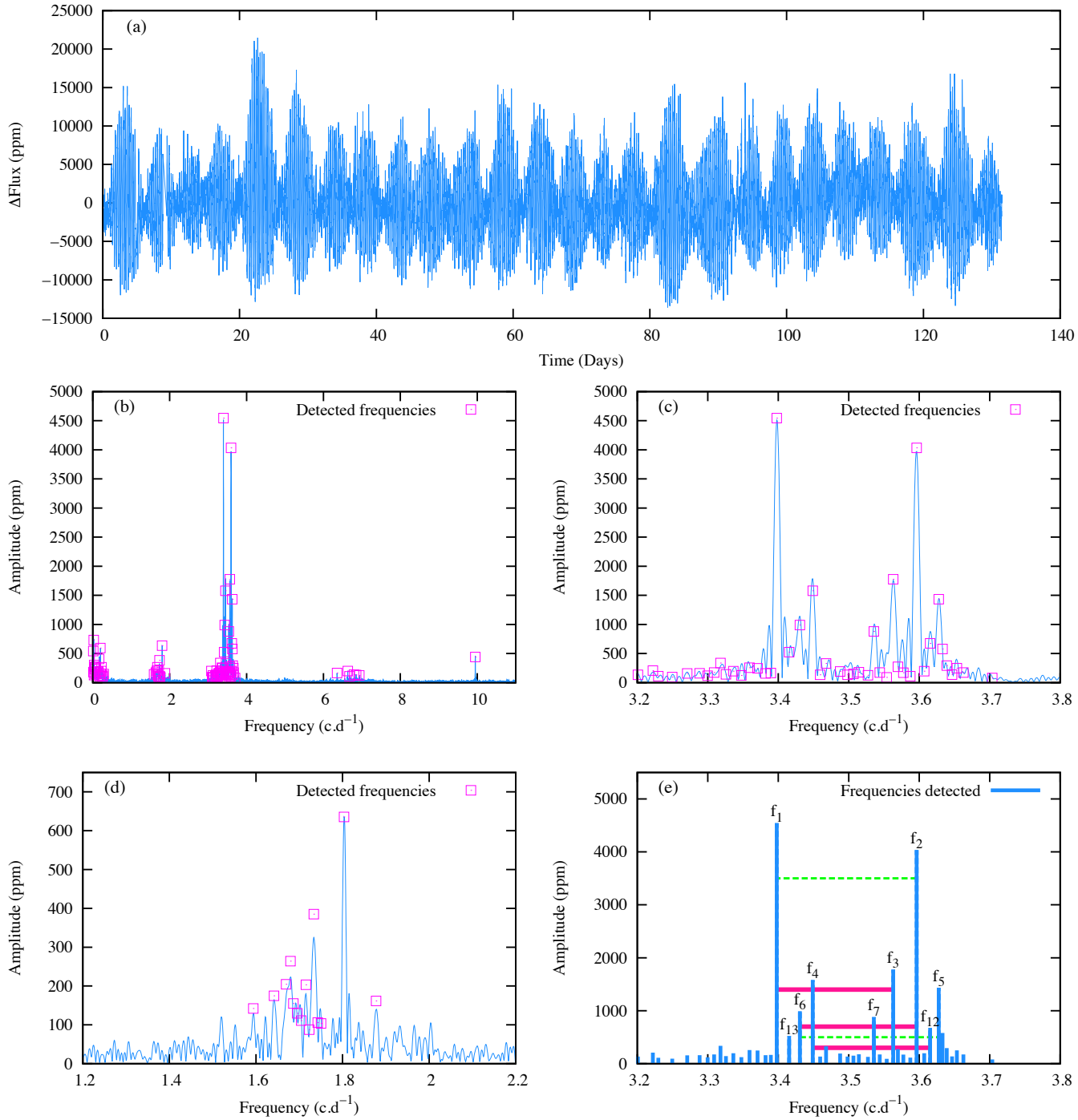

Fig. 13. Frequency analysis of the Be star CoRoT 102656190 (star No 4) observed in the LRA1 run. *Panel a*: rectified light curve is shown; *panel b*: DFT of the rectified light curve is shown; *panel c*: DFT zoomed in on the second frequency group located at 1.7 c d^{-1} is represented; *panel d*: DFT zoomed in on the third frequency group located at 3.5 c d^{-1} is shown; and *panel e*: frequency spacings inside the third group are shown. The spacings in dashed green are comparable to f_{17} and those in pink are comparable to f_{14}.

curves, of which each corresponds to different degree of variability, are stable (see Tables 12 and 13) and reproduce the same frequency patterns. This result suggests that in the three epochs we are dealing with oscillations that have a stellar origin.

Transients and sometimes broad structures of low amplitude appear separated (or not) from the stellar frequencies, frequently not far from the stellar rotational frequency. These features are of circumstellar origin. However, the estimation of their contribution is difficult.

6. Main frequency properties of the studied Be stars according to their position in the H-R diagram

In Paper I we determined the apparent fundamental parameters and those corrected for rotational effects of the Be stars studied in the present work. The corrected parameters and rotational frequency, $f_{\rm rot}$, given in Table A.1, were calculated assuming $\Omega/\Omega_{\rm c}$ = 0.95. The apparent and corrected positions of our Be star sample in the H-R diagram are shown in Fig. 14. Each star

Table 2. Dominant stellar frequencies (≥ 6/ΔT) and main characteristics in CoRoT light curves of Be stars.

No	CoRoT ID	Frequencies ($c\,d^{-1}$) Amplitudes (ppm) $\pm\sigma_{Amplitudes}$ (ppm)						Comments
1	CoRoT 101486436	5.0333	5.0024	4.9741	2.6755	2.4703	2.5624	Strong beatings (~32 d)
	(LRC1)	2996	1775	625	541	388	225	
		±2	±7	±7	±6	±7	±7	
2	CoRoT 102595654	0.0494	0.1156	0.0867	0.1461	0.2366	0.2153	QPO (20–35 d)
	(LRA1)	264	127	124	106	86	81	
		±14	±9	±13	±9	±3	±12	
4	CoRoT 102656190	3.3979	3.5965	3.5630	3.4489	3.6277	3.4306	Strong beatings (~5 d)
	(LRA1)	4545	4035	1776	1580	1433	990	
		±15	±10	±1	±1	±7	±11	
5	CoRoT 102672979	0.8322	0.8466	0.8253	0.8192	0.8124	1.6065	Strong brightening + QPO (~10–20 d) + beatings?
	(LRA1)	2443	1630	1718	1379	744	659	
		±5	±13	±13	±13	±13	±3	
6	CoRoT 102686433	2.2562	2.2790	1.2947	1.3046	2.2638	2.2881	Strong fading + beatings (~6–9 d)
	(LRA1)	3425	3359	2186	1819	1481	1598	
		±18	±2	±17	±16	±14	±17	
9	CoRoT 102719279	1.1351	1.1699	1.1525	2.3241	1.0028	0.9836	Strong fading
	(IR1)	11137	8928	8843	5312	5259	5981	
		±128	±75	±91	±133	±62	±125	
9	CoRoT 102719279	1.1425	2.3398	2.3239	1.1981	2.3680	2.3908	Strong fading + weak ones (or beatings?)
	(LRA1)	6486	6715	5258	4730	4146	4922	
		±69	±16	±66	±64	±55	±78	
9	CoRoT 102719279	1.1956	2.3663	2.3911	2.3219	2.2906	1.1460	QPO and/or beatings ?
	(LRA6)	6960	4704	4534	3772	3553	34901	
		±15	±26	±26	±10	±26	±6	
11	CoRoT 102725623	0.8966	–	–	–	–	–	
	(IR1)	391	–	–	–	–	–	
		±27	–	–	–	–	–	
11	CoRoT 102725623	0.1453	0.0700	0.1187	0.2419	0.8946	0.2145	
	(LRA1)	511	286	291	249	224	179	
		±7	±20	±21	±20	±17	±21	
12	CoRoT 102728404	1.9161	1.8576	1.9390	1.8644	1.9017	1.8850	Strong beatings (~15–25 d)
	(LRA1)	6980	3401	1920	879	866	761	
		±4	±2	±2	±2	±3	±5	
14	CoRoT 102766835	0.9297	0.8809	0.8235	1.7531	0.1201	0.76427	Fadings or QPO (~18 d ; sawtooth var.)
	(IR1)	8003	4718	3776	3311	2101	1920	
		±35	±32	±4	±18	±44	±3	
14	CoRoT 102766835	0.9288	1.7506	0.8757	0.8218	0.1077	0.7433	Fadings or QPO (~ 18 d ; sawtooth var.)
	(LRA1)	12576	6675	6702	6821	6129	4852	
		±5	±5	±11	±7	±9	±10	
16	CoRoT 102785204	1.2127	2.6740	1.2489	1.1650	1.4012	1.2858	
	(LRA1)	21471	4923	2235	2084	1970	1620	
		±12	±12	±13	±11	±8	±4	
17	CoRoT 102785480	2.2346	1.1288	1.0150	2.1430	1.0465	1.1065	Weak fading? + QPO (~40 d)
	(LRA1)	8263	6277	2785	1963	1167	2166	
		±8	±7	±9	±9	±9	±7	
18	CoRoT 102825808	4.1312	2.3764	4.2305	4.3419	1.9655	6.1907	Weak beatings (~7–10 d)
	(IR1)	1825	1314	1090	981	790	663	
		±9	±6	±8	±16	±14	±3	
19	CoRoT 102829773	5.6118	2.7067	2.8261	2.6148	2.8482	0.1672	QPO (~7–15 d)
	(IR1)	2143	1141	1010	932	602	559	
		±29	±14	±20	±20	±35	±30	
20	CoRoT 102847615	2.7193	2.7875	2.7635	3.0802	5.5087	–	
	(IR1)	554	381	288	227	99	–	
		±14	±10	±15	±13	±14	–	
22	CoRoT 102904910	3.9745	3.8457	3.8179	1.9272	3.7308	3.7952	Weak brightening + beatings (~4–8 d)
	(IR1)	3249	2519	2368	2086	1400	913	
		±19	±4	±18	±22	±4	±23	

Notes. The uncertainty Δf of frequencies is given for each star and for each run in Table 1.

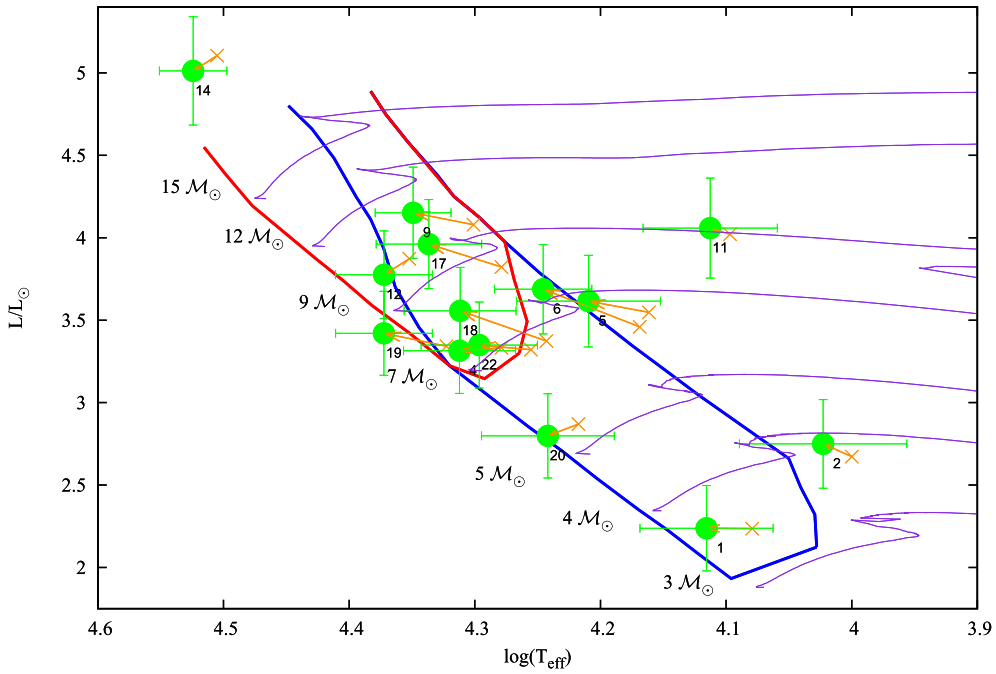

Fig. 14. H-R diagram of our sample of Be stars. Each star is identified with its sequence number, "No", given in Table 1. The cross and filled circle symbols are for stars non-corrected and corrected from the rotation, respectively. The β Cephei (thick red curve) and SPB (thick blue curve) domains calculated by Miglio et al. (2007) with the OP opacity table and the AGS05+Ne chemical abundances are shown. The pink curves represent the evolutionary tracks of rotating stars with various solar masses calculated for $(\Omega/\Omega_c)_{ZAMS} = 0.90$ by Georgy et al. (2013).

is identified with its sequence number "No" given in Table 1. Figure 14 shows the instability domains of the β-Cephei and slowly pulsating B-type variables (hereafter SPB) calculated by Miglio et al. (2007) with the OP opacity table and AGS05+Ne chemical abundances. This figure also shows the evolutionary tracks of rotating stars calculated by Georgy et al. (2013) for $\Omega/\Omega_c = 0.90$. Observational overviews of β Ceph and SPB stars can be found in Pamyatnykh (1999); De Cat (2002); Waelkens (1991); Waelkens et al. (1998), while early instability strips for these types of stars were determined by Dziembowski & Pamiatnykh (1993); Dziembowski et al. (1993).

6.1. Location of Be stars in β-Cephei and SPB domains

In the H-R diagram, the Be stars are generally situated in the same region in which the classic B-type variables β Cephei and SPB stars are found. According to Dziembowski et al. (1993), these pulsators show oscillations driven by the kappa-excitation mechanism acting in the metal opacity bump region. β Cephei stars have B0–B2 spectral types and pulsate in low radial order p- and g-modes, while the SPB stars, less massive variables with spectral types ranging from B2 to B9, pulsate in high radial order g-modes. Frequencies detected for observed p-modes in β Cephei generally range from 3 to 12 c d^{-1}, while in SPB stars, the frequencies of g-modes range from 0.3 to 3.5 c d^{-1}. Pulsation modes are influenced by the centrifugal and Coriolis force (e.g., Townsend 2005; Saio 2013, and references therein). However, p-modes are more affected by the centrifugal force effects than g-modes (e.g., Ballot et al. 2012); conversely, low frequency g-modes are more affected by the Coriolis force than p-modes. In rapidly rotating stars, toroidal oscillations (r-modes) are also expected (e.g., Townsend 2005) and the predicted frequencies of high-order g-modes and r-modes are concentrated in groups.

Among the Be stars studied, only four locate in the SPB domain. These stars are No 1, 5, 6, and 20.

For the Be stars No 5, 6, and 20, the frequencies detected in their CoRoT light curve are in the range of values found for SPB stars. Their groupings are similar to those of other pulsating Be stars with intermediate mass, the so-called slowly pulsating Be stars (SPBe stars; Walker et al. 2005). For star No 1, the dominant frequencies range around 5 c d^{-1}, which are higher than the pulsation frequencies of SPB stars. However, Be stars rotate more rapidly than classic SPB, thus, in the observers referential the frequencies corresponding to prograde modes are higher than for slowly rotating SPB, as is illustrated by the late Be star No 1, which has the higher rotation frequency in the sample, $f_{rot} = 2.12$ cd^{-1} (see Sect. 8).

The B1 Ve star No 19 could be the only star belonging to the β-Cephei domain. The isolated high frequency $f_{24} = 5.6118$ c d^{-1} detected in this star, which also has the highest amplitude ($A \sim 2100$ ppm), could then be attributed to a p-mode; in fact, this value is consistent with the main frequencies reported in the catalog of Stankov & Handler (2005) for β-Cephei stars of B1V spectral types.

An independent high frequency, $f_{62} = 4.5040$ c d^{-1}, is also detected in star No 12, but with a rather weak amplitude ($A \sim 300$ ppm) as compared with that of the dominant low frequency ($f_{41} = 1.9161$ c d^{-1}, $A \sim 7000$ ppm). This B1 Ve star is located in the β-Cephei domain, but it is also near the border of the early type SPB domain. This star could therefore be located in the common part of the two instability domains. The high frequency can be associated either with a p-mode or a zonal g-mode if we consider the frequency spectrum provided by the new pulsation model established for the early Be star HD 163868 (Cameron et al. 2008), although this object is even less massive. Zonal modes are very sensitive to models and rotational frequency Ω, while staying weak and hardly excitable.

The Be stars No 4, 9, 17, 18, and 22 are located inside the common zone of β-Cephei and SPB domains. They show low and high frequencies, which could be attributed to g- and p-modes. However, most high frequencies that have rather low amplitudes are harmonics or can be combinations.

The hottest Be star of the sample, star No 14, has a O9 IV spectral type determined using spectroscopic criteria. It shows frequencies $f < 3.5$ c d^{-1}. The most important characteristic deduced for this star is rotational modulation; see Sect. 8.

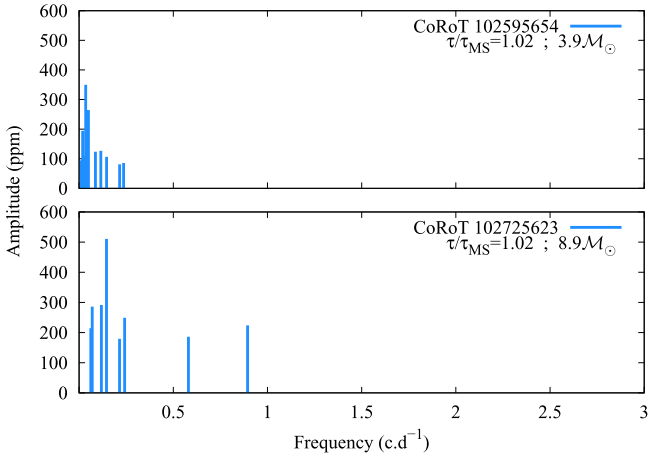

Fig. 15. Frequency pattern of the Be stars located outside the main sequence.

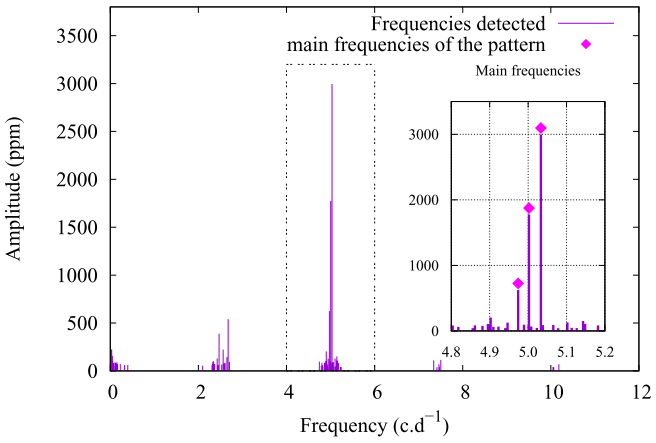

Fig. 16. Concentration of closely spaced frequencies in groups. The insert in the right part of the figure shows the pattern of the three dominant and closely spaced frequencies inside the third frequency group of the Be star CoRoT 101486436 observed in the LRC1 run.

6.2. Main properties on the main sequence

All the main sequence Be stars depict a frequency spectrum concentrated in one, two, three, or even more groups. This characteristic has been reported for bright Be stars whatever their spectral type, thanks to satellite photometry, first with MOST (e.g., Cameron et al. 2008), then CoRoT (e.g., Diago et al. 2009; Huat et al. 2009; Neiner et al. 2009), and more recently *Kepler* (Kurtz et al. 2015) and BRITE (Baade et al. 2016). Theoretical models predict the groupings of frequencies in rapidly rotating stars, which are attributed to high radial g-modes and r-modes of non-radial oscillations (e.g., Saio et al. 2007; Saio 2013). However, mode couplings produce damping effects on retrograde g-modes and for prograde, tesseral g-modes (Lee 2008; Townsend 2005). Therefore, low-degree prograde sectoral-g modes and retrograde r-modes should be visible in Be stars. Dense frequency groupings observed in MOST and CoRoT bright Be stars of 4–8 solar masses are consistent with prograde g-modes (Cameron et al. 2008; Neiner et al. 2009). Nevertheless, these results conflict with those of Rivinius et al. (2003), who claim that the spectroscopic variability is better reproduced with retrograde g-modes ($\ell = 2, m = 2$). In several stars of our sample we also note the presence of some isolated high frequencies that could be attributed to p-modes. Moreover, most stars show a pattern of three (sometimes more) dominant and closely spaced frequencies located in the same group, see Fig. 16. Close and high amplitude frequencies are responsible for beatings in the light curves, as observed, for instance, in stars No 1 (f_{55} and f_{52}), No 4 (f_{60} and f_{78}, f_{60} and f_{74}), No 6 (f_{28} and f_{20}, f_{29} and f_{20}).

6.3. Be stars outside the main sequence

The quasi-totality of the sample stars belong to the MS evolutionary phase in the H-R diagram, except two stars, No 2 and 11, which are beyond the terminal-age main sequence (TAMS). The power spectrum of these two evolved stars is poor (Fig. 15). All the frequencies detected are low frequencies (<1 c d^{-1}). The highest amplitudes detected in these two stars are <300 ppm and <600 ppm for No 2 and No 11, respectively. For the sake of comparison, we note that the amplitude of the dominant frequency in most MS Be stars studied in this work ranges from 2000 to 8000 ppm.

6.4. Frequency patterns as a function of stellar age

The frequency spectrum has been analyzed as a function of the evolutionary phase of each star located in the MS. For this purpose we used the age ratio τ/τ_{MS} determined for $\Omega/\Omega_c = 0.95$, see Paper I (τ = stellar age; τ_{MS} = time spent by a rotating star in the MS evolutionary phase). Thus, the frequency spectrum of each main sequence star was plotted against τ/τ_{MS} (Fig. 17).

A distinction can readily be made between stars near the zero-age main sequence (ZAMS) and those approaching the TAMS. Except for the group of very low frequencies close to 0 c d^{-1}, which is mainly populated by combinations of frequencies and slow flux variation frequencies, stars with $0 < \tau/\tau_{MS} < 0.2$ show only one frequency group. For $\tau/\tau_{MS} > 0.2$ two thick frequency groups are seen. Most often, in stars with $0.2 < \tau/\tau_{MS} < 0.5$, the groups populated by the higher frequencies also have the highest amplitudes.

In more evolved stars, i.e., $\tau/\tau_{MS} > 0.5$, there are two groups with a similar number of frequencies and/or comparable amplitudes. The separation between frequency groups seems to be larger for stars close to the ZAMS than for those near the TAMS. To better reflect this tendency we considered only stars with similar masses. This limited sample encompasses stars No 4, 5, 6, 18, 19, and 22 that have masses from $M = 6.4$ to 8.2 $M_\odot$. In Fig. 17, a tendency is brought out that concerns the spacing of groups. The two main groups seem to be nearer to each other and closer to the origin of abscissas. We find that

– For the younger stars, i.e., $0 < \tau/\tau_{MS} < 0.63$, the tendency is that the larger is τ/τ_{MS} the wider becomes the separation between the two main groups. We note that for star No 19 only a frequency group was seen, since the frequency at 5.6118 c d^{-1} is isolated.

– For older stars, i.e., $0.63 < \tau/\tau_{MS} < 1.00$), the tendency is that the spacing between the groups does not vary continuously, but in any case it attains a maximum value at the middle of the MS. This property deserves to be confirmed with larger samples of stars that have about the same mass and age. Finally, it is worth highlighting that all the stars (except one, No 22), which show one or more light outbursts (stars No 5, 6, 9, 14, and 17) are also those which are the more evolved in the sample, i.e., $0.63 < \tau/\tau_{MS} \rightarrow 1.0$ (see Fig. 17).

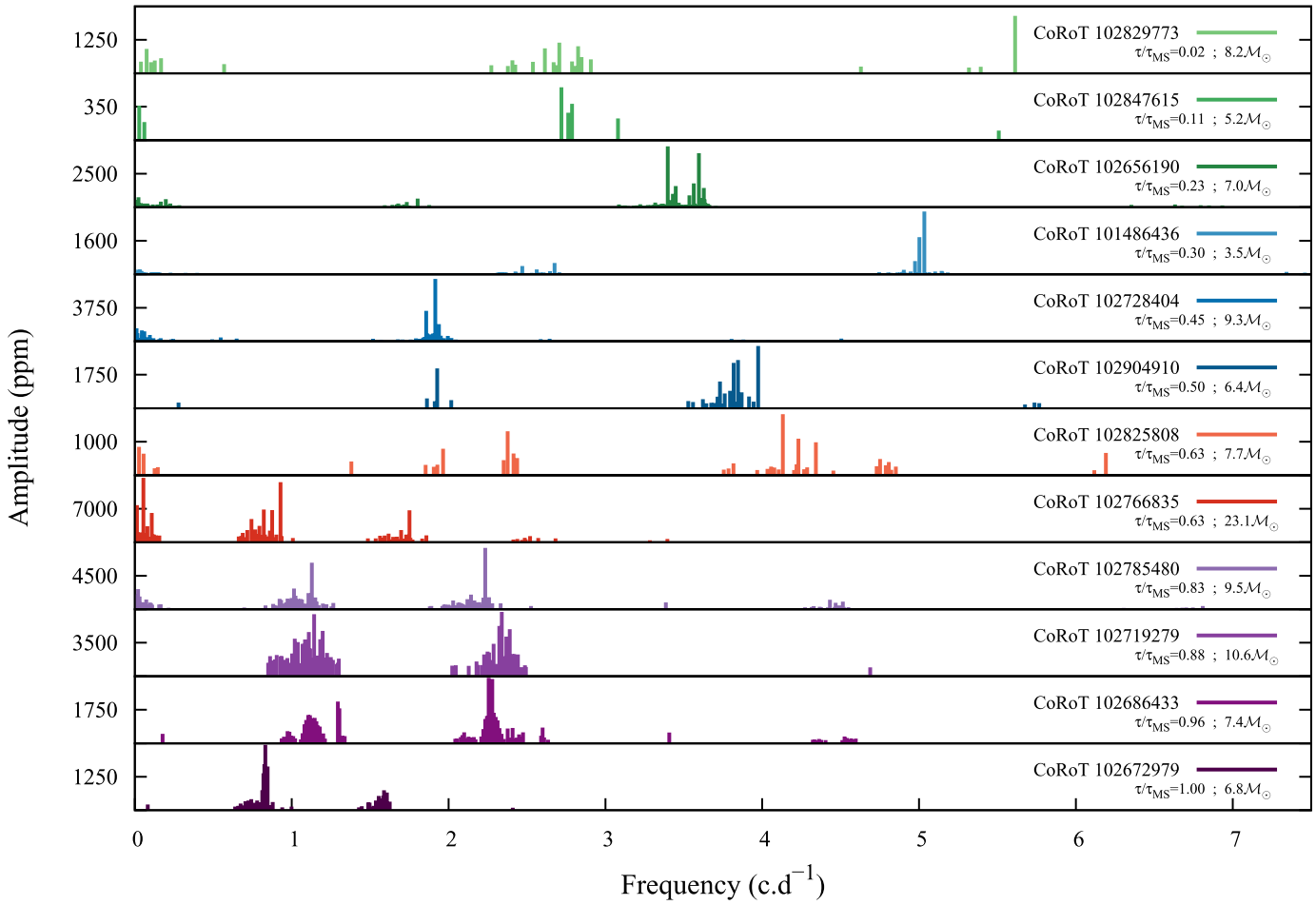

Fig. 17. Evolution of the frequency patterns linked to the evolutionary status of the stars. The more evolved stars in the sample ($0.5 \lesssim \tau/\tau_{MS} \rightarrow 1.0$) are those which show one or more light outbursts.

6.5. Visibility of the rotational frequency in the power spectra of light curves

We searched for a link between the frequency groups present in the CoRoT light curves of Be stars and a rotational modulation of spots and/or blobs of material attached to the stellar surface. First, we compared the rotational frequency domain provided by spectroscopic fundamental parameters corrected from effects due to rapid rotation at a ratio $\Omega/\Omega_c = 0.95$ with the main groups of frequencies found in light curves. As shown in Fig. 18, about three-quarters of the sample stars have their rotational frequency outside the groups. The rotational frequency domain can only correspond to one of the main groups for stars No 4, 14, 17, and 19. Moreover, except for star No 14, the group in question does not contain the higher amplitude frequencies.

Then, for each star we determined the intervals between subsequent groups and compared them with the rotational frequency (see Table 3). We found that five stars (among these those quoted above and star No 5) show a mean spacing between groups compatible with the rotational frequency (Fig. 19). The most important disagreement between rotational frequency and group spacing is found for the two stars that have strong outbursts: i.e., stars No 6 and 9, as well as for the highly emissive star No 12. The latter has recently been suspected to be a Herbig star (Negueruela et al. 2015).

Finally, we plotted in Fig. 20 the mean separation between the groups as a function of the rotational frequency and we found a well-defined linear relation between these two quantities. This result, obtained with our sample, agrees with the proposition made by Saio and co-workers (Cameron et al. 2008; Saio et al. 2007) to explain the frequency distributions in several intermediate-mass Be stars observed with the MOST satellite, the so-called SPBe. According to these authors, the position of frequency groups in the Fourier spectrum attributed to g- and r-mode oscillations depends on the azimuthal degree m and the separation of the frequency groups corresponding to prograde g-modes is close to the rotational frequency. However, the spacing between the groups of frequencies detected in CoRoT Be stars does not coincide entirely with the rotational frequency. We find that the main frequency groups are separated by $\delta f = (1.24 \pm 0.28) f_{\rm rot}$ (its uncertainty is discussed in Appendix A). This spacing is fairly in agreement with recent models of prograde sectoral g-modes ($m = -1, m = -2$) of a highly rotating, 4.5 $M_\odot$ main sequence star (Saio 2013).

The frequency forests found in the power spectra of Be stars is a known phenomenon since the works by Saio et al. (2007); Saio (2013); Dziembowski et al. (2007b,a) and Cameron et al. (2008), who interpreted them as dense populations of low-order g-modes. Rivinius et al. (2016) suggest, however, that they likely represent short-term circumstellar variability.

Table 3. Average separation δf of frequency groups and their uncertainty $\sigma_{\Delta f}$.

Star No:	1	2	4	5	6	9	11	12	14	17	18	19	20	22
Groups No:	1, 2, 3	–	1, 2, 4	1, 2	1, 2, 4	1, 2	–	1, 2	1, 2, 3	1, 2, 4	1, 2, 3, 4	1, 2	–	1, 2, 3, 4
δf c d^{-1}	2.51	–	1.75	0.67	1.14	1.20	–	1.90	0.85	1.07	1.99	2.83	–	1.89
$\sigma_{\delta f}$	0.23	–	0.23	0.15	0.22	0.22	–	0.14	0.19	0.23	0.34	0.25	–	0.16

Notes. Frequency groups are numbered according to increasing values of frequencies. Group 0, near 0 c d^{-1}, also contains very low frequencies of intrinsic or instrumental origin. This group is not used in this work.

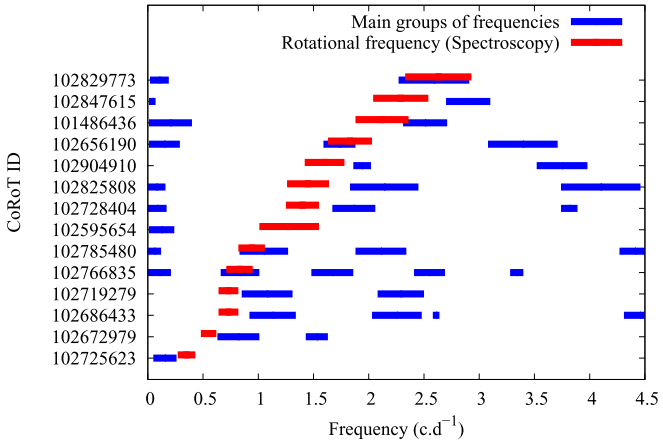

Fig. 18. Location of the groups of frequencies compared with the rotational frequency established by spectroscopy. The length of each blue dash in c d^{-1} corresponds to the uncertainty on the location of the frequency group. The length of the red dashes corresponds to the uncertainty of the stellar spectroscopic rotational frequencies.

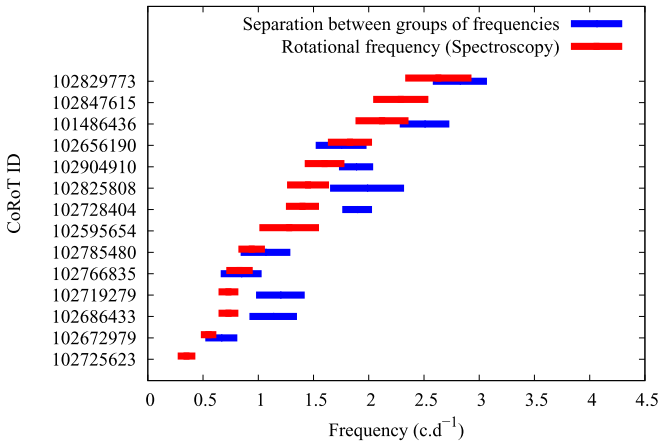

Fig. 19. Separation of the groups of frequencies compared with the rotational frequency established by spectroscopy. The length of the blue dashes corresponds to the uncertainty of the group spacings.

7. Stars showing light outbursts

Thanks to the high precision and the samplings of CoRoT data, we have been able to detect short-lived outbursts in a large percentage of our Be star sample with magnitude changes $|\Delta V| \simeq 0.03$ mag. Five objects in the sample, stars No 5, 6, 9, 14, and 17 showed light jumps. Another object, star No 22, also depicted similar light variations but of much weaker amplitude. Flux increases (brightenings) were observed in stars No 5, 6, and 22, while flux decreases (fadings) were seen in stars No 9,

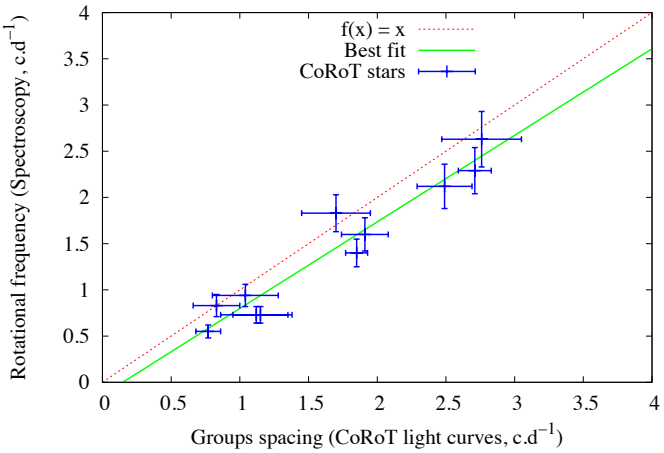

Fig. 20. Relation between the separation of the groups of frequencies and rotational frequency deduced from spectroscopy. The uncertainties are the same as in Fig. 19.

14, and 17. For stars No 9 and 14, the VLT/GIRAFFE spectroscopic observations (Semaan et al. 2013, Paper I) have revealed the presence of a strong Be-shell spectrum.

It may be worth noting that among stars No 1, 2, and 11, which have the lowest effective temperatures in our sample, only star No 2 shows the QPO, and that stars No 2 and 11 are above the instability region in the H-R diagram. Other activities were not detected in any of these stars.

In contrast with Sect. 5 in which the light curves are analyzed globally, in this section we consider the light curves divided in several parts according to the outburst phases. This is carried out for stars No 5, 6, and 9, which have shown outbursts that lasted more than 20 days. It is also done for star No 17, which depicted an isolated, but short outburst at the beginning of the observational run. The event was too short to identify properly the successive phases of the light curve. In star No 22, the suspected outburst at the middle of the run was hardly distinguished from beatings.

In those cases in which the outbursts lasted during a large portion of the CoRoT run, we searched for temporal variations in the frequency spectrum of our sample stars that accompanied their light outbursts similarly as in Huat et al. (2009) for HD 49330. Thus, whenever it was possible, the CoRoT light curves displaying outbursts, either brightenings or fadings, were cut into four separate sections that closely follow the schematic picture of the spectroscopic phases proposed by Rivinius et al. (1998b) to characterize an outburst in the Be star μ Cen:

– the quiet or relative quiescence phase, during which the outburst is not yet identified and the star can a priori be considered inactive;

Table 4. Different phases in the light curve of CoRoT 102672979 (star No 5).

Phases	Time (d)		Resolution
	t_i	t_f	$1/\Delta T$ (c d^{-1})
Brightening phase	0.00	40.40	0.03
Relaxation phase	40.41	71.29	0.03
Relative quiescence phase	71.30	131.46	0.02

– the precursor phase of the outburst, which precedes the sudden stellar brightness jump and the stellar brightness fades very weakly and gradually;
– the outburst phase, which corresponds to the sudden brightness jump;
– the relaxation phase, during which the star brightness progressively recovers the level of its quiet phase.

Since we do not have simultaneous spectroscopic and photometric observations of outbursts, a comprehensive correspondence between the descriptions of spectroscopic and photometric phases cannot be established.

We note that not all the stars observed with outbursts during the two CoRoT runs IR1 and LRA1 showed all the above-mentioned phases. In some cases, recurrent minor outbursts followed one another very closely in time, which did not enable us to identify the phases correctly. Sometimes, an outburst occurred just at the beginning or at the end of the CoRoT run, so that some phases were probably missed.

We point out that the cutting in different phases was made from the complete light curve rectified from instrumental discontinuities, but frequencies in each phase were sought in the DFT of the complete light curve rectified as mentioned above, then detrended from the shape of stronger outburst(s). Finally we performed a time-frequency analysis across the complete CoRoT light curve to better investigate the change of the number and amplitude of dominant frequencies and/or groups of frequencies.

7.1. CoRoT 102672979 (star No 5 – LRA1)

This star has shown a prominent brightening (30 000 ppm) at the very beginning of the CoRoT run. The expected precursor phase must have appeared just before the start of the observational run. The amplitude of light oscillations is higher during the first half of the brightening phase.

7.1.1. Separation of different phases

The cutting up of the light curve is depicted in Fig. 21 (top left panel). The different phases, their time duration, and frequency resolution ($1/\Delta T$) are given in Table 4. Only three phases could be identified.

We analyzed each phase using the same method as for the complete light curve described in Sect. 4. We calculated the DFT for each phase, shown in Fig. 21 (left panels).

7.1.2. Follow-up of main groups of frequencies

In each light-curve phase, we focused on the behavior of the main frequencies or on groups of frequencies. The height of each step is given by the highest amplitude in the group of frequencies. Because we mainly search for tendencies of the amplitude changes with time, the following description is schematic. The low frequency resolution in each phase of outbursts does not allow any study of their frequencies individually. For this star only two groups of frequencies around 0.83 and 1.58 c d^{-1} are conspicuous. We investigated their amplitude changes during the three phases, (shown in Fig. 21; right panels), as follows:
– The amplitude of the frequency group around 0.83 c d^{-1}, which is high in the outburst phase, decreases by a factor 3 in the relaxation phase, and then weakly increases in the relative quiescence phase.
– The amplitude behavior of the group around 1.58 c d^{-1} is opposite to that of the group around 0.83 c d^{-1}. The frequency amplitude, at a minimum during the brightening, gradually increases across the two following phases to become twice as large as in the relative quiescence phase. In this later phase, the group recovered its initial amplitude level before the outburst event.

Our analysis implies that frequencies are stable in position across each outburst phase.

7.1.3. Time-frequency analysis

For this study, we used a 40d-window moving with a 1d-constant step across the light curve. The frequency accuracy is 0.006 c d^{-1} (Fig. 22). This method provides some additional information as follows:
– The dominance of the 0.83 c d^{-1} group of frequencies in the first part of the CoRoT light curve, which corresponds to a brightening, is confirmed in addition to the consecutive drop during the relaxation phase. However, we see that at the epoch of this later phase, weak frequencies appeared at about 0.7 c d^{-1} (see also Fig. 4(d)), which always remained visible by the end of the run, while the frequencies at 0.83 c d^{-1} increased their amplitude.
– The frequency beam at 0.83 c d^{-1} contains several frequencies variable in amplitude but rather stable in position according to the respective frequency resolution of each phase (Table 4 and Figs. 21 and 22). According to the DFTs of the different phases we find that the frequency f_{21} = 0.832 c d^{-1} is dominant at the beginning of the run during the brightening phase (phase a), then the frequency beam temporary becomes double, at 0.822 c d^{-1} and 0.858 c d^{-1}, during the relaxation phase (phase b). It is again single but broad and recovers its position at 0.835 c d^{-1} with a low amplitude in the relative quiescence phase (phase c).
– The structure between 1.5 and 1.6 c d^{-1} contains many weak amplitude frequencies that form several beams, such as the narrow frequency beam at 1.50 c d^{-1} with a variable amplitude across the run, and the frequency beam at 1.58–1.60 c d^{-1}. From the DFTs we find that this latter frequency beam is single with a low amplitude in phase (a), double in phase (b), and again single with a higher amplitude at the beginning of phase (c) and then broader at the end.

7.2. CoRoT 102686433 (star No 6 – LRA1)

This object has shown one of the more prominent and best characterized light outbursts among the stars in our sample. The brightening (50 000 ppm) was observed at the middle of the CoRoT run. The amplitude of light oscillations is higher at the maximum of the brightening phase.

7.2.1. Separation of different phases

The cutting up of the light curve is shown in Fig. 23 (top, left panel) and the values of the different phases are given in

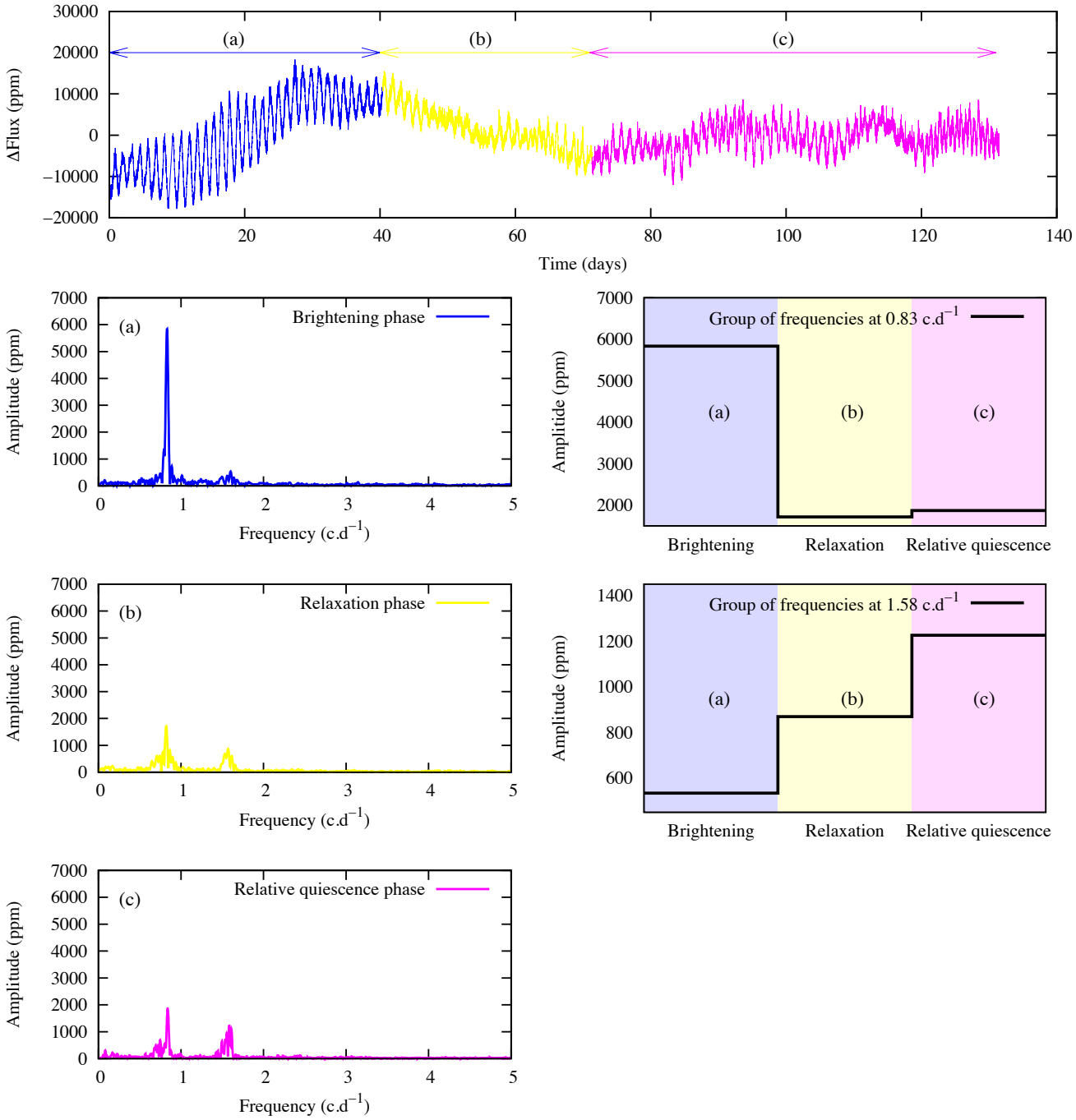

Fig. 21. Analysis of the rectified light curve of star CoRoT 102672979 (star No 5, in the LRA1) in parts. Three phases are found in the complete light curve: (a) brightening phase ⟷,(b) relaxation phase ⟷ and (c) relative quiescent phase ⟷ (*upper left panel*). The DFT in each phase is shown (*lower left panels*); changes in amplitude of the main groups of frequencies at 0.83 and 1.58 c d^{-1} between the different phases (*right panels*) is shown; errors of the amplitude estimates are ∼ ±10% ppm on average are represented. The amplitudes of the two frequency groups are clearly anticorrelated during the brightening phase.

Table 5. For this star we were able to obtain all four phases that characterize the outburst in HD 49330 (Huat et al. 2009).

We calculated the DFT for each phase (Fig. 23, left panels).

7.2.2. Follow-up of main groups of frequencies

First, we consider the behavior of the two subgroups at 1.15 and 1.30 c d^{-1} in the group around 1.20 c d^{-1}. Then, we follow the three subgroups at 2.27, 2.42, and 2.60 c d^{-1} in the group around 2.40 c d^{-1}. Finally, we consider the frequencies at 3.40 c d^{-1} and 4.57 c d^{-1}. The variation of the maximum amplitude in the different frequency subgroups plotted as a function of each light curve phase is depicted in Fig. 23 (right panels). We note two types of frequency behavior:

– For the frequency subgroups at 1.15, 2.27, 2.42 c d^{-1}, and for the frequencies at 3.40 c d^{-1} and 4.57 c d^{-1}, we note a clear amplitude increase during the outburst phase proper. This is generally of about a factor 3. However, for the subgroup at 1.15 c d^{-1}, the amplitude increase in the outburst phase is particularly high, about 10 times the amplitude in the relative quiescent phases.

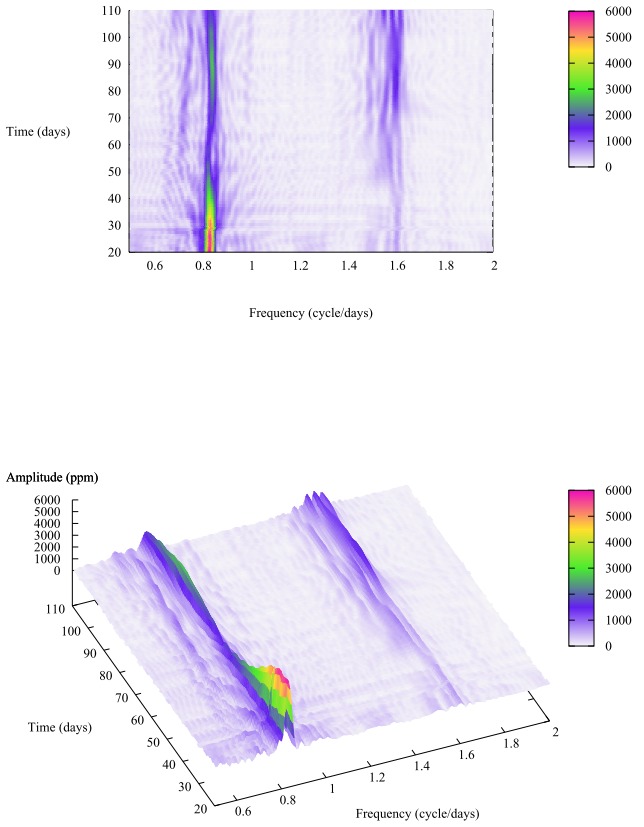

Fig. 22. DFT evolution with time for the star CoRoT 102672979 (star No 5, in the LRA1) seen under different angles; this was made with a sliding 40-d window width and a 1-d constant step. The colors denote the amplitude of frequency peaks in ppm. The structure evolution of the two groups at 0.83 and 1.58 c d^{-1} is complex: amplitudes of frequencies vary through the whole light curve.

Table 5. Different phases identified in the light curve of CoRoT 102686433 (star No 6).

Phases	Time (d)		Resolution
	t_i	t_f	$1/\Delta T$ (c d^{-1})
Relative quiescence phase 1	0	30.56	0.03
Precursor phase	30.57	57.56	0.04
Brightening phase	57.56	70.56	0.08
Relaxation phase	70.57	84.26	0.07
Relative quiescence phase 2	84.26	131.46	0.02

In the following relaxation phase we observed a strong decrease of the amplitude that is, however, higher or of the same level as those in the quiescent and precursor phases.
– For the two frequency subgroups at 1.30 and 2.60 c d^{-1} we observe an opposite behavior. During the precursor and outburst phases the signal amplitude is lower than in the quiescent phases 1 and 2. However, after the strong drop in the precursor phase the signal amplitude increases in the outburst phase proper to reach, in the next relaxation phase, the same level as in the quiescent phases.

7.2.3. Time-frequency analysis

We performed a time-frequency analysis with a moving 40d-window as previously carried out for CoRoT 102672979 (star No 5). The evolution of the Fourier spectrum as a function of time (Fig. 22) shows that changes occur inside the different groups of frequencies as follows:
– In the group around 1.15 c d^{-1}, which is not very populated in the quiet phase, numerous frequencies appear in two subgroups around 0.95 and 1.12 c d^{-1} during the brightening; they have slightly higher values than the spectroscopic rotational frequency f_{rot} = 0.73 ± 0.09 c d^{-1}. The amplitude level of the main frequencies 1.12–1.15 c d^{-1} attained 4000–5000 ppm. All frequencies that appear during the outburst exhibit a very low amplitude or disappear afterward, except the 0.97 c d^{-1} frequency whose amplitude is 1600 ppm during the outburst and about 800 ppm in the following phases.
– In the same way, in the 2.3 c d^{-1} group many low amplitude frequencies appear during the brightening and then disappear. However, some low amplitude frequencies between 2.35 and 2.5 c d^{-1} do not seem to vary across the run. The two close and main frequencies 2.26 and 2.28 c d^{-1} oscillate around a mean and single value during the precursor phase. They are both present during the outburst and have the same amplitude, which gives the impression that there is a frequency doubling with the same phase.
– Numerous frequencies of small amplitude also appear in the range from 4.0 to 4.5 c d^{-1} during the outburst, as shown in Fig. 23 (left panel).
– The amplitudes of dominant frequencies are affected during outbursts but their positions in the periodogram often remain stable from one phase to another in the run (Fig. 23). This is the case for the narrow beam at 1.3 c d^{-1} and 2.3 c d^{-1} (Fig. 24). Thus, the 2.3 c d^{-1} beam is conspicuous during the first relative quiescence phase (a) and the precursor phase (b), appears double during the outburst (phases c and d); and is again single as it recovers its position in a new quasi-quiet phase (phase (e)). Moreover, many low amplitude frequencies, such as those in the blue and red sides of the frequency beam at 2.3 c d^{-1}, appear stable in position (Fig. 24).

7.3. CoRoT 102719279 (star No 9 – IR1 and LRA1)

This star has shown very strong activity in the first two CoRoT runs, which is characterized by the presence of several fadings. Moreover, stellar brightness increased by 0.06 mag over the 200 days that separated the IR1 from the LRA1 run. First, in the IR1 we observed a very strong fading (about 100 000 ppm) just at the beginning of the run (see Fig. 25; top, left panel). Afterward, in the LRA1 we detected at least six fadings of weak intensity, and another fading, at the middle of the run, of longer duration and with somewhat higher amplitude, about 120 000 ppm (see Fig. 26; top, left panel). The amplitude of light oscillations is higher three or four days prior to the minimum flux related to the fading in the IR1 and the most important fading in the LRA1. We analyzed the fading in the IR1 and compared it with the stronger fading in the LRA1.

7.3.1. Separation of different phases

The cutting up into several phases of the two fadings that we have analyzed is summarized in Table 6. Only three phases are identified in each one. It was not easy to cut the strong fading in the LRA1 due to the strong activity of the star at that epoch. Because recurrent and very weak fadings first preceded and then followed the main fading, we were not able to isolate the precursor phase in the latter, which has probably been blended with the relaxation

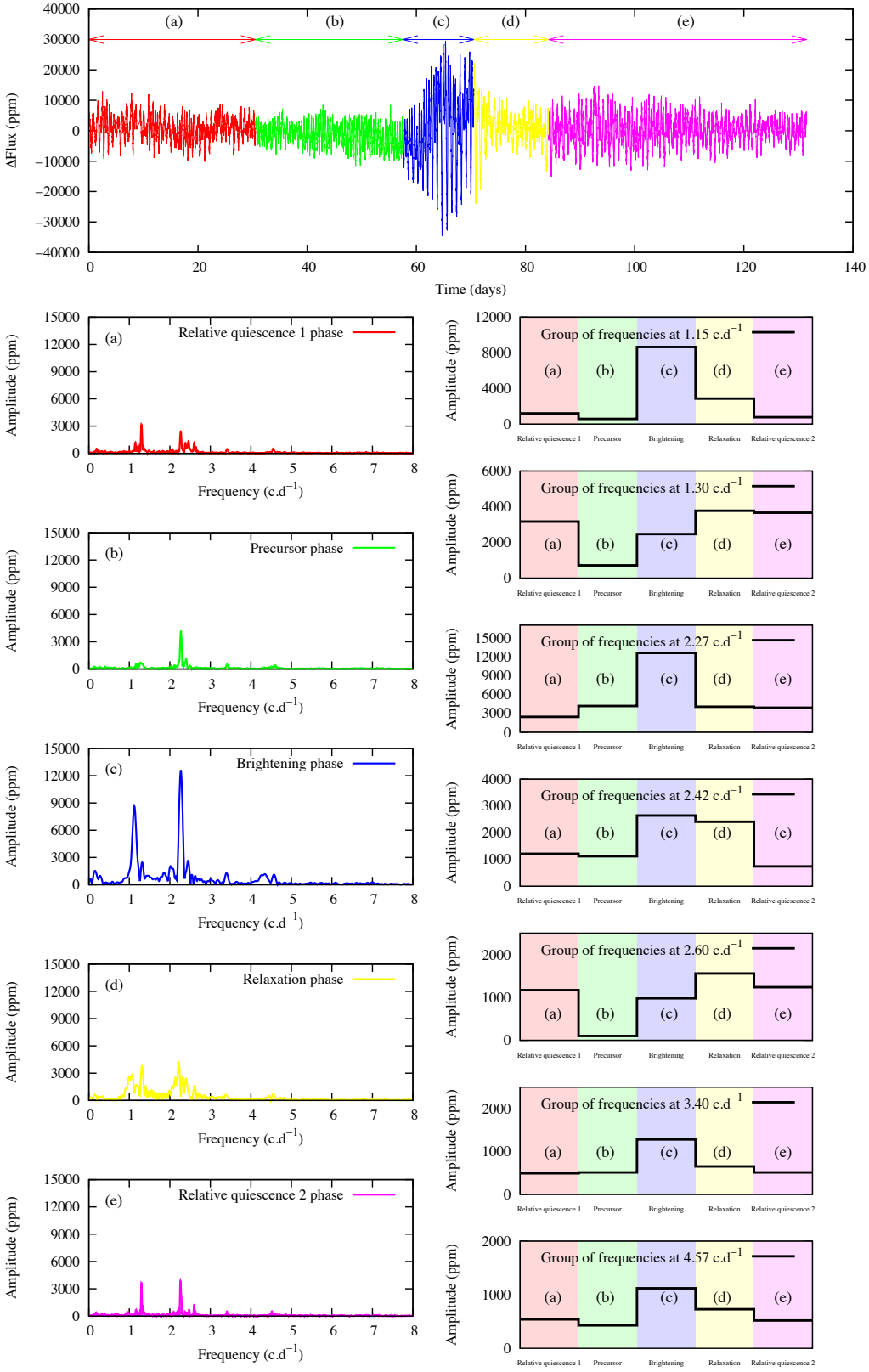

Fig. 23. Similar as for Fig. 21, but for star CoRoT102686433 (star No 6) in the LRA1. Five phases are found in the light curve: (a) relative quiescent phase 1 ⟷, (b) precursor phase ⟷, (c) brightening phase ⟷, (d) relaxation phase ⟷, and (e) relative quiescent phase 2 ⟷ (*upper left panel*). Changes in amplitude of the five groups of frequencies at 1.15, 1.30, 2.27, 2.42, 2.60, 3.40, and 4.57 c d^{-1} are seen between the different phases (*right panels*); errors of the amplitude estimates are ∼ ±10% ppm on average. The behavior of the amplitudes of the two frequency groups at 1.30 and 2.60 c d^{-1} in relaxation phase (d) and the relative quiescent phases (a) and (e) differs from that of the other groups.

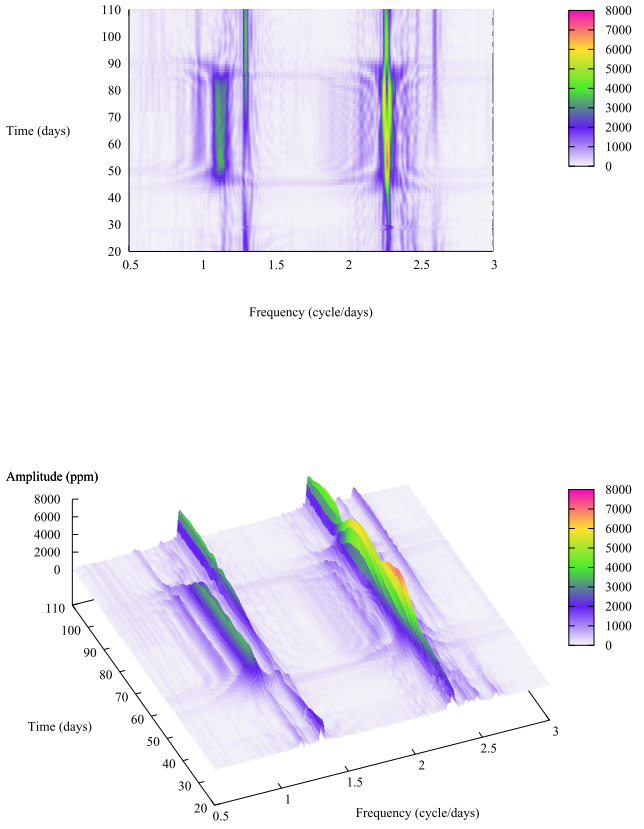

Fig. 24. Idem Fig. 22, but for star CoRoT 102686433 (star No 6) in the LRA1. The peak amplitude of each frequency group is variable through the light curve; transient frequencies appear during the brightening phase (c) and form the broad groups at 1.15 and around 2.27 c d^{-1}. This latter frequency appears double in the relaxation phase (d).

Table 6. Different phases identified in the light curve CoRoT 102719279 (star No 9) observed in the IR1 and LRA1 runs.

Run	Phases	Time (d)		Resolution
		t_i	t_f	$1/\Delta T$ (c d^{-1})
IR1	Fading phase	0.00	17.73	0.06
	Relaxation phase	17.73	26.68	0.11
	Relative quiescence phase	26.68	45.00	0.06
LRA1	Fading phase	39.60	54.96	0.07
	Relaxation phase	54.96	71.47	0.06
	Relative quiescence phase	71.47	82.31	0.09

phase of an earlier weak fading, as shown in the complete light curve. Moreover, the relative quiescence phase that we isolated after the main fading in the LRA1 is probably contaminated by the next weak fading that occurred at t = 85 d. The two fading phases that we have considered in detail are depicted in Figs. 25 and 26 (top level, left panel). The phase durations are given in Table 6.

We calculated the DFTs of the two major fading events observed in the IR1 and LRA1. They are shown in the left panels of Figs. 25 and 26, respectively.

7.3.2. Follow-up of main groups of frequencies

We consider four frequency groups present in the DFT of each phase of both fadings. The more important groups are located around 0.30, 1.12, and 2.32 c d^{-1} along with a weaker one around 4.66 c d^{-1}. The amplitude variations for each group along the three phases are schematically depicted in the right panels of Figs. 25 and 26; we note that the group around 1.12 c d^{-1} is highly dominant during the fading in the IR1 compared with that in the LRA1:
– The group around 0.30 c d^{-1} in the IR1 and the LRA1 displays a moderate amplitude, which remains approximately constant during the fading and over the relaxation phases, but it decreases in the subsequent quiescence phase by a factor between 2.5 and 3.
– On the contrary, the amplitude variation in the groups around 1.12 and 2.32 c d^{-1}, which is larger in the fading phase proper, drops in the subsequent relaxation phase in both IR1 and LRA1. However, the transition between the relaxation and relative quiescence phases is slightly different between the two runs. This may be due to the presence of weak recurrent fadings, which precede and follow the main fading in the LRA1.
– Unlike the first three groups, the amplitude of the fourth group around 4.66 c d^{-1} does not seem to vary greatly across the three successive phases.

7.3.3. Time-frequency analysis

The time-frequency evolution in the CoRoT light curve concerns only the LRA1 run. This shows that in the sliding 40d-window that includes stronger fadings, the frequencies at 2.3 c d^{-1}, and the compact group at 1.1–1.2 c d^{-1} dominate and are surrounded by numerous low amplitude frequencies. Moreover, other additional weaker frequencies appeared around 0.9 c d^{-1} at the epoch of the larger fading (Fig. 27, mean time 35–75 d). These last frequencies are close to those already detected by Gutiérrez-Soto et al. (2010) during the large fading observed in the first part of the initial run (IRA1), but their positions in the LRA1 DFT are slightly different and their amplitudes are considerably weaker than in the IR1. However, they always remain higher than the spectroscopic rotational frequency f_{rot} = 0.73 ± 0.09 c d^{-1}. The dominant frequency beams at 1.15 and 2.33 c d^{-1} each contain several close frequencies that according to the time-frequency analysis appear stable in position (Fig. 27) in the LRA1 run. This also happens in the follow up of the different phases studied in the two runs IR1 and LRA1 (see Figs. 25 and 26, respectively). Mainly at epochs of fadings, the frequency beam seen at 0.9 c d^{-1} in the time-frequency graph for the LRA1 run is variable in width (Fig. 27). As depicted in Figs. 25 and 26, this broad feature is strong in the DFTs of phases (a) and (b); in the IR1 we note a dominant component at 0.98 c d^{-1}.

7.4. Other stars

We mentioned at the beginning of this section that it was rather difficult to separate and thus to analyze the different phases of brightenings or fadings detected in the three other CoRoT stars: 102766835, 102785480, and 102904910 (stars No 14, 17,

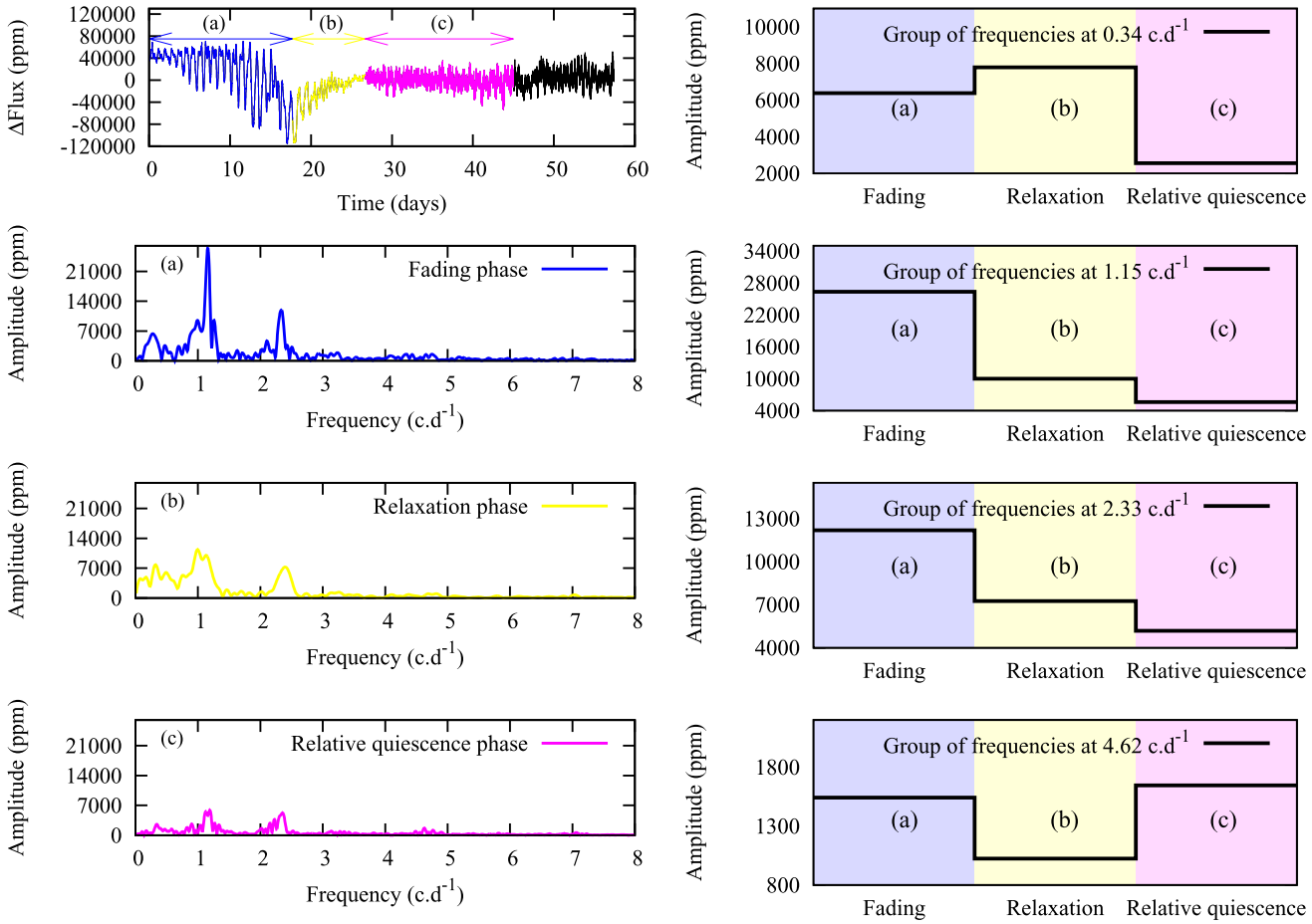

Fig. 25. Similar as for Fig. 21, but for star CoRoT 102719279 (star No 9) in the IR1. Three phases are found in the light curve: (a) fading phase ⟷, (b) relaxation phase ⟷ , and (c) relative quiescent phase ⟷; we note the high peak amplitude at 1.15 c d^{-1} during fading phase (a).

and 22). Their respective light curves are affected by numerous beatings or QPO; moreover, outbursts are too short and sometimes difficult to distinguish from strong beatings. In stars No 17 and 22, the amplitude of light oscillations is higher in the very short fading phase. Nevertheless, some very interesting analogies could be drawn from the time-frequency analysis between the CoRoT star No 17 and the three stars reported in Sects. 7.1–7.3.

– In the light curve of star No 17 [Fig 9(a)], we observe a very short fading that occurred just at the beginning of the run (t = 11.80 d) and seems to be superposed on a slow variation, and possibly another fading of lower amplitude at t = 108.88 d. In the groups of frequencies identified around 0.15, 1.04, 2.25, 3.34, and 4.50 c d^{-1} (Fig. 28), we note an amplitude increase by a factor varying between 2 and 3 at the epoch of the first fading compared with that in the other parts of the light curve. The time-frequency analysis that we performed with a sliding 40-day window (Fig. 29) reveals that at the epoch of the first and more important fading, the groups around 1.04 c d^{-1} contain not only the main frequency 1.1288 c d^{-1}, but also a close and preponderant group of frequencies between 0.95 and 1.05 c d^{-1}. This group vanishes in the quiet part of the light curve (20 d < t < 100 d) and becomes conspicuous again by the end of the run when a new fading of lower intensity occurs. Conversely, the signal associated with the main frequency 1.1288 c d^{-1} slightly decreases during the fadings. The other groups of frequencies around 2.25, 3.34, and 4.50 c d^{-1} show some similarity with the group around 1.04 c d^{-1}. However, the main frequency 2.2346 c d^{-1} dominates during the fadings. A secondary and lower frequency group at 2.15 c d^{-1} is conspicuous during the first fading, which then vanishes in a similar way to the 0.95–1.05 c d^{-1} group. Finally, a myriad of frequencies of very weak and variable amplitude are seen on both sides of the dominant frequencies. The transient group 0.95–1.05 c d^{-1}, which appears during fadings, is very close to $f_{\rm rot}$ = 0.94 ± 0.12 c d^{-1}, and the rotational frequency is determined spectroscopically. The main frequencies f_{46} = 1.129 and f_{86} = 2.235 c d^{-1} remain stable in position across the run (Fig. 29). The frequency beams at 1.01–1.04 c d^{-1} and 2.15 c d^{-1} are conspicuous with the same position during the two outbursts that occurred at the beginning and the end of the run, but they are poorly seen between these two epochs.

– The light curve of star No 22 depicts an outburst of short duration, ≤10 days, superposed on the beatings at the middle of the 60-d observational run (Fig. 5a); the amplitude level increases greatly during the brightening phase in the frequency group around 3.85 c d^{-1} (Fig. 30). The other groups, at 1.92, 5.75 and 7.75 c d^{-1}, show a moderate amplitude increase at that time, which then becomes low during the quiescence phase. Yet, the outburst is very short and very difficult to cut in different phases. Frequencies 1.927, 3.72, and 3.974 c d^{-1} are stable in position according to the DFTs of the different phases (Fig. 30, top level): the frequency f_4 = 1.927 c d^{-1} is present in each phase; the frequency f_{23} = 3.974 c d^{-1} is dominant in the precursor and in the relative quiescence phases (a) and (d), but it has a very weak amplitude or is poorly detectable in the brightening and relaxation phases (b) and (c); on the contrary, the

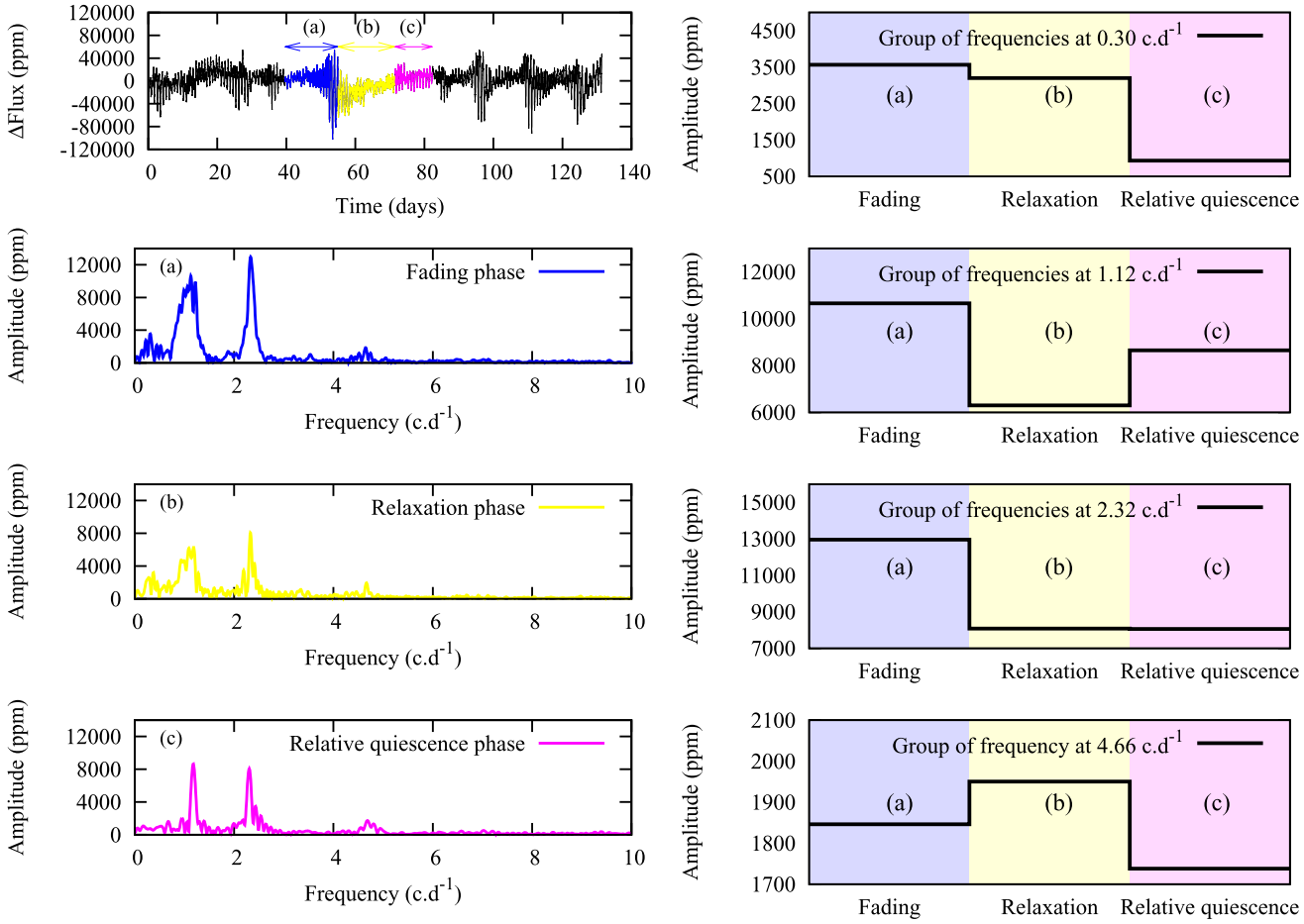

Fig. 26. Similar as for Fig. 21, but for star CoRoT 102719279 (star No 9) in the LRA1. Only the stronger outburst at the middle of the light curve is analyzed. Three phases are found: (a) fading phase ⟷, (b) relaxation phase ⟷ , and (c) relative quiescent phase ⟷. As in the IR1, four groups of frequencies are present at 0.30, 1.12, 2.32, and 4.66 c d^{-1} and their behavior from one phase to another is rather similar in the two runs, but their amplitude level is different.

blend formed by f_{12} = 3.715 c d^{-1} and f_{13} = 3.731 c d^{-1} has a weak amplitude in phase (a), and is more conspicuous in the following phases, mainly in the relaxation phase (c). Finally, the duration of the IR1 is not sufficient for reliable time-frequency analysis.

– The light curve of star No 14 shows many conspicuous light jumps, which could be interpreted as recurrent fadings with a timescale of about 18 days. However, it was not possible to determine the duration of each fading phase nor to analyze them. Moreover, spectroscopic data are needed to identify properly the nature of this object, whose spectral type is compatible with a late O-type star (Paper I).

7.5. Concluding remarks

In stars No 5 and 6 that show brightenings and whose light curves we analyzed in detail, we mainly observe two types of amplitude changes, depending on the groups of frequencies:

– The first type consists of a strong amplitude level in the peak of several frequency groups during the brightening phase proper, followed by a return to a lower level when the outburst ends. The degree of the variation depends on the group of frequencies and on the star itself; it may attain a factor 3.

– The second type shows a drop in amplitude in other frequency groups during the precursor (star No 6) or outburst (star No 5) phases. We note that the decrease in amplitude is larger in the precursor phase than in the increase in the outburst proper (star No 6).

Contrary to the first two stars, star No 9 shows numerous fadings of various intensities in its light curve (LRA1), where we observe only the first type of amplitude changes in many different groups.

The following very interesting points deserve to be noted:

– In two stars, No 5 and 6, we find two types of amplitude changes in frequency groups that are similar to those observed in the CoRoT light curve of the Be star HD 49330 studied by Huat et al. (2009). For this bright star showing an outburst at the middle of the LRA run (seismology field), two types of amplitude changes were found: a type with frequencies showing higher amplitude level before and after the outburst episode, and another type with frequencies of higher amplitude level during the outburst episode.

– Dominant frequencies of variable amplitude can be considered stable in position across the runs (at the accuracy of 0.02–0.03 c d^{-1}). From the time-frequency graphs (Figs. 22, 24, 27 and 29), the same conclusion can be drawn for numerous low amplitude frequencies located on both sides of the dominant frequencies. The origin of variable amplitude frequencies, which were first detected in HD 49330, is an open question. We ask whether these frequencies are g-modes and/or r modes; what physical process is involved in producing such variations; and if they are of circumstellar nature, as is claimed by Rivinius et al. (2016) and

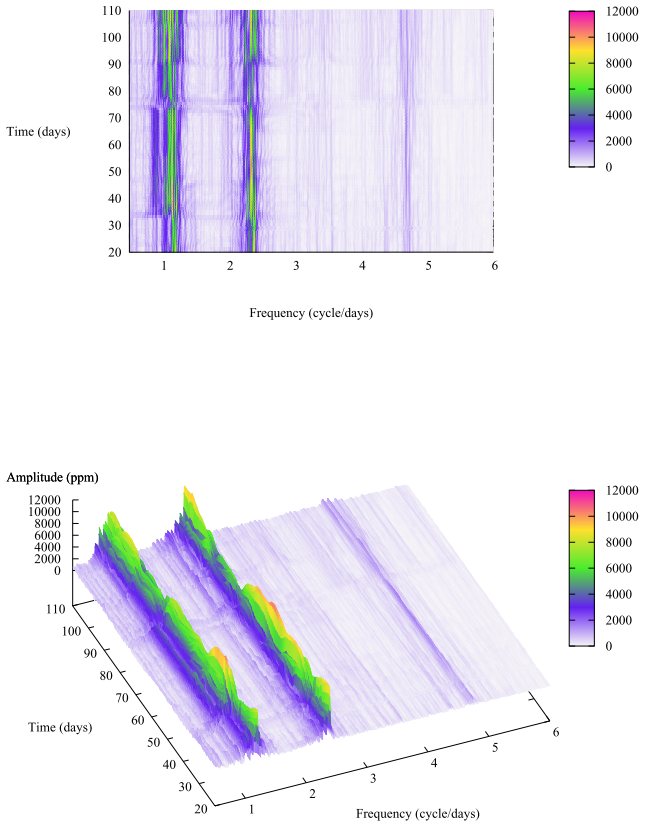

Fig. 27. Idem Fig. 22, but for star CoRoT 102719279 (star No 9) in the LRA1. Transient frequencies appear during the strong fading phase (a) and form the broad structure at 0.9 c d^{-1}.

Baade et al. (2016). Probably new and more appropriate models of pulsations for Be stars with and without outburst episodes are needed to fit observed frequency spectra (see discussion Sect. 9).

– At epochs of stronger light brightenings and fadings in stars No 5, 6, 9, and 17, we detect groups of weak transient and/or unstable frequencies. Some of these frequencies are not too far from the rotational frequency determined spectroscopically (Paper I), but their values are slightly higher in the second and third stars. In HD 49330, Huat et al. (2009) found a group of frequencies compatible with the rotation frequency, whose emergence they attributed to ejected material co-rotating with the star. In the four stars mentioned above, a group of transient and unstable frequencies appears during the time of the outbursts, whose mean frequency is situated about 10% below the next stable frequency that can be attributed to a stellar g-mode. These are the pairs of groups at 0.75 and 0.83 c d^{-1} in star No 5, 1.06 and 1.21 c d^{-1} in star No 6, 0.9 and 1.1 c d^{-1} in star No 9 (less clear in this case) and 1.0 and 1.12 c d^{-1} in star No 17. This behavior detected in CoRoT light curves has been observed spectroscopically in several other Be stars: transient frequencies at the time of strong emission-line episodes were first discovered by Stefl et al. (1998) in 28 CMa and μ Cen. Baade et al. (2016) argued that this kind of short-lived variability affecting spectral lines with a circumstellar component, which these authors call "Štefl frequencies" (Stefl et al. 1998, 2003), originates in the lower part of the circumstellar disk at the time when the disk is fed by ejecta from the surface of the star, rather than in the photosphere. The fact that all stars of our sample displaying outbursts (for which time-series analysis could be performed) present a similar behavior seems to confirm the existence of a common pattern of frequency spectra for all Be stars during outbursts.

8. Peculiar patterns in the frequency spectrum of some sample stars

8.1. Stars without outbursts

In rapidly rotating stars, the period spacing between two consecutive high-radial order g-modes that have the same effective degree ℓ and azimuthal order m is expected to be fairly constant Ballot et al. (2013). This frame may correspond to stars No 1 and 4. We also tried to identify the rotational period through the rotational modulation of some frequencies, and we made a comparison with the rotational frequencies $f_{\rm rot}$ determined spectroscopically in Paper I (see also Table A.1).

8.1.1. CoRoT 101486436 (star No 1)

This late Be star is located toward the red edge of the SPB domain (Fig. 14). Since it is not affected by outbursts, it is a good candidate to search for steady stellar pulsations. The two main groups of frequencies are located at 5 c d^{-1} and 2.3 – 2.7 c d^{-1} in the DFT spectrum. The major group at 5 c d^{-1} is greater than twice the spectroscopic rotational frequency $f_{\rm rot}$ = (2.12 c d^{-1} ± 0.24) c d^{-1}. The other group is larger than $f_{\rm rot}$. In the DFT we identified the low amplitude frequency f_{19} = 2.0960 c d^{-1}, which is very close to the spectroscopic $f_{\rm rot}$.

As rotation frequency increases, according to Saio (2013) prograde g-modes remain excited while retrograde g-modes are damped. We may then consider that the two groups at 5 c d^{-1} (~2.4$f_{\rm rot}$) and 2.3–2.7 c d^{-1} (~1.2–1.3 $f_{\rm rot}$) are compatible with prograde g-modes m = −2 and m = −1, respectively. As far as fundamental parameters are concerned, CoRoT 101486436 (star No 1) can be considered a twin of β Canis Minoris, the late Be star (B8Ve) observed by MOST in which Saio et al. (2007) identified prograde m = −1 g-modes. In CoRoT 101486436 (star No 1), we considered the group of frequencies at 5 c d^{-1}, which is the most populated. The corresponding frequency spectrum was converted in the co-rotating frame for m = −2 using $f_{\rm rot}$ = 2.1 c d^{-1}. The periodogram is shown in Fig. 31. Considering that f_{56} and f_{53} are numerical repeats (doublons) of the main frequencies f_{55} and f_{52}, respectively, we find eight periods (P_{62}, P_{59}, P_{57}, P_{55}, P_{52}, P_{50}, P_{49}, and P_{47}) nearly all consecutive with a spacing period of 4400 ± 200 s in the co-rotating frame. In the DFT the corresponding spacing between two consecutive frequencies ranges from 0.040 to 0.020 c d^{-1} , which is very significant since it is from 3 to 6 times higher than the Rayleigh frequency (0.0066 c d^{-1}). These frequency spacings are similar to those in the rapidly rotating late-type Be star β Canis Minoris, from 0.035 to 0.020 c d^{-1}, calculated by Saio et al. (2007) for consecutive high n-order prograde modes with m = −1.

Figure 31 also shows the periods calculated in the stellar co-rotating frame P_{61}, P_{60}, P_{58}, P_{56}, P_{54}, P_{53}, P_{51}, and P_{48}, which correspond to low amplitude frequencies that are "doublons[3]", harmonics, or perhaps combinations.

[3] The French term "doublons" indicates numerical repeats of frequencies, possibly due to numerical origin, which appear beside other frequencies with much higher amplitude.

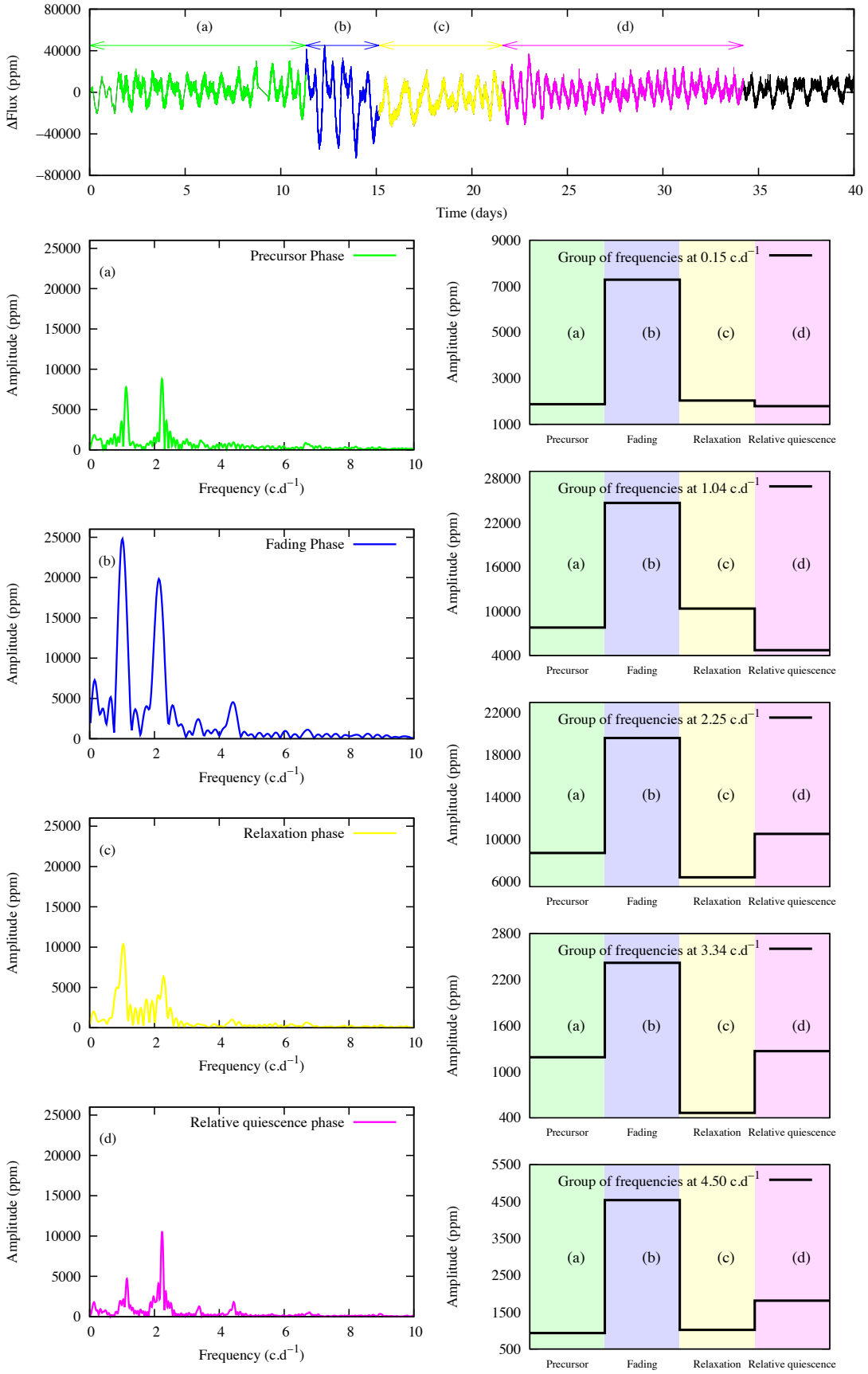

Fig. 28. Similar as for Fig. 21, but for star CoRoT 102785480 (star No 17) in the LRA1. Only the weak outburst at the very beginning of the run is analyzed. Three phases are found: (a) precursor phase/quiescent phase ⟷, (b) fading phase ⟷, (c) relaxation phase ⟷ , and (d) relative quiescent phase ⟷. The amplitude of the five groups of frequencies at 0.15, 1.04, 2.25, 3.34, and 4.50 c d^{-1} is highest at the time of fading.

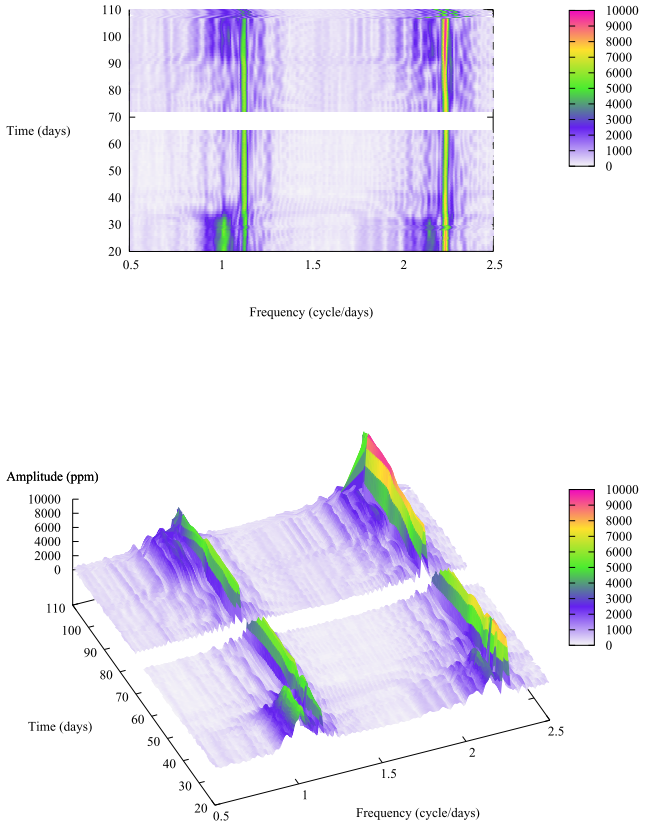

Fig. 29. Idem Fig. 22, but for star CoRoT 102785480 (star No 17) in the LRA1. Broad structures formed by transient low amplitude frequencies are observed at 0.95-1.05 c d^{-1} and 2.15 c d^{-1} during the first fading, then they vanish and are recovered at the time of very weak second fading.

We finally remark that because, our observed frequency patterns are qualitatively comparable to those predicted by Saio (2013) from models of structures of rapidly rotating stars and the separation of the main groups of frequencies agrees with that predicted theoretically (see Sect. 9.2), we consider that we are dealing with prograde modes. On the contrary, from Sect. 6 in Rivinius et al. (2003) it can be concluded that owing to several uncertainties 59% of their studied Be stars perhaps pulsate with retrograde modes $\ell = m = +2$, which is a result that is also based on a qualitative comparison of line profile variations with those modeled for ω CMa as seen from different aspect angles.

8.1.2. CoRoT 102656190 (star No 4)

This B2 Ve star is located at the red edge of the β-Cephei domain (Fig. 14). This is a hybrid β Cep/SPB star. As shown in Fig. 13(a), the light curve depicts numerous beatings of variable amplitude, but it does not seem to be contaminated by outbursts. The most important group of frequencies is located at 3.5 c d^{-1}. It contains two subgroups located at 3.4 and 3.6 c d^{-1} in the DFT spectrum; the latter is at about twice the spectroscopic rotation frequency $f_{\rm rot} = 1.83 \pm 0.20$ c d^{-1}. The other main group of weaker amplitude is located at about 2.3–2.7 c d^{-1}. The isolated high frequency $f_{95} = 9.9504$ c d^{-1} ($A \sim 400$ ppm) could be a p-mode. We searched unsuccessfully for the signature of the spectroscopic rotational frequency, but we found a common spacing in the DFT, $\Delta f = 1.56$ c d^{-1}, which is a lower limit of the spectroscopic rotational frequency $f_{\rm rot}$.

– Between $f_9 = 0.0799$ c d^{-1}, $f_{25} = 1.6415$ c d^{-1}, $f_{44} = 3.2009$ c d^{-1} we obtain 1.5617 c d^{-1} and 1.5594 c d^{-1}, respectively. The f_9, f_{25}, and f_{44} could belong to a rotational triplet.
– In the same way, between $f_{11} = 0.1149$ c d^{-1}, $f_{26} = 1.6697$ c d^{-1} and $f_{46} = 3.2298$ c d^{-1} we derive $f_{26} - f_{11} = 1.5548$ and $f_{46} - f_{26} = 1.5601$ c d^{-1}, respectively; between $f_{17} = 0.1978$ c d^{-1} and $f_{52} = 3.3181$ c d^{-1} we find $f_{52} - f_{17} = 2 \times 1.5601$ c d^{-1}. The 1.56 c d^{-1} frequency, which as shown can be obtained with combinations implying the beating frequencies f_{11} and f_{17}, does not however appear among the frequencies identified in the DFT, but nevertheless may represent the correct value of the rotational frequency. In this case, the two dominant frequency groups at 1.7 c d^{-1} ($m = -1$) and 3.5 c d^{-1} ($m = -2$) could be prograde g-modes. On the contrary, if $f_{\rm rot} = 1.83$ c d^{-1} is correct, the group at 1.7 c d^{-1}, as well as the two subgroups at 3.4 and 3.6 c d^{-1}, would not be consistent with prograde g-modes.
– Finally, we find that the spacing between consecutive frequencies in each group is often close to the frequency resolution $1/\Delta T = 0.0076$ c d^{-1}, particularly in the dominant group of frequencies 3.4–3.6 c d^{-1}, which is very dense. Adopting the 1.56 c d^{-1} value as the correct rotational frequency and considering that the group at 3.5 c d^{-1} contains $m = -2$ high order g-mode frequencies, we find that the spacing between the periods associated with the consecutive frequencies f_{61}, f_{62}, f_{63}, f_{65}, and f_{66} is very constant at 14 400 ± 400 seconds in the co-rotating frame.

8.2. Stars with outbursts

During outbursts, many patterns of transient frequencies appear in the DFTs forming arc-shaped picket fence-like or comb-like structures (see Fig. 32) near or inside groups of permanent frequencies that have variable amplitudes. These transient frequencies are depicted in time-frequency graphs and DFTs. Examples of these frequencies are shown in Figs. 3d and 32, Fig. 6f, and Fig. 9c, for stars No 6, 9, and 17, respectively. Although highly variable in time and amplitude, these structures resemble those that Rivinius et al. (2016) call "bumps h", which they assign to be of circumstellar origin.

Because many transient frequencies are compatible with combinations of dominant permanent frequencies, we may wonder whether they are permanent frequencies with very low amplitudes (undetectable) during the stellar quiescent phases, or whether they are genuine new frequencies that appear at the outburst epochs. Since these apparently new frequencies are on the order of $f_{\rm crit}$ (critical rotation frequency), and since they are sometimes above the escape frequency $f_{\rm tran} \gtrsim f_{\rm esc} = \sqrt{2} f_{\rm crit}$, Gutiérrez-Soto et al. (2010) in their study of star No 9 (discussed here below) asked if transients could be formed in the matter ejected from the star.

8.2.1. CoRoT 102686433 (star No 6)

During the outburst, we observe in different parts of the 2D map (see Fig. 24) the appearance of patterns inside transient frequency groups, which form what look like combs of discrete structures. Thanks to frequencies that we have identified in the 0.94–1.02 c d^{-1} range (see also Fig. 3d), we observe eight consecutive frequencies (Fig. 32) showing a nearly constant spacing $\Delta f = 0.012$ c d^{-1}, which is about 1.6 times the Rayleigh limit $1/\Delta T = 0.0076$ c d^{-1}. This group is slightly higher than $f_{\rm rot} = 0.73 \pm 0.06$ c d^{-1} and nearly the same as $f_{\rm crit} = 0.97$ c d^{-1}. In

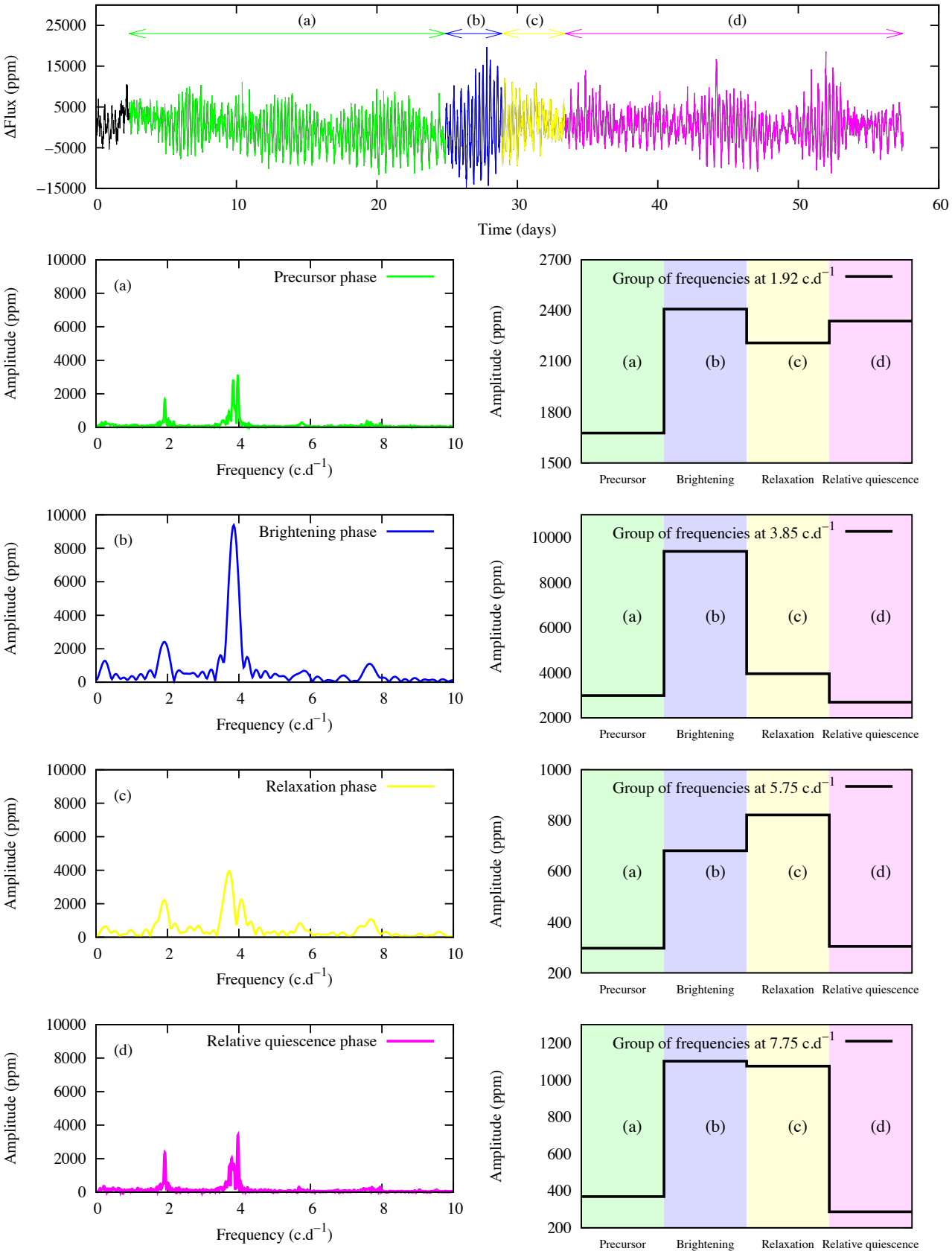

Fig. 30. Similar as in Fig. 21, but for star CoRoT 102904910 (star No 22) in the IR1. The outburst is very short and results are only indicative. Four phases are found: (a) precursor phase ⟷, (b) brightening phase ⟷, (c) relaxation phase ⟷, (d) relative quiescent phase ⟷. Four groups are present at 1.92, 3.85, 5.75 and 7.75 c d^{-1}. The amplitude of the group at 3.85 c d^{-1} is very high during the brightening phase.

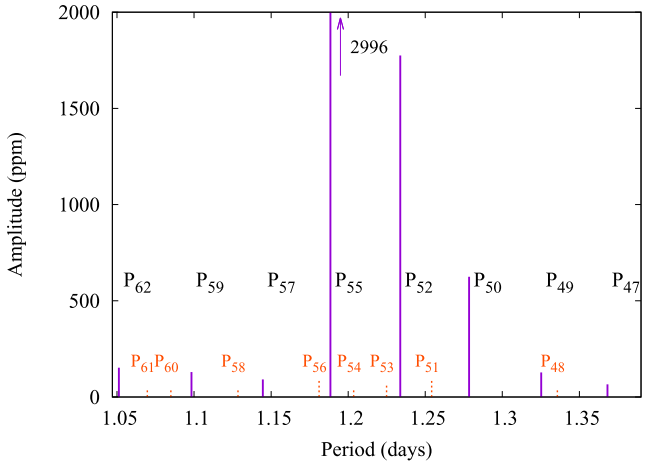

Fig. 31. Period diagram in the $m = -2$ gravity mode spectrum for star CoRoT 101486436 (star No 1, LRC1). The periods shown are calculated in the co-rotating frame for $m = -2$ with $f_{\rm rot} = 2.1$ c d^{-1}; eight periods (P_{62}, P_{59}, P_{57}, P_{55}, P_{52}, P_{50}, P_{49}, and P_{47}) are nearly all consecutive with a spacing period of 4400 ± 200 s (magenta ticks). The red ticks are periods also computed in the co-rotating frame of the star. These periods correspond to low amplitude frequencies, which are "doublons", harmonics, or perhaps combinations.

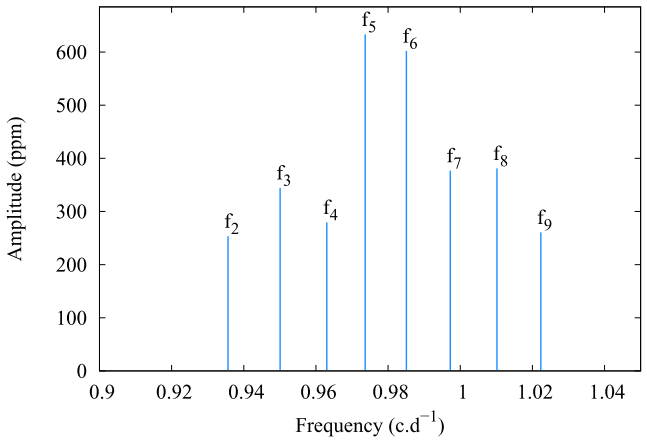

Fig. 32. Group of transient frequencies in the 0.94–1.02 c d^{-1} range for star CoRoT 102686433 (star No 6) observed in the LRA1. Eight consecutive frequencies (Fig. 32) show a nearly constant spacing Δf = 0.012 c d^{-1} larger than the Rayleigh limit $1/\Delta T$ = 0.0076 c d^{-1}. These frequencies form a curved picket fence-like or comb-like structure.

the same way, we find another comb between 1.06 c d^{-1} and 1.21 c d^{-1} that has a similar spacing of 0.012 c d^{-1} easily detected at each edge of the comb, which is superposed on a group of permanent frequencies. The same remark could be made for the region between 2.08 c d^{-1} and 2.17 c d^{-1} (Fig. 3e) and probably for the other group in the 2.21 − 2.35 c d^{-1} range. However, this structure is disturbed in its center by the presence of the main frequencies f_{48} = 2.2562 c d^{-1} and f_{51} = 2.2790 c d^{-1} that dominate the DFT spectrum. Nevertheless, we detect on each side of the comb a spacing going from Δf = 0.011 c d^{-1} on the left edge to Δf = 0.013 c d^{-1} on the right edge. We note that at the center of the comb the spacing between the dominant frequencies f_{48}, f_{49}, f_{50}, f_{51}, and f_{52} corresponds to the resolution limit 0.0076 c d^{-1}.

In conclusion, the spacing found inside different groups of weak transient frequencies quoted above as the spacing between dominant frequencies, generally corresponds to the maximum frequency resolution. The behavior of weak, transient or variable amplitude frequencies, which are larger than the spectroscopic $f_{\rm rot}$ = 0.73 c d^{-1}, is closely linked with the outburst, yet their nature is still not understood.

8.2.2. CoRoT 102719279 (star No 9)

This star has presented several fadings of different intensity in the CoRoT light curves. In particular, during the stronger and longer fading that occurred at the middle of the LRA1, in different parts of the 2D map (Fig. 27) we observe a strengthening of low amplitude close frequencies, whose spacing Δf corresponds to the resolution limit $\sim 1/\Delta T$ = 0.0076 c d^{-1}. Additional frequencies are observed at 0.90–0.93 c d^{-1} at epochs of strong fadings (Fig. 6f). These transient frequencies are higher than the rotational frequency $f_{\rm rot}$ = 0.73 ± 0.09 c d^{-1} determined spectroscopically and close to $f_{\rm crit}$ = 1.05 c d^{-1}, so they may also be related to episodic mass ejections.

8.2.3. CoRoT 102785480 (star No 17)

During the isolated outburst that occurred at the beginning of the run (Figs. 9a and 29), we observed the presence of numerous close frequencies of low and moderate amplitude at the resolution limit $\sim 1/\Delta T$ = 0.0076 c d^{-1}. These form what appear as arc-shaped picket-fences or combs of discrete features such as those located on each side of f_{33} = 1.0150 c d^{-1} in the range extending from 0.90 c d^{-1} to 1.05 c d^{-1} as shown in Fig. 9c. The resulting complex structure, which is very close to the spectroscopic rotational frequency $f_{\rm rot}$ = 0.94 ± 0.12 c d^{-1} vanished afterward, keeping room only for several isolated frequencies, which remain visible in the following relative quiescence phase (Fig. 28). In the same way, we also observed other combs around f_{64} = 2.0291 and f_{75} = 2.1430 c d^{-1} ranging from about 2.05 c d^{-1} to 2.20 c d^{-1} (Fig. 9d), which has a spacing extending from $1/\Delta T$ to $1.7/\Delta T$. The same comments could be made for the presumed second outburst at the end of the run. We note that the spacing between the weak amplitude frequencies f_{51} = 1.1719 c d^{-1}, f_{91} = 2.2785 c d^{-1}, f_{94} = 3.3858 c d^{-1}, and f_{104} = 4.4907 c d^{-1} is constant $\Delta f \sim$ 1.1065 c d^{-1}. This corresponds to the beating frequency f_{43} between the two dominant frequencies f_{86} and f_{46}. The two dense packs of transient frequencies at 0.95–1.05 c d^{-1} and 2.05–2.20 c d^{-1} are also separated by the beating frequency f_{43}. Moreover, not only several dominant frequencies, such as f_{27} = 0.9634 c d^{-1} that combines with f_{46} and f_{33}, but also f_{43}, are very close to the estimated spectroscopic value $f_{\rm rot}$ = 0.94 ± 0.12 c d^{-1}.

8.3. Be star in a binary

A very indirect signature of the stellar rotation may exist as a combined frequency with the orbital motion.

8.3.1. CoRoT 102766835 (star No 14)

This is a late O-type star. In the LRA1, we note the same spacing between the frequencies f_6 = 0.0546 c d^{-1}, f_{32} = 0.8757 c d^{-1}, f_{49} = 1.6975 c d^{-1}, and f_{64} = 2.5201 c d^{-1}, and between this other series f_{10} = 0.1077 c d^{-1} ∼ $2f_6$, f_{35} = 0.9288 c d^{-1}, f_{54} = 1.7506 c d^{-1}, f_{65} = 2.5716 c d^{-1}, and f_{68} = 3.3958 c d^{-1}. The spacing corresponds to f_{27} = 0.8218 c d^{-1}, which closely

corresponds to the rotational frequency $f_{\rm rot} = 0.83 \pm 0.12$ c d^{-1} determined spectroscopically. We conclude that the light curve must have a strong rotational modulation because the frequencies $f = n \times f_{\rm rot}$ have high amplitudes. From the Hα line profile, we suggested in Paper I that the star was a multiple system with a circumbinary envelope. The frequency $f_6 = 0.0546$ c d^{-1} that governs the recurrent outbursts could correspond to the orbital motion. In this picture the light curve is dominated by the interaction between an orbital motion and the stellar rotation with frequencies $f = f_{\rm bin} + n \times f_{\rm rot}$.

9. Discussion and conclusions

9.1. General remarks

The CoRoT satellite observed many Be stars during short and long runs. Thanks to the high photometric quality and temporal resolution of the light curves obtained, for the first time we have been able to identify a large number of reliable frequencies in all the stars studied, some observed in both runs. Nevertheless, it is frequently difficult to determine frequencies in Be stars because irregular variations either of circumstellar origin or several other variations, mainly those due to outbursts, strongly affect the correct understanding of the more or less regular behavior of the intrinsic stellar light curves. For rapidly rotating stars, the frequencies are most often concentrated in several densely packed groups and their correct determination depends on the temporal resolution. In stars that were observed at different epochs, two types of changes are detected: for a same star differences are expected depending on the accuracy of the frequency determination, which is inherent to the unequal durations of observing runs; during the outbursts most frequencies are unstable in amplitude over the whole run and many of them are transients (stars No 9 and 14, see Sect. 7).

Owing to the lack of models of NRP for stellar masses, evolutionary stages, and metallicities comparable to those of our program stars, today we cannot decide to what pulsation modes the frequencies observed correspond. Neither can we say which pulsation modes best fit the mass ejection phenomena or obtain any information on stellar structure.

It is worth noting that in the last 10 years, models have been developed in which rotation was treated as non-perturbative (Reese et al. 2009b, and references herein). New types of acoustic modes have thus been found in rotating polytropes, which are classified into island, chaotic, and whispering gallery modes (Lignières & Georgeot 2009). The visibility of these modes in differentially rotating stars has been discussed by Reese et al. (2009a). Similarly, a new theory of gravito-inertial modes in rapidly rotating massive stars has recently been investigated by Prat et al. (2016). According to these authors, the predicted chaotic modes could help to account for the discrete mass ejection events in Be stars.

9.2. Frequencies

To perform the frequency determination, in the PASPER and FREQFIND codes it was assumed that the oscillation components can be described with sinusoidal functions, which are then used to prewhiten the signal at successive frequency identifications. The use of simple circular functions may not be appropriate for all kinds of variations, in particular for the mid-term variations found in several program stars that are irregular in amplitude and duration. The detection of first harmonics in the frequency spectrum of several stars indicates that in some cases the signal is non-sinusoidal. This is something that is common in classic pulsators such as SPB, γ Dor, or δ Scuti (e.g., Breger et al. 2011; Degroote et al. 2012).

In spite of all these difficulties, the present analysis of CoRoT data for Be stars provides a number of interesting results that we summarize as follows:

– Frequencies are gathered in several regularly spaced groups, except in three stars, No 2, 11, and 20. The second and third groups are most populated by increasing frequencies. Depending on the target, the frequencies with the largest amplitude are seen either in the second or third group. The first group, situated next to the origin, i.e., $f \sim 0$ c d^{-1}, may include non-stellar frequencies. When the light curves are cleaned from the global trends induced by outbursts, the number of very low frequencies in this group greatly decreases, as shown in Fig. 17 (stars No 5, 6, and 9). Except for stars No 9 and 14, which show several fadings in their LRA1 light curve, the very low frequencies do not correspond to any outburst interval. However, in star No 14 the interval between fadings, or sawtooth variations, is compatible with the high amplitude low frequency 0.054 c d^{-1}; in star No 9, moderate fadings are separated by about 10–15 d, while in the LRA1, as in the IR1 runs, the duration of the major outburst is at least 30 d. In main sequence stars of intermediate mass showing no outbursts during the CoRoT runs or just short outbursts of very low intensity, (fx–fy) combinations between dominant frequencies of a same group, where beatings are the main characteristics, largely contribute to determine the global behavior of their light curve.

– According to the fundamental parameters corrected for effects induced by rapid rotation, stars No 2 and 11 are located beyond the main sequence evolutionary phase of the H-R diagram. Analysis of their light curves shows a very poor spectrum of frequencies, less than 20, and all are of weak amplitude. These objects may have formed a circumstellar envelope during the secondary contraction phase when stellar surface rotational velocity greatly increases. In such circumstances, if the external stellar layers attain the escape velocity, $v_{\rm esc} = \sqrt{2} v_{\rm crit}$, discrete mass ejection episodes may occur.

– In stars of similar masses situated close to the ZAMS, the spacing between the groups of frequencies is larger than in those which are near the TAMS. The spacing between frequency groups does not vary in a monotonic way during the MS evolutionary phase, but it is greatest at the middle of the MS. This behavior resembles the speeding up of surface rotation in A-type stars discovered by Zorec & Royer (2012). With a sufficiently numerous sample, it would be possible to confirm this finding and eventually establish a relation between the spacing of groups and the fractional evolutionary age $\tau/\tau_{\rm MS}$.

– The rotation frequency derived spectroscopically, $f_{\rm rot}$, was compared with the main frequencies detected in the DFT of the CoRoT light curves and with the average location of group frequencies and the separation of groups. In spite of uncertainties, from these comparisons we conclude that in three-quarters of the stars studied the rotational modulation of the light curves induced by spots, or co-rotating clouds, cannot explain the frequency spectrum.

– Excited prograde g-modes and r-modes are expected in most of our sample stars that are main sequence stars of intermediate mass (3–8 $M_\odot$, Saio 2013). In most objects, the second and third groups of frequencies are spaced by a quantity slightly larger than the rotational frequency. Using as reference the

models calculated for rapidly rotating B-type stars by Cameron et al. (2008); Saio et al. (2006, 2007), we find that the location of the second and third frequency groups in the DFT is consistent with prograde $m = -1$ and $m = -2$ g-modes. The separation between them is $\delta f = (1.24 \pm 0.28) \times f_{\rm rot}$. The first group of frequencies near 0 c d^{-1} contains combinations of dominant frequencies and according to theoretical predictions, they are probably odd r-modes with $m = 1$. Even r-modes with $m = 2$ could be excited and observed at about $(5/3)f_{\rm rot}$, although this frequency agrees very poorly with our frequency measurements. According to Baade et al. (2016), the 0.03 c d^{-1} variability in η Cen may reveal a causal connection with the mass-loss phenomenon during outbursts.

In the late Be star No 1, the dominant 5 c d^{-1} group might be attributed to prograde $m = -2$ g-modes. According to the rotation frequency $f_{\rm rot} = 2.1$ c d^{-1} of this star, the spacing between eight significant periods running in the co-rotating frame is 4400 ± 200 s.

The dominant frequency group in four objects, stars No 4, 14, 17, and 19, is compatible with their rotational frequency $f_{\rm rot}$ inferred spectroscopically. In these cases, it cannot be excluded that in the observed light variations there could be signatures of some rotational modulation. In star No 14, the 18-d recurrence of fadings seems to be constant and is likely linked to a multiplicity. In star No 17, several dominant frequencies could be associated with the rotational frequency. The situation is not so clear for star No 4 because there is some evidence for a rotational modulation implying the frequency separation $\Delta f = 1.56$ c d^{-1}, which is slightly lower than $f_{\rm rot} = 1.83 \pm 0.20$ c d^{-1}.

9.3. Outbursts

Outbursts (brightenings or fadings) are detected in the CoRoT light curve of six objects, which represent 40% of the sample studied: brightenings occurred in stars No 5, 6, and likely in No 22, while fadings were detected in stars No 9, 14, and 17. All these stars have spectral types earlier than B4.

The photometric variations related to the outbursts studied in this work are similar or smaller than that observed in HD 49330 (Huat et al. 2009), i.e., $|\Delta V| \lesssim 0.03$ mag.

The study of frequencies carried out over different time intervals show that during the light outbursts there is a strong increase of the amplitude of many frequencies, which can attain up to a factor 3. However, in stars No 5 and 6, contrary to the preceding cases, the amplitude of some groups increases, while the amplitude markedly decreases in other groups of frequencies. At the same time, numerous transient and weak-amplitude frequencies appear. Many of these frequencies are slightly lower than those in the second group of stable frequencies, and they are not far from the rotational frequency $f_{\rm rot}$. The most interesting examples are stars No 5, 6, 9, and 17. Similarities to this behavior of frequencies have been previously found in HD 49330 (Huat et al. 2009). Transient frequencies have also been observed spectroscopically in other bright Be stars at the time of enhanced emission-line episodes (Stefl et al. 1998) and were interpreted as being formed in the inner part of the circumstellar disk (Baade et al. 2016).

9.3.1. Outbursts and mass ejection

The photometric variations related to the outbursts studied in this work are characterized by increases or decreases in radiation flux that, depending on the object, last from 5 to 20 days and imply photometric variations ranging from $\Delta V \simeq \pm 0.01$ to $\Delta V \simeq \pm 0.03$ mag. Some are similar to those observed in HD 49330, where $\Delta V \sim -0.03$ mag (Huat et al. 2009). In the past, several other outbursts in Be stars have been reported in the literature, which also imply photometric variations ranging from $\Delta V \simeq \pm 0.01$ to $\Delta V \simeq \pm 0.08$ mag, observed changes of equivalent widths of line-emission components, and detected polarimetric changes characterized by timescales on the order of 10 days; these outbursts have been reported in μ Cen (Smith et al. 1996; Hanuschik et al. 1993), EW Lac (Floquet et al. 2000), η Cen (Levenhagen et al. 2003), and ω Ori by (Hayes & Guinan 1984; Guinan & Hayes 1984). The authors cited interpreted these phenomena as due to discrete mass ejections, where the amount of mass ejected could range from $\Delta M \simeq 10^{-11}$ to $10^{-10} M_{\odot}$. Harmanec (1983) proposed a different explanation of brightening and fading phenomena based on density variations of a highly flattened Be star envelope viewed under different angles. Continuum flux changes correlated with the phase of a binary system produced by truncation of the circumstellar and accumulation of material inward of truncation, caused by both radiative and gravitation interaction of the decretion disk with the companion, were proposed by Panoglou et al. (2016).

9.3.2. Outbursts and inclination angles

Apart from the above cited suggestion by Harmanec (1983), it is worth highlighting the statistical study carried out by Hubert & Floquet (1998), where it is clearly shown that photometric outbursts implying magnitude changes up to $\Delta V \sim \pm 0.3$ mag are likely seen as brightenings in pole-on Be stars, while those implying fadings are seen in equator-on Be stars. Haubois et al. (2012) simulated the photometric variation produced by episodic mass injections into circumstellar disks and predicted brightenings at the V-photometric band when inclination angles are $i \lesssim 70°$; these authors found almost no variation at $i \simeq 70°$ and fadings for $i \gtrsim 70°$. Associating the outbursts detected in our program Be stars with mass-ejection events and aiming at determining whether a similar tendency exists for our stars, we looked for possible correlations with $V \sin i$, the inferred inclination angles i, and the shape of the Hα emission lines. Although the stars that displayed brightening phases may conform with these predictions, the fadings do not agree with them. However, owing to many uncertainties we dealt with, in particular the small number of stars showing outburts (six stars) and the unclear physical nature of some of the stars, no conclusive result could be obtained.

The relations observed between outbursts and indicators of inclination angles are, however, uncertain because (1) the outburst statistics are poor; (2) $V \sin i$ and mostly i, can be uncertain, in particular the inclination angle, which strongly depends on the assumed value of the ratio $\Omega/\Omega_{\rm c}$ (see Appendix A); (3) star No 14 is suspected to be a binary; (4) the quoted Hα emission-line profiles are generally variable in Be stars and, in this case, these profiles were not obtained simultaneously with the CoRoT observations; (5) double-peaked Hα emission-line profiles, believed to be a kind of signature for circumstellar disks seen at rather high inclination angles, can also exist in pole-on Be stars if the circumstellar disks are vertically extended and have high optical depth (Hummel & Dachs 1992; Hummel 1994); and (6) apart from the interpretation of outburst carried out by Haubois et al. (2012), based on a sudden increase of the flux of matter injected into a thin and regular disk, it would also be useful to explore the photometric consequences of clumpy circumstellar environments produced by discrete and localized mass ejections. This implies that we should implement model

calculations with the physics of wind-clump interactions (Dyson & Hartquist 1992; Dyson et al. 1993) and thermo-radiative mechanisms in differentially rotating fluids (Kakouris & Moussas 1998; Kakouris 2001). The geometrical frame in which outbursts may then take place can be significantly different and the correlation of brightenings and fadings with inclination angles less obvious.

We would then be inclined to say that the inclination angle and the structure and optical depth of the ejected material determine together whether an outburst is perceived as brightening or fading.

9.3.3. Pulsations and mass ejections

Because NRP have angular momentum and kinetic energy associated with the waves, they can be transported from the wave-driven zone and deposited near the stellar surface. Osaki (1986) suggested that the accumulation of angular momentum in the outermost layers, mostly by prograde non-radial pulsation modes, could favor discrete mass ejections. Recently, Kee et al. (2016) estimated that the pulsation-related mass equatorial ejections may be on the order of $\Delta M \sim 10^{-11}\,M_{\odot}$. They could then be responsible for the outbursts reported in this work and for the spectroscopic signatures mentioned in Sect. 9.3.1.

9.4. Outlooks

We noted in Sect. 8.2 that transient frequencies appear near to or superposed on groups of permanent frequencies. Since many transient frequencies are combinations of prominent permanent frequencies, which also have variable amplitudes, we may ask whether the transient frequencies are also of stellar origin. These frequencies could not exist or would have very small amplitudes at quiescent phases. But owing to physical conditions in the layers not far from the surface created by the energy and angular momentum deposited by the NRP pulsations, combinations and/or enhancement of some modes in these same regions could lead to the changes observed in the amplitudes of the permanent frequencies and to the presence of transient oscillations.

According to Saio (2013) in main sequence rapidly rotating stars of intermediate mass (3–8 $M_{\odot}$), high-order g-modes can be excited by the kappa-mechanism at the Fe-opacity bump, which appears in frequency groupings associated with azimuthal order m. In principle, they are also separated a little more than the rotational frequency likely to be observed in our program stars among the frequency groups 1 and 2. However, these theoretical predictions were made for rotating stars, where the Fe-opacity bump region that excites the waves has not been modified by rotational effects. So we may ask what might be the properties of NRP and the associated discrete mass ejections when the following characteristics of rotating stars are also taken into account:

– Both subphotospheric convection regions in rapid rotating B-type stars, caused by opacity peaks associated with iron and helium ionization (Cantiello et al. 2009), are strongly enlarged by the rotationally induced increase of the radiative gradient (Clement 1979; Maeder et al. 2008). These wider subsurface convective zones could then excite pulsations either by the kappa-mechanism (Saio & Cox 1980; Lee & Baraffe 1995; Lee & Saio 1997), stochastic mechanisms (Belkacem et al. 2010; Samadi et al. 2010; Shiode et al. 2013; Mathis et al. 2014), or in the way that it is presumed to occur for some g-modes near the convective stellar core (Lee & Saio 1986, 1987). The excited modes may then combine and/or transport energy and angular momentum to the surface stellar layers through a substantially enlarged subatmospheric region unstable to convection. The accumulation of angular momentum in the stellar surface could finally help to free a given amount of mass (Lee & Saio 1993; Pantillon et al. 2007; Neiner et al. 2013).

– At the present time, the number of B-type stars where ordered magnetic fields of some kG have been detected is rather small (Brown et al. 1985; Shore et al. 1990; Sikora et al. 2015, 2016). However, still undetected and more or less disordered magnetic fields $H \lesssim 10^2$ G may originate in the extended subphotospheric convection zones (Cantiello et al. 2009). Among the unexplored phenomena in rapidly rotating B-type stars is the interaction between pulsations and magnetic fields. In addition, the subphotospheric convection zones may undergo differential rotation (Zorec et al. 2011, 2016, 2017) to induce new characteristics to the pulsation spectra. It must be noted that the current spectropolarimetric observations and numerical simulations rule out the presence of any ordered small-scale fields stronger than some 50-250 G in Be stars (Wade et al. 2016; Kochukhov & Sudnik 2013). This concerns emerging magnetic fields from the stellar surface. The question is open regarding the nature and strength of internal magnetic fields. They could be maintained by the mentioned Clement-Maeder subphotospheric convection rotationally induced over a large percentage of the envelope.

– The loaded surface layers of the angular momentum transported by the NRP can be retained by magnetic fields not stronger than $H \lesssim 10^2$ G. Rayleigh–Taylor type instabilities may then unleash huge discrete mass ejections (Apparao et al. 1987) and produce more intense light outbursts than those listed in Sect. 9.3. To this particular class of outburst may belong the long- and short-lived outbursts observed in Galactic Be stars with the HIPPARCOS satellite, reported by Hubert & Floquet (1998), and similar outbursts, reported by Cook et al. (1995); Keller et al. (2002), and Mennickent et al. (2002), for Be stars observed during MACHO (Alcock et al. 1993) and OGLE (Udalski et al. 1997) and EROS (Aubourg et al. 1995) microlensing experiments in the Small and Large Magellanic Clouds. These outbursts imply timescales of light brightening or fading that range from 50 days to some 100 days. These outbursts are characterized by magnitude changes that can attain $\Delta V \simeq \pm 0.3$ mag. According to Hubert et al. (2000), Moujtahid et al. (1999), and de Wit et al. (2006), the amount of mass accumulated around the star in these timescales needs to be around $\Delta M \simeq 10^{-9} - 10^{-8} M_{\odot}$ to account for the observed photometric properties of these strong outbursts.

– A large fraction of Be stars are binaries (Oudmaijer & Parr 2010). Resonances can be expected from combinations between rotation, orbital frequencies, and tidally excited modes (Moreno et al. 2005; Aerts 2007).

The changes observed in the pulsation characteristics of Be stars near and during the outbursts, and the amount of the ejected material, can then be associated with perturbations of the outermost stellar layers produced by the subphotospheric chain of related phenomena: rapid rotation, enlarged subatmospheric convection, differential rotation, pulsation, transport of angular momentum and magnetic fields.

The results obtained in the present work need to be extended to a larger sample of stars in order to provide better founded constraints to the modeling of stellar pulsations and their relation

with sporadic huge matter ejections. Our ongoing analysis of the light curves of all remaining stars listed in Paper I will contribute to this purpose.

Acknowledgements. The CoRoT space mission, launched on December 27 2006, has been developed and was operated by CNES, with the contribution of Austria, Belgium, Brazil, ESA, Germany, and Spain. T.S. warmly thanks Cyril Georgy and Sylvia Ekström for discussions on the evolutionary tracks and Sébastien Salmon for the discussions on the instability trips. We are also very grateful to the referee, Dr. D. Baade, whose critical reading of the manuscript helped to improve the presentation of our results.

References

Aerts, C. 2007, in IAU Symposium, Vol. 240, Binary Stars as Critical Tools and Tests in Contemporary Astrophysics, eds. W. I. Hartkopf, P. Harmanec, & E. F. Guinan, 432
Alcock, C., Akerlof, C. W., Allsman, R. A., et al. 1993, Nature, 365, 621
Apparao, K. M. V., Antia, H. M., & Chitre, S. M. 1987, A&A, 177, 198
Aubourg, E., Bareyre, P., Brehin, S., et al. 1995, A&A, 301, 1
Auvergne, M., Bodin, P., Boisnard, L., et al. 2009, A&A, 506, 411
Baade, D. 1987, in IAU Colloq. 92: Physics of Be Stars, eds. A. Slettebak, & T. P. Snow, 361
Baade, D., Rivinius, T., Pigulski, A., et al. 2016, A&A, 588, A56
Baglin, A., Auvergne, M., Barge, P., et al. 2006, in ESA Special Publication, Vol. 1306, eds. M. Fridlund, A. Baglin, J. Lochard, & L. Conroy, 33
Ballot, J., Lignières, F., Prat, V., Reese, D. R., & Rieutord, M. 2012, in ASP Conf. Ser., Vol. 462, Progress in Solar/Stellar Physics with Helio- and Asteroseismology, eds. H. Shibahashi, M. Takata, & A. E. Lynas-Gray, 389
Ballot, J., Lignières, F., & Reese, D. R. 2013, in Lecture Notes in Physics, Vol. 865 (Berlin: Springer Verlag), eds. M. Goupil, K. Belkacem, C. Neiner, F. Lignières, & J. J. Green, 91
Baudin, F., Baglin, A., Orcesi, J.-L., et al. 2006, in ESA Special Publication, Vol. 1306, The CoRoT Mission Pre-Launch Status – Stellar Seismology and Planet Finding, eds. M. Fridlund, A. Baglin, J. Lochard, & L. Conroy, 145
Belkacem, K., Dupret, M. A., & Noels, A. 2010, A&A, 510, A6
Boisnard, L., & Auvergne, M. 2006, in ESA Special Publication, Vol. 1306, The CoRoT Mission Pre-Launch Status – Stellar Seismology and Planet Finding, eds. M. Fridlund, A. Baglin, J. Lochard, & L. Conroy, 19
Breger, M., Stich, J., Garrido, R., et al. 1993, A&A, 271, 482
Breger, M., Balona, L., Lenz, P., et al. 2011, MNRAS, 414, 1721
Brown, D. N., Shore, S. N., & Sonneborn, G. 1985, AJ, 90, 1354
Cameron, C., Saio, H., Kuschnig, R., et al. 2008, ApJ, 685, 489
Cantiello, M., Langer, N., Brott, I., et al. 2009, A&A, 499, 279
Clement, M. J. 1979, ApJ, 230, 230
Cook, K. H., Alcock, C., Allsman, H. A., et al. 1995, in ASP Conf. Ser., Vol. 83, IAU Colloq. 155: Astrophysical Applications of Stellar Pulsation, eds. R. S. Stobie, & P. A. Whitelock, 221
Cranmer, S. R. 2005, ApJ, 634, 585
Cranmer, S. R. 2009, ApJ, 701, 396
De Cat P. 2002, in ASP Conf. Ser., Vol. 259, IAU Colloq. 185: Radial and Non-radial Pulsations as Probes of Stellar Physics, eds. C. Aerts, T. R. Bedding, & J. Christensen-Dalsgaard, 196
de Wit, W. J., Lamers, H. J. G. L. M., Marquette, J. B., & Beaulieu, J. P. 2006, A&A, 456, 1027
Degroote, P., Briquet, M., Catala, C., et al. 2009, A&A, 506, 111
Degroote, P., Aerts, C., Michel, E., et al. 2012, A&A, 542, A88
Diago, P. D., Gutiérrez-Soto, J., Auvergne, M., et al. 2009, A&A, 506, 125
Doazan, V., Franco, M., Sedmak, G., Stalio, R., & Rusconi, L. 1983, A&A, 128, 171
Dyson, J. E., & Hartquist, T. W. 1992, Astrophys. Lett. Commun., 28, 301
Dyson, J. E., Hartquist, T. W., & Biro, S. 1993, MNRAS, 261, 430
Dziembowski, W. A., Daszyńska-Daszkiewicz, J., & Pamyatnykh, A. A. 2007a, MNRAS, 374, 248
Dziembowski, W. A., Moskalik, P., & Pamyatnykh, A. A. 1993, MNRAS, 265, 588
Dziembowski, W. A., & Pamiatnykh, A. A. 1993, MNRAS, 262, 204
Dziembowski, W. A., Daszyńska-Daszkiewicz, J., & Pamyatnykh, A. A. 2007b, Commun. Asteroseismol., 150, 213
Ekström, S., Georgy, C., Eggenberger, P., et al. 2012, A&A, 537, A146
Floquet, M., Hubert, A. M., Hirata, R., et al. 2000, A&A, 362, 1020
Frémat, Y., Zorec, J., Hubert, A. M., & Floquet, M. 2005, A&A, 440, 305
Georgy, C., Ekström, S., Granada, A., et al. 2013, A&A, 553, A24
Guinan, E. F., & Hayes, D. P. 1984, ApJ, 287, L39
Gutiérrez-Soto, J., Floquet, M., Samadi, R., et al. 2009, A&A, 506, 133
Gutiérrez-Soto, J., Semaan, T., Garrido, R., et al. 2010, ArXiv e-prints [arXiv:1010.1910]
Hanuschik, R. W., Dachs, J., Baudzus, M., & Thimm, G. 1993, A&A, 274, 356
Harmanec, P. 1983, Hvar Observ. Bull., 7, 55
Haubois, X., Carciofi, A. C., Rivinius, T., Okazaki, A. T., & Bjorkman, J. E. 2012, ApJ, 756, 156
Hayes, D. P., & Guinan, E. F. 1984, ApJ, 279, 721
Huat, A.-L., Hubert, A.-M., Baudin, F., et al. 2009, A&A, 506, 95
Hubert, A. M. 2007, in ASP Conf. Ser., Vol. 361, Active OB-Stars: Laboratories for Stellare and Circumstellar Physics, eds. A. T. Okazaki, S. P. Owocki, & S. Stefl, 27
Hubert, A. M., & Floquet, M. 1998, A&A, 335, 565
Hubert, A. M., Floquet, M., & Zorec, J. 2000, in ASP Conf. Ser., Vol. 214, IAU Colloq. 175: The Be Phenomenon in Early-Type Stars, eds. M. A. Smith, H. F. Henrichs, & J. Fabregat, 348
Hubert-Delplace, A.-M., & Hubert, H. 1979, An atlas of Be stars (Obs. Paris-Meudon)
Hummel, W. 1994, A&A, 289, 458
Hummel, W., & Dachs, J. 1992, A&A, 262, L17
Kakouris, A. 2001, A&A, 373, 665
Kakouris, A., & Moussas, X. 1998, A&A, 333, 678
Kallinger, T., Reegen, P., & Weiss, W. W. 2008, A&A, 481, 571
Kee, N., Owocki, S., Townsend, R., & Müller, H.-R. 2016, ASP Conf. Ser., 506, 47
Keller, S. C., Bessell, M. S., Cook, K. H., Geha, M., & Syphers, D. 2002, AJ, 124, 2039
Kochukhov, O., & Sudnik, N. 2013, A&A, 554, A93
Kurtz, D. W., Shibahashi, H., Murphy, S. J., Bedding, T. R., & Bowman, D. M. 2015, MNRAS, 450, 3015
Kuschnig, R., Weiss, W. W., Gruber, R., Bely, P. Y., & Jenkner, H. 1997, A&A, 328, 544
Lee, U. 2008, Commun. Asteroseismol., 157, 203
Lee, U., & Baraffe, I. 1995, A&A, 301, 419
Lee, U., & Saio, H. 1986, MNRAS, 221, 365
Lee, U., & Saio, H. 1987, MNRAS, 225, 643
Lee, U., & Saio, H. 1993, MNRAS, 261, 415
Lee, U., & Saio, H. 1997, ApJ, 491, 839
Lenz, P., & Breger, M. 2005, Commun. Asteroseismol., 146, 53
Leroy, B. 2012, A&A, 545, A50
Levenhagen, R. S., Leister, N. V., Zorec, J., et al. 2003, A&A, 400, 599
Lignières, F., & Georgeot, B. 2009, A&A, 500, 1173
Maeder, A., Georgy, C., & Meynet, G. 2008, A&A, 479, L37
Mathis, S., Neiner, C., & Tran Minh, N. 2014, A&A, 565, A47
Mennickent, R. E., Pietrzyński, G., Gieren, W., & Szewczyk, O. 2002, A&A, 393, 887
Miglio, A., Montalbán, J., & Dupret, M.-A. 2007, Commun. Asteroseismol., 151, 48
Moreno, E., Koenigsberger, G., & Toledano, O. 2005, A&A, 437, 641
Moujtahid, A., Zorec, J., & Hubert, A. M. 1999, A&A, 349, 151
Negueruela, I., Simón-Díaz, S., Lorenzo, J., Castro, N., & Herrero, A. 2015, A&A, 584, A77
Neiner, C., Gutiérrez-Soto, J., Baudin, F., et al. 2009, A&A, 506, 143
Neiner, C., Mathis, S., Saio, H., & Lee, U. 2013, in ASP Conf. Ser. , Vol. 479, Progress in Physics of the Sun and Stars: A New Era in Helio- and Asteroseismology, eds. H. Shibahashi, & A. E. Lynas-Gray, 319
Osaki, Y. 1986, PASP, 98, 30
Oudmaijer, R. D., & Parr, A. M. 2010, MNRAS, 405, 2439
Pamyatnykh, A. A. 1999, Acta Astron., 49, 119
Panoglou, D., Carciofi, A. C., Vieira, R. G., et al. 2016, MNRAS, 461, 2616
Pantillon, F. P., Talon, S., & Charbonnel, C. 2007, A&A, 474, 155
Prat, V., Lignières, F., & Ballot, J. 2016, A&A, 587, A110
Reese, D. R., MacGregor, K. B., Jackson, S., Skumanich, A., & Metcalfe, T. S. 2009a, A&A, 506, 189
Reese, D. R., Thompson, M. J., MacGregor, K. B., et al. 2009b, A&A, 506, 183
Rivinius, T., Baade, D., Stefl, S., et al. 1998a, in Astronomical Society of the Pacific Conference Series, Vol. 135, A Half Century of Stellar Pulsation Interpretation, eds. P. A. Bradley, & J. A. Guzik, 343
Rivinius, T., Baade, D., Stefl, S., et al. 1998b, A&A, 333, 125
Rivinius, T., Baade, D., & Štefl, S. 2003, A&A, 411, 229
Rivinius, T., Carciofi, A. C., & Martayan, C. 2013, A&ARv, 21, 69
Rivinius, T., Baade, D., & Carciofi, A. C. 2016, A&A, 593, A106
Saio, H. 2013, in Lecture Notes in Physics, Vol. 865 (Berlin: Springer Verlag), eds. M. Goupil, K. Belkacem, C. Neiner, F. Lignières, & J. J. Green, 159
Saio, H., & Cox, J. P. 1980, ApJ, 236, 549
Saio, H., Kuschnig, R., Gautschy, A., et al. 2006, ApJ, 650, 1111
Saio, H., Cameron, C., Kuschnig, R., et al. 2007, ApJ, 654, 544
Samadi, R., Belkacem, K., Goupil, M. J., et al. 2010, Ap&SS, 328, 253

Schild, R. 1973, ApJ, 179, 221
Semaan, T., Hubert, A. M., Zorec, J., et al. 2013, A&A, 551, A130
Shimazaki, H., & Shinomoto, S. 2007, Neural Comput., 19, 1503
Shiode, J. H., Quataert, E., Cantiello, M., & Bildsten, L. 2013, MNRAS, 430, 1736
Shore, S. N., Brown, D. N., Sonneborn, G., Landstreet, J. D., & Bohlender, D. A. 1990, ApJ, 348, 242
Sikora, J., Wade, G. A., Bohlender, D. A., et al. 2015, MNRAS, 451, 1928
Sikora, J., Wade, G. A., Bohlender, D. A., et al. 2016, MNRAS, 460, 1811
Smith, M. A., Plett, K., Johns-Krull, C. M., et al. 1996, ApJ, 469, 336
Stankov, A., & Handler, G. 2005, ApJS, 158, 193
Stefl, S., Baade, D., Rivinius, T., et al. 1998, in ASP Conf. Ser., Vol. 135, A Half Century of Stellar Pulsation Interpretation, eds. P. A. Bradley, & J. A. Guzik, 348
Štefl, S., Baade, D., Rivinius, T., et al. 2003, A&A, 411, 167
Townsend, R. H. D. 2005, MNRAS, 364, 573
Udalski, A., Kubiak, M., & Szymanski, M. 1997, Acta Astron., 47, 319
Underhill, A., & Doazan, V. 1982, B Stars with and without emission lines, parts 1 and 2
Wade, G. A., Petit, V., Grunhut, J. H., Neiner, C., & MiMeS Collaboration 2016, in Astronomical Society of the Pacific Conference Series, Vol. 506, Bright Emissaries: Be Stars as Messengers of Star-Disk Physics, eds. T. A. A. Sigut, & C. E. Jones, 207
Waelkens, C. 1991, A&A, 246, 453
Waelkens, C., Aerts, C., Kestens, E., Grenon, M., & Eyer, L. 1998, A&A, 330, 215
Walker, G. A. H., Kuschnig, R., Matthews, J. M., et al. 2005, ApJ, 635, L77
Weiss, W. W., Aerts, C., Aigrain, S., et al. 2004, in ESA Special Publication, Vol. 538, Stellar Structure and Habitable Planet Finding, eds. F. Favata, S. Aigrain, & A. Wilson, 435
Zorec, J., & Royer, F. 2012, A&A, 537, A120
Zorec, J., Frémat, Y., Domiciano de Souza, A., et al. 2011, A&A, 526, A87
Zorec, J., Frémat, Y., Domiciano de Souza, A., et al. 2016, A&A, 595, A132
Zorec, J., Frémat, Y., Domiciano de Souza, A., et al. 2017, A&A, 602, A83

Appendix A: Fundamental parameters

Table A.1 gives the fundamental parameters of the Be stars studied. These fundamental parameters represent the so-called *pnrc*−parameters (parent-non-rotating-counterpart objects) introduced in Frémat et al. (2005), which represent an approach to the parameters of a nonrotating object that has the same mass and nearly the same age as the rotating star studied. These parameters are calculated from the apparent (observed) fundamental parameters of a classic nonrotating plane-parallel stellar atmosphere that fits the spectrum in the visual range emitted by the rotating stellar hemisphere observed. The rotational effects in the fundamental parameters are estimated with the FASTROT code (Frémat et al. 2005), which produces synthetic spectra emitted by stellar atmospheres with rigid rotation. Models of stellar evolution with rotation (Ekström et al. 2012) are used to infer the *pnrc* masses and ages. The set of *pnrc*−parameters given in Table A.1 were calculated assuming that stars rotate at the angular velocity ratio $\Omega/\Omega_c = 0.95$. The *pnrc*−parameters for other values of the ratio Ω/Ω_c from 0.8 to 1.0 are given in Semaan et al. (2013). We note that rather small differences from star to star with rapid rotation of the ratio Ω/Ω_c represent significant differences in the rotation rate η = [centrifugal force/gravity] and consequent sensitive changes in the estimate of the inclination angle i. This change can be estimated readily by writing $i = \arcsin[(V\sin i/V_c)/(V/V_c)]$, where the ratio V/V_c passes from 0.6 to 1.0 as Ω/Ω_c varies from 0.8 to 1.0.

The uncertainty assigned to each f_{rot} in Table A.1 is the 1σ dispersion of several hundreds of individual estimates of each rotational frequency distributed over a wide range of values from $f_{rot} - 3\sigma$ to $f_{rot} + 3\sigma$. They are calculated using a subtle procedure detailed in Zorec et al. (2016), where the apparent stellar parameters are transformed into pnrc-parameters considered also with their individual errors ranging from -3σ to $+3\sigma$ and whose distributions are characterized by the respective 1σ Gaussian dispersions indicated in Table A.1. The individual rotational frequencies of the program stars for rotational rates $0.8 \leq \Omega/\Omega_c \leq 1.0$ are given in Semaan et al. (2013).

The average separation between the main frequency groups presented in Sect. 6.5: $\delta_f = (1.24 \pm 0.28) \times f_{rot}$ is characterized by a 1σ dispersion, which was estimated through a Monte Carlo simulation where the uncertainties of δ_f and f_{rot} are indicated in Table 3 and Table A.1, respectively. These uncertainties represent the 1σ dispersion of the normal distributions of errors affecting δ_f and f_{rot}. Hence, the calculation of the ratio $a = \delta_f/f_{rot}$ was carried out with $\delta_f + \epsilon_{\delta_f}$ and $f_{rot} + \epsilon_f$, where the individual errors ϵ_{δ_f} and ϵ_f range from $-3\sigma_{\delta_f}$ to $+3\sigma_{\delta_f}$ and $-3\sigma_f$ to $+3\sigma_f$, respectively. Although the above $\delta_f = \langle a \rangle f_{rot}$ relation assumes that stars rotate at $\Omega/\Omega_c = 0.95$, we recall that the average $\langle f_{rot} \rangle$ range from $\langle f_{rot} \rangle = 1.12 \pm 0.58$ for $\Omega/\Omega_c = 0.80$, $\langle f_{rot} \rangle = 1.33 \pm 0.69$ at $\Omega/\Omega_c = 0.95$ to $\langle f_{rot} \rangle = 1.36 \pm 0.69$ if $\Omega/\Omega_c = 1.00$.

It is also timely to ask whether the inclination angles presented in Table A.1 are reliable. To this end, we compared their distribution with that of angles distributed at random by definition. Hence, the inclination angles of the stars observed were sampled taking into account the uncertainties of their $V\sin i$ parameters and assuming that errors have a normal distribution characterized by the 1σ dispersion reproduced in Table A.1. We also assumed that the stellar ratios V/V_c of the program stars have a normal distribution in the $0 \leq V/V_c \leq 1$ interval centered at $\langle V/V_c \rangle = (4/\pi)\langle V \sin i/V_c \rangle$, whose dispersion is established by the corresponding standard deviation of $\langle V/V_c \rangle$. Since the reduced number of stars observed, 14 in our case, unavoidably suffers from significant sampling uncertainty, we calculated a distribution of the same number of theoretical objects whose inclination angles are distributed at random by definition. In both cases, 10^4 independent samplings were produced and the class-steps of the histogram were established using the bin-width optimization method of Shimazaki & Shinomoto (2007). It is worth noting that in each sampling the errors of the intervening parameters are assigned according to a Monte Carlo procedure, such that they range from -3σ to $+3\sigma$ according to their respective σ dispersions. Figure A.1 shows the averages of both distributions obtained. The error bars correspond to the standard deviation obtained for each bin. These bars are not equal, though they are very similar. The theoretical distribution corresponding to an infinite number of objects is also superposed for comparison. This test suggests that, in spite of the uncertainties we are dealing with, our estimates of inclination angles depict very reliable orientations of the studied objects.

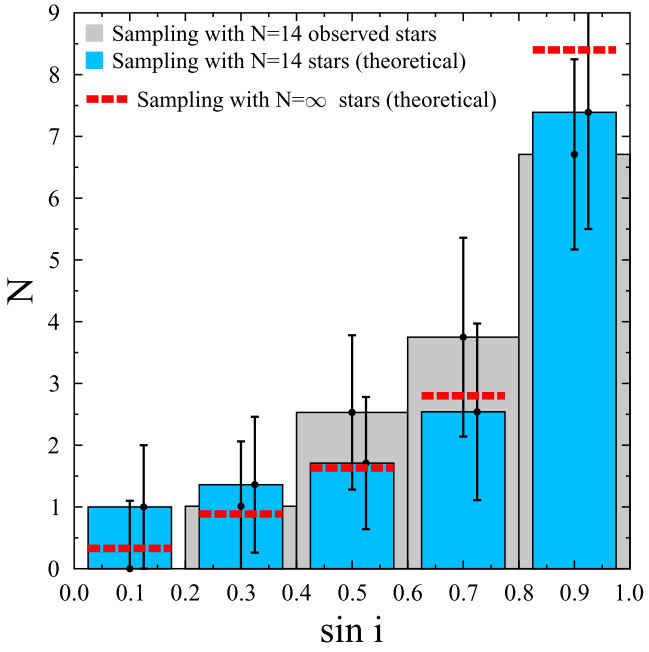

Fig. A.1. Comparison of the distribution of calculated inclination angles of the program stars with those for random oriented inclinations by definition, which are labeled "theoretical".

Appendix B: Description of individual light curves

We studied the rectified light curves and their corresponding DFT for 15 Be stars. The list of the frequencies, amplitudes, and phases and the signal-to-noise ratio is reported in Tables 7 to 22 (at the CDS). We give below a short description of the light-curve properties of each star, and when available, its Hα emission feature described in Paper I is briefly recalled.

B.1. CoRoT 101486436 (star No 1)

A strong beating of about 33 d is clearly detected in the detrended light curve (Fig. 2a). It is the signature of the combination of two close dominant frequencies, but the beating duration is not strictly constant. The maximal peak-to-peak amplitude remains at about 12000 ppm. The DFT and the 74 frequencies of stellar origin detected are shown in Fig. 2b and listed in Table 7. Frequencies are concentrated in several well-separated

Table A.1. Fundamental parameters and rotational frequencies with their respective 1σ uncertainties.

CoRoT ID	No	SpT	$T_{\rm eff}$ K	$\log g$ dex	$v\sin i$ km s^{-1}	$\log L$	R $R_\odot$	M $M_\odot$	$\tau/\tau_{\rm MS}$	$f_{\rm rot}$ c d^{-1}	i°
CoRoT 101486436	1	B7 V	13000 ± 1500	4.1 ± 0.2	242 ± 30	2.24 ± 0.26	2.6 ± 0.5	3.5 ± 0.2	0.30 ± 0.23	2.12 ± 0.24	40 ± 15
CoRoT 102595654	2	B9 III	10500 ± 1500	3.4 ± 0.3	328 ± 30	2.75 ± 0.27	7.3 ± 1.5	3.9 ± 0.3	1.02 ± 0.01	1.28 ± 0.27	90 ± 10
CoRoT 102656190	4	B2 V	20500 ± 2000	4.1 ± 0.2	278 ± 30	3.31 ± 0.26	3.7 ± 0.7	7.0 ± 0.4	0.23 ± 0.21	1.83 ± 0.20	40 ± 15
CoRoT 102672979	5	B3 IV	16200 ± 2000	3.5 ± 0.4	222 ± 30	3.62 ± 0.28	8.4 ± 1.8	6.8 ± 0.5	1.00 ± 0.03	0.55 ± 0.07	50 ± 10
CoRoT 102686433	6	B3 IV	17600 ± 1500	3.7 ± 0.2	300 ± 30	3.69 ± 0.27	7.7 ± 1.6	7.4 ± 0.5	0.96 ± 0.05	0.73 ± 0.09	60 ± 20
CoRoT 102719279	9	B1 IV	22300 ± 1500	3.7 ± 0.2	287 ± 20	4.15 ± 0.28	8.1 ± 1.8	10.6 ± 0.8	0.88 ± 0.07	0.73 ± 0.09	50 ± 10
CoRoT 102725623	11	B7 III	13000 ± 1500	2.8 ± 0.3	296 ± 40	4.06 ± 0.30	21.8 ± 5.1	8.9 ± 1.0	1.02 ± 0.01	0.35 ± 0.08	90 ± 10
CoRoT 102728404	12	B1 V	23600 ± 2000	4.0 ± 0.3	200 ± 30	3.78 ± 0.27	4.7 ± 1.0	9.3 ± 0.5	0.45 ± 0.21	1.40 ± 0.15	40 ± 15
CoRoT 102766835	14	O9 IV	33400 ± 2000	3.8 ± 0.3	262 ± 50	5.01 ± 0.33	9.9 ± 2.5	23.1 ± 2.8	0.63 ± 0.12	0.83 ± 0.12	30 ± 10
CoRoT 102785480	17	B2 IV	21700 ± 2000	3.8 ± 0.2	331 ± 30	3.96 ± 0.27	6.9 ± 1.5	9.5 ± 0.7	0.83 ± 0.09	0.94 ± 0.12	60 ± 10
CoRoT 102825808	18	B2 V	20500 ± 2000	4.0 ± 0.3	369 ± 40	3.56 ± 0.26	4.9 ± 1.0	7.7 ± 0.4	0.63 ± 0.17	1.45 ± 0.19	60 ± 10
CoRoT 102829773	19	B1 V	23600 ± 2000	4.3 ± 0.3	409 ± 40	3.42 ± 0.25	3.1 ± 0.6	8.2 ± 0.4	0.02 ± 0.04	2.63 ± 0.30	60 ± 10
CoRoT 102847615	20	B3 V	17500 ± 2000	4.2 ± 0.3	220 ± 30	2.80 ± 0.26	2.8 ± 0.6	5.2 ± 0.3	0.11 ± 0.13	2.29 ± 0.25	30 ± 15
CoRoT 102904910	22	B2 V	18900 ± 2000	4.1 ± 0.2	296 ± 30	3.23 ± 0.26	4.0 ± 0.8	6.4 ± 0.3	0.50 ± 0.20	1.60 ± 0.18	40 ± 10

Notes. No = sequence number of stars attributed in Paper I. SpT = spectral type. Stellar luminosity L, mass M, and radius R are given in solar units. τ = stellar age; $\tau_{\rm MS}$ = time that a rotating star spends in the main sequence phase. $f_{\rm rot}$ = rotational frequency. i° = estimated inclination angle of the rotation axis.

groups. The more important group, around 5 c d^{-1} [Fig. 2(c)], contains one-third of the detected frequencies and two close dominant frequencies, f_{55} = 5.0333 c d^{-1} (A ~ 3000 ppm) and f_{52} = 5.0024 c d^{-1} (A ~ 1800 ppm), which are mainly responsible for the 33 d beating. The second group is located at 2.3–2.7 c d^{-1} (Fig. 2d). Very low frequencies are present in the 0.05–0.25 c d^{-1} range. Several high frequencies are detected around 7.5 c d^{-1} and 10.1 c d^{-1}, most of these may be combinations.

For this late Be-type star we observed a faint double-peaked emission in the bottom of the photospheric Hα line profile.

B.2. CoRoT 102595654 (star No 2)

The light curve is noisy and does not reveal any particularity except weak, slow, and irregularly spaced variations going from 20 to 35 days [Fig. 10(a)]. The Fourier spectrum is very poor [Fig. 10(b)]. Only 10 frequencies have been detected that have low values (<0.24 c d^{-1}) most often with very low amplitudes, A < 200 ppm (Table 8). For this late Be-type star we observed an asymmetrical double-peaked emission at the center of the Hα photospheric line profile.

B.3. CoRoT 102656190 (star No 4)

The light curve shows conspicuous and recurrent beatings with a timescale of about 5 days and with a variable and large peak-to-peak amplitude of 25 000 ppm on average [Fig. 13(a)]. For this star, 95 frequencies have been detected (Table 9) that are mainly distributed in 4 groups at 0.15 c d^{-1}, 1.7 c d^{-1}, 3.5 c d^{-1} and 6.6 c d^{-1} (Fig. 13b–d). The dominant frequencies belong to the 3.5 c d^{-1} group. We note the high frequency f_{95} = 9.9504 c d^{-1} (A ~ 400 ppm) that does not seem to be the result of combinations. Two common spacings are detected between several dominant frequencies that belong to the group at 3.5 c d^{-1} (Fig. 13e); the first spacing is between f_{60} and f_{78} and between f_{62} and f_{81}, which corresponds to f_{17} = 0.1978 c d^{-1}; the second is between f_{60} and f_{74}, f_{62}, and f_{78}, and f_{63} and f_{80} that corresponds to the frequency f_{14} = 0.1658 c d^{-1}. Both spacings are compatible with the occurrence of beatings observed in the light curve. Several frequencies and their first harmonics of lower amplitude are detected. Sometimes, the fundamental and first harmonics have similar amplitudes, such as the couples f_{33} and f_{65} and f_{27} and f_{56}. Conversely, some first harmonics are identified with a larger amplitude than their fundamental; this is the case for frequencies f_6 (A = 990 ppm) = 2f_{31} (A = 203 ppm), which are possibly linked.

For this early Be-type star we observed a strong double-peaked Hα emission line profile.

B.4. CoRoT 102672979 (star No 5)

The light curve of this star is complex. On the first 75 days, the light curve depicts a large oscillation; then in the second part of the run, it shows beatings or quasi-periodic oscillations (QPO) with a variable timescale going from 10 to 20 days [Fig. 4(a)]. Moreover, short-period oscillations are observed in the whole run, but their amplitude is much larger in the first part of the light curve. A phenomenon such as a light outburst, similar to that discovered in CoRoT 102686433 (star No 6, see Sect. B.5), might have occurred a short time prior to the start of observations. To study the DFT we removed the general trend from the light curve (Fig. 4b), which thus suppresses nearly all frequencies lower than 0.08 c d^{-1} (Fig. 4c) resulting from long-term variations. A list

of 48 frequencies is reported in Table 10. They are mainly distributed in two dense groups at 0.8 c d^{-1} and 1.55 c d^{-1} (Fig. 4d and e). The first four frequencies ($A \geq 1300$ ppm) belong to the main group at 0.8 c d^{-1}. The frequency $f_1 = 0.0822$ c d^{-1} may correspond to beatings or QPO observed in the second part of the run. We only detected the first harmonics of lower amplitude for frequencies showing a moderate amplitude such as f_9, f_{12}, f_{14}, and f_{18}. Furthermore, as in other stars, we find a first harmonics having a larger amplitude than the fundamental, $f_{45} = 2f_{17}$. We also note the second harmonics of f_{17}.

A time-frequency analysis was presented in Sect. 7, where we have inquired whether the occurrence of a light brightening phenomenon could be validated.

For this early Be-type star we observed a strong, single-peaked Hα emission.

B.5. CoRoT 102686433(star No 6)

The CoRoT light curve shows a prominent brightening similar to that observed in HD 49330 by Huat et al. (2009); see Fig. 3a. During the first 63 days of the LRA1 run the flux has decreased as in the precursor phase of the light outburst in HD 49330. Short-time beatings, from six to nine days, are then conspicuous during the first part of the light curve, which we call the precursor phase. The brightening phase occurred at $t = 63$ d and the magnitude of the star increased by 0.01 mag within two days; at the same time, the amplitude of oscillations suddenly got larger by a factor 4. Afterward, the star entered a relaxation phase and the oscillation amplitude as well as the brightness of the star decreased to recover nearly its level before the outburst. We removed the general trend in the light curve produced by the outburst (Fig. 3b). The Fourier spectrum of the detrended light curve depicts three broad groups and several isolated frequencies (Fig. 3c and Table 11). We detected 84 frequencies mainly concentrated around 0.9–1.3 c d^{-1}, 2.1–2.6 c d^{-1}, and in a small pack around 4.5 c d^{-1}. The first two patterns consist of several subfeatures (Fig. 3d and e), whose frequencies are very close to each other with spacings that approach the resolution limit. The main frequencies form two couples. The first couple consists of $f_{48} = 2.2561$ c d^{-1} and $f_{50} = 2.2790$ c d^{-1}, which has the highest amplitude $A \sim 3400$ ppm. The second couple is formed by $f_{28} = 1.2947$ c d^{-1} and $f_{29} = 1.3046$ c d^{-1} with amplitude $A \sim 2000$ ppm. Dominant frequencies at 1.3 c d^{-1} and 1.15 c d^{-1} are probably responsible for beatings. The first harmonics of dominant frequencies, such as f_{15}, f_{28}, f_{29} and f_{50}, and f_{51}, are detected. The first and third harmonics of f_{12} are also detected. A lot of frequencies, including dominant harmonics, could be considered as the result of combinations (addition and/or subtraction). In particular we note the combinations $f_{48} \pm f_1$, $f_{51} \pm f_1$ and $f_{51} + 2f_1$ with $f_1 = 0.1772$ c d^{-1}.

The time-frequency analysis of this stars was presented in Sect. 7.

For this early Be-type star we observed a double-peaked emission Hα line.

B.6. CoRoT 102719279 (star No 9)

At the beginning of the CoRoT mission, this star was observed twice: first in the IR1 during 57.45 d, and 206 days later, in the LRA1 during 131.46 d (Fig. 6a and c). Meanwhile, the stellar flux had increased by about 0.06 mag. The star was reobserved in the LRA6 during 76.62 d about five years after the first two runs. The flux level was again comparable to that in the IR1 light curve on average (see Fig. B.1). Fadings and substantial changes

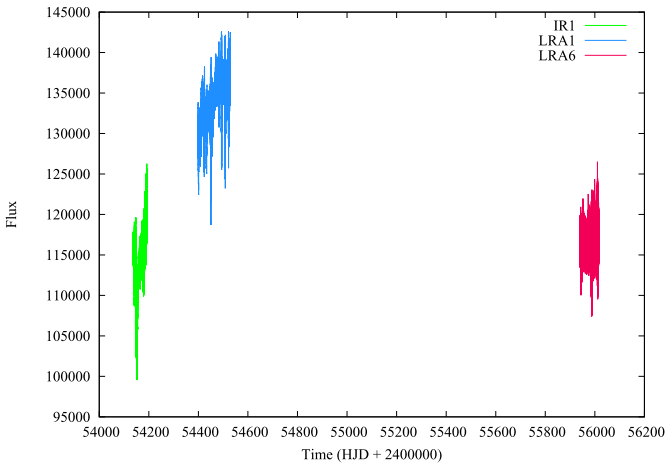

Fig. B.1. Changes of flux that the Be star CoRoT 102719279 (star No 9) underwent during the IR1 (green), LRA1 (blue) and LRA6 (red) runs.

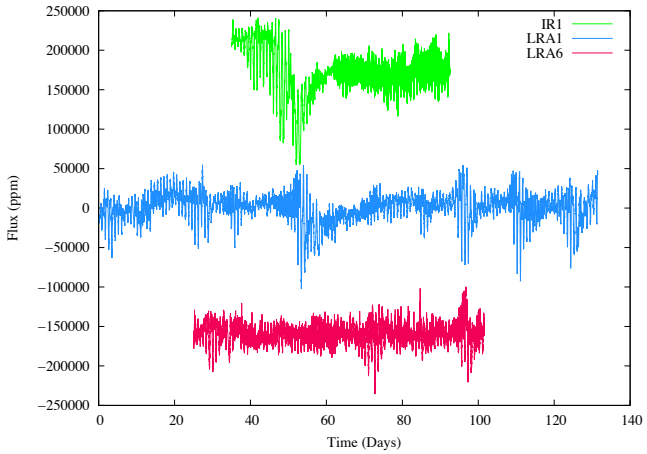

Fig. B.2. Comparison of non-rectified light curves for fading effects of the Be star CoRoT 102719279 (star No 9) observed during the IR1, LRA1, and LRA6 runs. The light curves are arbitrarily displaced in the ordinates, while their right flux levels are shown in Fig. B.1. The same sampling is used for all light curves (S1). The time in the abscissas indicates only the duration of the respective runs.

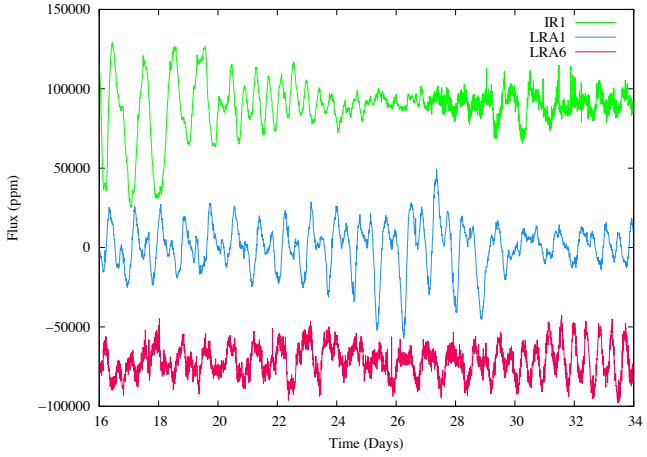

Fig. B.3. Comparison of zoomed light curve parts free from fadings of the Be star CoRoT 102719279 (star No 9) observed during the IR1, LRA1, and LRA6 runs. The same sampling is used for all light curves (S1).

in the amplitudes of the frequencies observed in the first two runs were first reported by Gutiérrez-Soto et al. (2010). These authors noted that the main frequencies 1.143 and 2.324 c d^{-1}, common to the two runs, simultaneously present maximal amplitude at a time close to the fadings. The third light curve obtained in 2012 revealed a more quiet phase since no prominent fading occurred as those in the first two runs (see Fig. B.2), but QPO with timescales varying from 15 to 25 d, and sometimes beatings, are easily detected.

At the beginning of the IR1, large amplitude variations over several days were followed by a rapid flux decrease of about 0.04 mag, which indicated the occurrence of an outburst seen as a fading. The flux then progressively increased, while the oscillation amplitude decreased.

For this star, spectroscopy revealed strong shell features (Paper I), which are expected to be observed under a rather large inclination angle. So it cannot be excluded that the outbursts detected as fadings are produced by ejecta in the equatorial regions, which have sufficient optical depth to produce absorption of the stellar light.

In the LRA1 run, large amplitude variations that can be assimilated to beatings occur intermittently and most are often followed by fadings. The most prominent fading, 0.02 mag, is comparable in strength and duration (about 30 days) to that observed during the IR1 run. Other fadings are less prominent (0.005 mag), but oscillations have globally the same amplitude. The recurrence of fadings in the LRA1 is about 15–20 days. Each data set was reanalyzed separately. The presence of strong fadings in the light curve adds low frequencies to the DFT. In this specific case, we tried to clean the DFT by removing the general trend produced by the dominant fadings (Fig. 6b and d). The Fourier spectra of the detrended light curves resemble each other (Fig. 6e) and two common groups of frequencies are found around 1.1 c d^{-1} and 2.3 c d^{-1}. The Fourier spectrum of the likely calm LRA6 light curve shows the same patterns (see Fig. 7c). Nevertheless, the frequencies in the ranges 0.9–1.0 c d^{-1} and 1.1–1.2 c d^{-1} have much stronger amplitudes in the IR1 than in the LRA1. We also note that a group of frequencies is also seen around 0.3 c d^{-1} in the DFT of the IR1 with a S/N slightly lower than the limit fixed by our detection criteria. The number of frequencies detected with $S/N \geq 4.0$ is lower in the IR1 than in the LRA6, and the number of frequencies in the LRA6 is lower than in the LRA1, i.e., 24, 42, and 64 frequencies, respectively (Tables 12 and 13). The temporal resolutions in the IR1, and to a lesser degree in the LRA6, do not allow separation of close frequencies detected in the LRA1. Thus, most of the frequencies detected in the IR1, and some in the LRA6, could be identified in the LRA1 as blends. In the LRA1, frequencies belonging to the denser groups 1.1 c d^{-1} and 2.3 c d^{-1} are very close and their spacing is often at the detection limit. Finally, the sole high frequency detected in the LRA1 is $f_{64} = 4.6880$ c d^{-1}. Independent of the stellar activity, which is different in the three runs, the quasi-totality of common frequencies detected are stable and the behavior of the light curve parts that are free from fadings are comparable (see Fig. B.3) and attributed to stellar pulsations.

Only the first harmonics of the frequencies f_{27}, f_{28}, and $f_{(51}$ were identified. A study of the main frequencies in the two dominant groups (Figs. 6f,g, and 7d,e) for the IR1, LRA1, and LRA6 runs reveals that the amplitudes of oscillations are strongly variable. A time-frequency analysis is presented in Sect. 7.

We observed a highly asymmetrical double-peaked Hα emission line in this very early Be-shell type star.

B.7. CoRoT 102725623 (star No 11)

This object was first observed in the IR1 and then in the LRA1 run (Fig. 11a and b). The light curves presented many instrumental jumps and steps that were corrected, but remained very noisy. They do not show any noticeable peculiar stellar variation (Fig. 11c). A small number of frequencies were detected in each run, 2 and 8, in the IR1 and LRA1, respectively. Most frequencies in the LRA1 are low frequencies with small amplitude, $A < 525$ ppm (Table 14). They are probably due to residuals in the detrended light curve. We note that there is only one common frequency identified as $f_2 = 0.8966$ c d^{-1} in the IR1 or $f_8 = 0.8946$ c d^{-1} in the LRA1, but which had a lower amplitude in this second run.

For this late Be-shell star, we observed a double-peaked Hα emission line.

B.8. CoRoT 102728404 (star No 12)

The light curve shows strong beatings varying in duration (from 15 to 25 days) and amplitude [Fig. B.4(a)]. In the Fourier spectrum (Fig. B.4b) 62 frequencies are identified (Table 15). Most of these frequencies belong to three groups at 0.05–0.25 c d^{-1}, 1.9 c d^{-1}, and 3.8 c d^{-1}. The two dominant frequencies, f_{41} and f_{35}, belong to the second group (Fig. B.4c). The group with frequencies lower than 0.25 c d^{-1} comprises f_7, which is close to the beating between the two dominant frequencies, $f_{41} - f_{35} = 0.0586$ c d^{-1} $= \Delta_1$. The low frequencies f_5 and f_6 are also compatible with beatings. The third group at 3.8 c d^{-1} includes the first harmonics of several frequencies with high to moderate amplitude (f_{39}, f_{43} and f_{50}). Other groups around 0.5 c d^{-1} and 2.6 c d^{-1} contain only a small number of frequencies. The highest frequency $f_{26} = 4.5040$ c d^{-1} is isolated. We note the combinations $f_{41} \pm f_{36}$, $f_{35} \pm f_{39}$, and $f_{35} \pm f_{38}$. We detected the spacing $\Delta_1 = 0.0586$ c d^{-1} between f_{37}, f_7 and f_{11}, which is close to f_7. We also find another spacing $\Delta_2 = 0.0373$ c d^{-1} between f_{36}, f_{39}, and f_{43}, which is close to f_4.

For this early Be-type star, no Hα line profile was available.

B.9. CoRoT 102766835 (star No 14)

The star was observed first in the IR1 and then in the LRA1 (Fig. 8a and b). The two light curves show the same complex structure. At each 18-d interval, the stellar flux decreases during about 10 days, accompanied by large oscillations that attain up to 40 000 ppm, and then it increases to recover its former level. This behavior is similar to a periodic sawtooth-shaped curve of varying amplitude similar to a series of fadings. Moreover, a secondary depression is very visible between consecutive sawteeth ticks. The DFT shows three groups that are regularly spaced (Fig. 8c) and located at 0.8 c d^{-1}, 1.7 c d^{-1}, and 2.5 c d^{-1} (Fig. 8d and e). Another group, of very low intensity, seems to be present near 3.4 c d^{-1}. In these groups we detected 23 and 68 frequencies in the IR1 and LRA1, respectively (Table 16). The frequencies detected in groups 0.8 c d^{-1} and 1.7 c d^{-1} in the LRA1 are very compact, so that the resolution in the IR1 is not high enough to separate them. Only 20 of the 23 frequencies detected in the IR1 were recovered in the LRA1, of which some are blends. A difference in signal amplitude can be noted in common frequencies of both data sets. Most often, the amplitudes are higher in the LRA1 than in the IR1 by a factor varying from 1.5 to 3, which explains the low number of frequencies found in the IR1 with a $S/N \geq 4.0$.

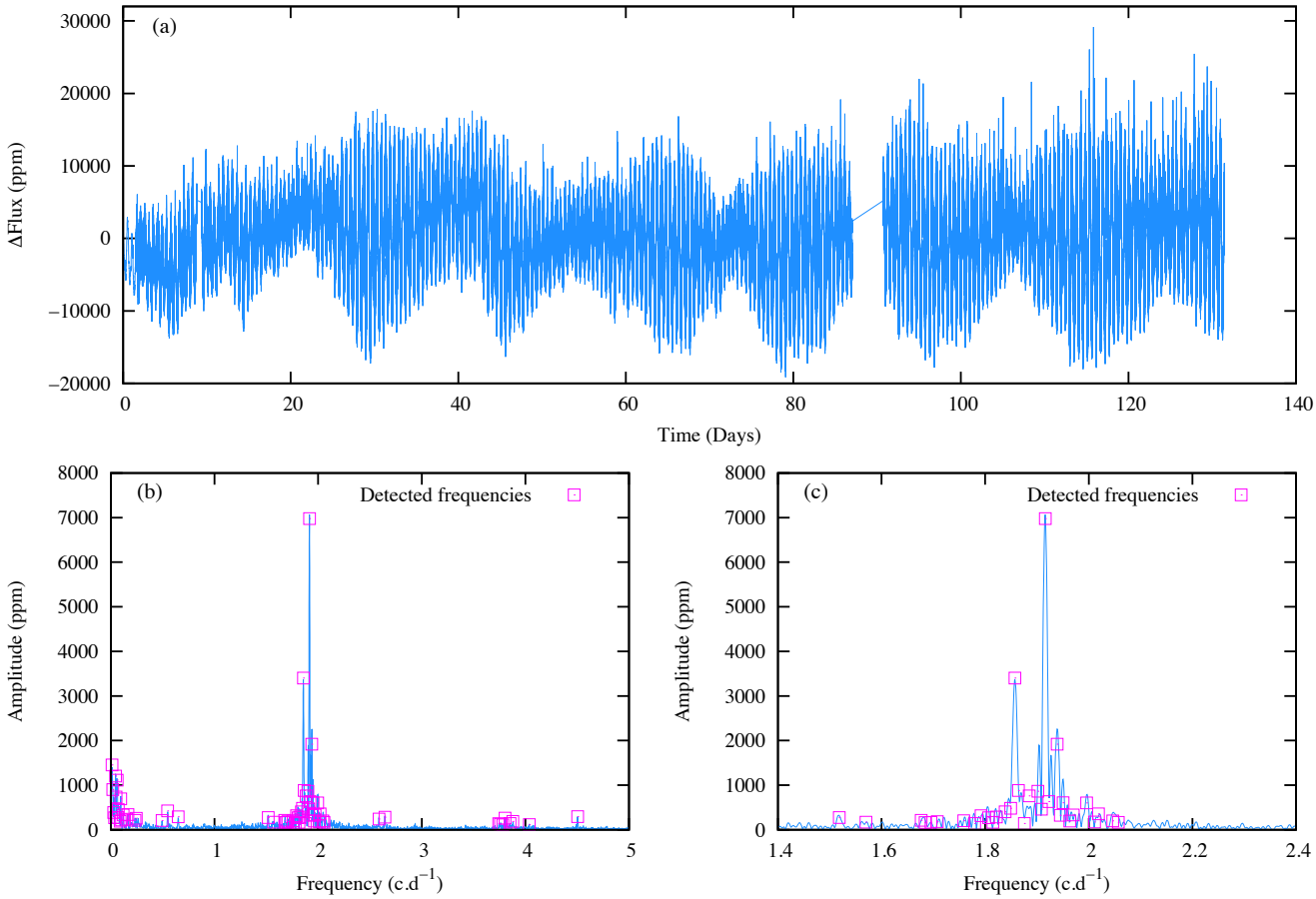

Fig. B.4. Frequency analysis of the Be star CoRoT 102728404 (star No 12) in the LRA1 (blue). *Panel a*: rectified light curve, *panel b*: DFT of the rectified light curve, and *panel c*: DFT zoomed on the second frequency group located at 1.9 c d^{-1}.

Here we comment only on the frequencies found in the LRA1. The first high amplitude frequency detected $f_6 = 0.0546$ c d^{-1} corresponds to the recurrent flux decrease of 18 days (Table 16); this is also more or less the spacing between the following frequencies $f_{23} = 0.7672$ c d^{-1}, $f_{27} = 0.8218$ c d^{-1}, $f_{32} = 0.8757$ c d^{-1}, and $f_{35} = 0.9288$ c d^{-1}.

We found the first harmonics of many frequencies such as f_6, f_{20}, f_{23}, f_{30}, f_{32}, f_{35}, and f_{49}. Finally, the first three harmonics of f_{27} are probably present. We also note combinations between the first main frequencies, such as $f_{54} \pm f_{27}$, $f_{35} \pm f_{25}$, and $f_{10} \pm f_{25}$.

For this late Oe-type star, we observed an asymmetrical Hα emission line. This object is also a star with strong He shell features and many metallic lines.

B.10. CoRoT 102785204 (star No 16)

The LRA1 light curve of this very peculiar Be star, probably a multiple system (see Paper I), is very noisy and does not reveal any obvious beating (Fig. B.5a). Nevertheless, long-time amplitude variations are conspicuous over the whole run. In the DFT (Fig. B.5b) we detected 30 frequencies that are mainly distributed in three groups at about 0.05–0.1 c d^{-1}, 1.3 c d^{-1}, and 2.7 c d^{-1}. We noted several low frequencies of high amplitude (Table 17). The dominant group at 1.3 c d^{-1} (Fig. B.5c) contains the very high amplitude frequency $f_8 = 1.2127$ c d^{-1} ($A \sim 21\,500$ ppm). The group around 2.7 c d^{-1} contains the other high amplitude frequency $f_{21} = 2.6740$ c d^{-1} ($A \sim 4900$ ppm) (Fig. B.5d) and other low amplitude frequencies that could be first harmonics such as $f_{17} = 2f_7$. The high amplitude frequency f_8 combines with many others since $f_8 = f_9 - f_4 = f_{23} - f_{16} = f_{20} - f_{15} = f_{30} - f_{28}$. The accuracy is not high enough to assess any other correlation.

For this very early Be-shell star, we observed an asymmetrical Hα line profile. Owing to the very strong circumstellar emissivity, we have not been able to determine the fundamental parameters of this object (see Paper I).

B.11. CoRoT 102785480 (star No 17)

The LRA1 light curve shows low amplitude variations (QPO) of about 40 d [Fig. 9(a)]. Moreover, at $t = 12$ d a noticeable sudden flux decrease resembling a low intensity fading was observed over four days. The same phenomenon repeated at $t = 109$ d and also lasted four days, but with a lower intensity. The DFT shows a rich spectrum of frequencies distributed in several groups. The first three groups are located at 0.008–0.15 c d^{-1}, 1.0–1.1 c d^{-1}, and 2.2 c d^{-1}; others of lower amplitude are present at 4.5 c d^{-1} and 6.8 c d^{-1} (Fig. 9b). A total of 114 frequencies were detected, but many of these may be combinations (Table 18). Dominant frequencies are concentrated in two groups at 1.0 c d^{-1} and 2.2 c d^{-1} (Fig. 9c and d).

Frequencies in the group at 0.06 c d^{-1} are probably due to beatings of close frequencies and to break residues of instrumental origin. Harmonics of dominant frequencies were identified. Hence, we note f_{33} and f_{37} with their first harmonics, f_{86} with its first two harmonics, and f_{46} with its first three harmonics.

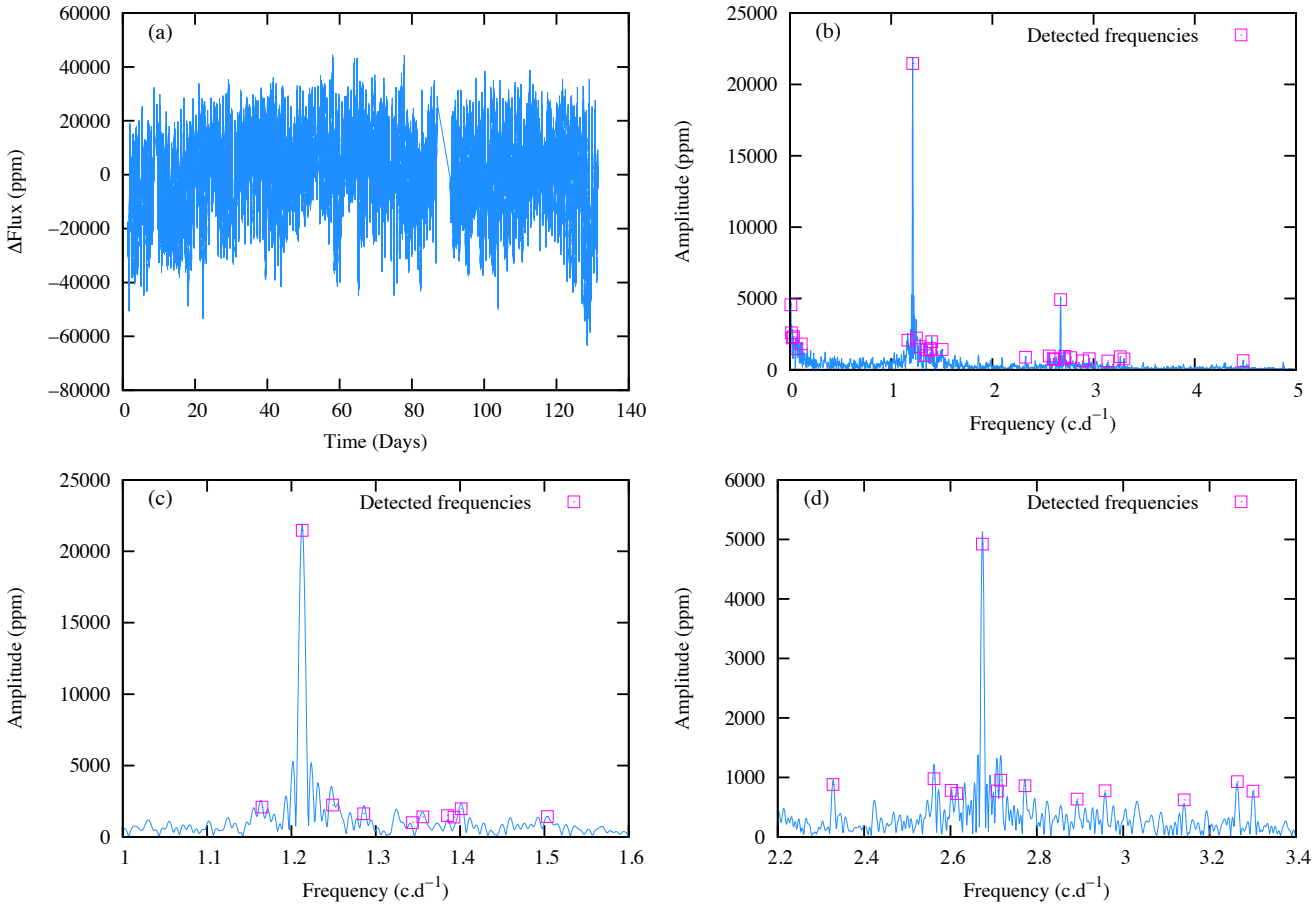

Fig. B.5. Frequency analysis of the Be star CoRoT 102785204 (star No 16) in the LRA1 (in blue). *Panel a*: rectified light curve; *panel b*: DFT of the rectified light curve; *panel c*: DFT zoomed on the second frequency group located at 1.3 c d^{-1}; and *panel d*: DFT zoomed on the third frequency group located at 2.7 c d^{-1}.

We also note the very high frequency f_{112} = 9.0407 c d^{-1} ($A \sim 200$ ppm), which could correspond to the first harmonics of the low amplitude frequency f_{98} = 4.5200 c d^{-1} ($A \sim 300$ ppm).

Among the combinations we detected are $f_{46} \pm f_{27}$, $f_{33} \pm f_{27}$, and $f_{37} \pm f_{33}$.

In the group at 4.5 c d^{-1}, f_{101} = 4.4315 c d^{-1}, which has the highest amplitude ($A \sim 1300$ ppm), does not seem to be the result of combinations. In the group at 6.8 c d^{-1}, the frequency f_{75} = 6.8084 c d^{-1}, which is dominant, is considered as independent.

For this early Be star no Hα line profile was available.

B.12. CoRoT 102825808 (star No 18)

The star was observed only in the IR1. Noticeable amplitude variations are present in the light curve and faint beatings with a timescale varying from about 7 to 10 days can also be seen (Fig. 12a). The Fourier spectrum is very complex as 44 frequencies were identified (Table 19), which is a comparatively high number for Be stars observed in the IR1. They are gathered mainly in eight groups located at 0.06–0.1 c d^{-1}, 2.0 c d^{-1}, 2.4 c d^{-1}, 3.8 c d^{-1}, 4.2 c d^{-1}, 4.8 c d^{-1}, 6.2 c d^{-1}, and 8.1 c d^{-1} (Fig. 12b). However the sets at 2.0 c d^{-1} and 2.4 c d^{-1} (Fig. 12d) could be the substructures of a single large group of frequencies. The sets at 3.8 c d^{-1}, 4.2 c d^{-1}, and 4.8 c d^{-1} could also form a single group (Fig. 12c). The high frequency f_{37} = 6.1907 c d^{-1} is rather isolated. The variable beating timescale in the light curve could be due to interference between f_{22} and f_{25} ($f_{25} - f_{22}$ = 0.0992 c d^{-1}), on the one hand, and between f_{25} and f_{28} ($f_{28} - f_{25}$ = 0.1114 c d^{-1}), on the other hand. The only first harmonic that we detected (f_{31}) corresponds to the dominant frequency f_{11} = 2.3764 c d^{-1}. We note the combinations $f_{11} \pm f_{37}$ and $f_{11} \pm f_{10}$. Other combinations may be present (Table 19).

In this early Be-type star, we observed a complex structure in the core of photospheric Balmer lines; it could be a faint Be star or a binary.

B.13. CoRoT 102829773 (star No 19)

The object was observed only in the IR1. It shows conspicuous, slow, and irregular amplitude variations in its light curve (Fig. B.6a) ranging from 7 to 15 days without any obvious beating. We detected only 26 frequencies in the Fourier spectrum (Fig. B.6b, Table 20). These frequencies are mainly gathered in three groups around 0.1 c d^{-1}, 2.7 c d^{-1}, and 5.2 c d^{-1} (Fig. B.6c,d); the most populated is the second group but the dominant frequency f_{24} = 5.6118 c d^{-1} ($A \sim 2100$ ppm) belongs to the third group. Only the first harmonics (f_{26} = 11.2254 c d^{-1}) of f_{24} were detected. Several frequencies are probably the result of combinations that involve low frequencies of the first group. Moreover, the frequencies f_{24} (Fig. B.6c) and f_6 = 0.5696 c d^{-1} are rather isolated.

For this early Be-type star we observed a complex Hα emission line.

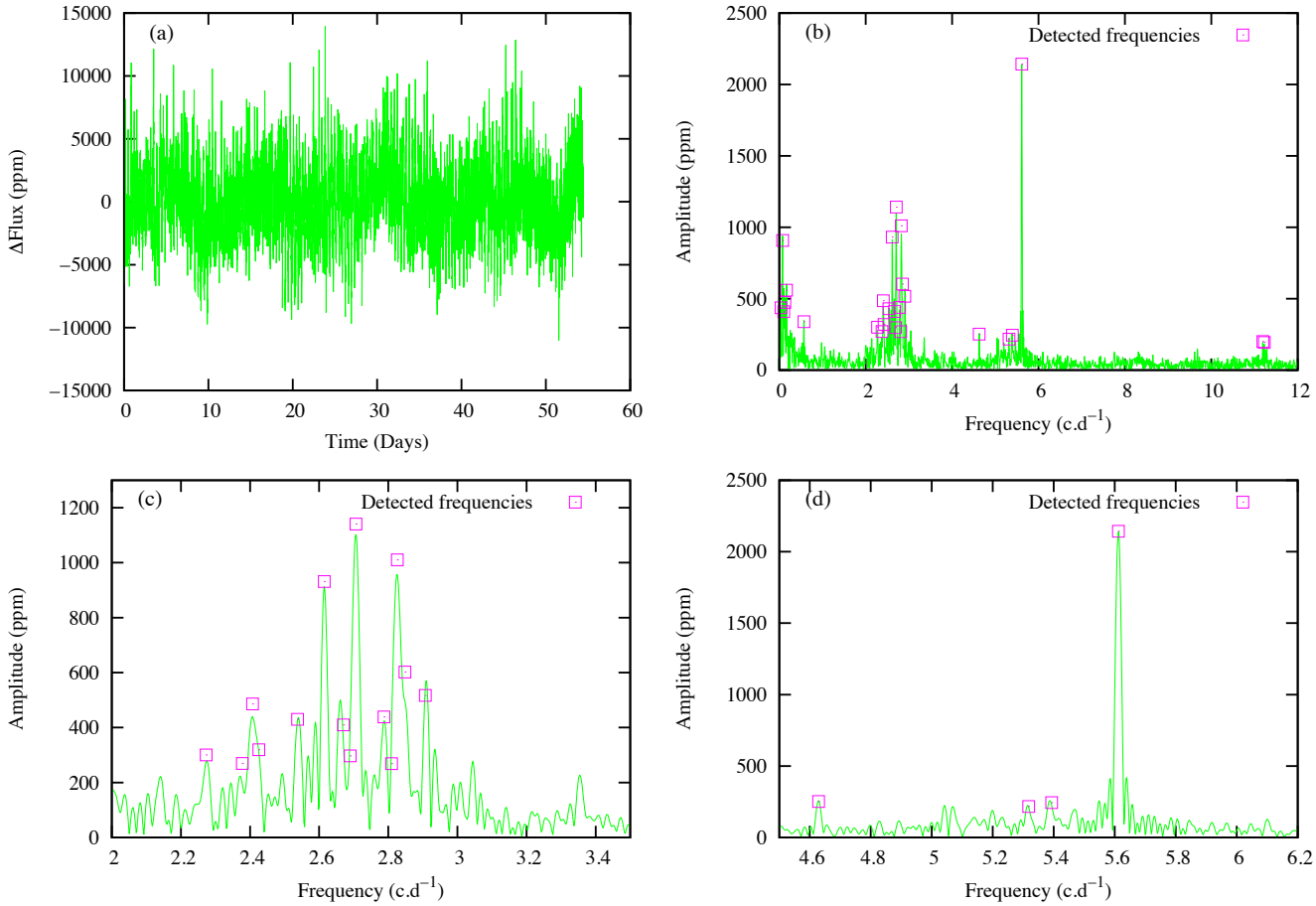

Fig. B.6. Frequency analysis of the Be star CoRoT 102829773 (star No 19) observed in the IR1 (green). *Panel a*: rectified light curve; *panel b*: DFT of the rectified light curve; *panel c*: DFT zoomed on the second frequency group located at 2.7 c d^{-1}, and *panel d*: DFT zoomed on the third frequency group located at 5.5 c d^{-1}.

B.14. CoRoT 102847615 (star No 20)

This object was observed only in the IR1. The light curve shows no remarkable characteristic and seems to be very noisy (Fig. B.7a). Only seven frequencies were detected (Fig. B.7b and Table 21). Three of these frequencies (f_3, f_4, f_5) are concentrated near 2.75 c d^{-1} (Fig. B.7c), and the highest amplitude (f_3) is only about 600 ppm. The two lower frequencies probably result from beatings between the frequencies close to 2.75 c d^{-1}. We note the combination $f_3 \pm f_5$.

For this early Be-type star we observed a strong Hα emission line.

B.15. CoRoT 102904910 (star No 22)

This object was observed only in the IR1. The light curve shows beatings irregularly spaced from four to eight days. An increase of brightness seems to occur at t = 26 d (Fig. 5a). The light curve corrected for the presence of the brightening is shown in Fig. 5b. Thirty-two frequencies (Table 22) were detected in the DFT that are distributed in distinct groups near 1.9 c d^{-1}, 3.8 c d^{-1}, 5.7 c d^{-1}, and 7.7 c d^{-1} (Fig. 5c). A zoom is shown on the two dominant groups at ∼3.8 c d^{-1} and 1.9 c d^{-1} (Fig. 5d and e); higher amplitudes are found in the first dominant group (about 3200 ppm for f_{23} = 3.9745 c d^{-1}). Combinations between frequencies f_{23}, f_{19}, f_{17}, and f_{13} such as $f_{23} - f_{19}$ = 0.1288 c d^{-1}, $f_{23} - f_{17}$ = 0.1567 c d^{-1}, and $f_{23} - f_{13}$ = 0.2437 c d^{-1} could be responsible for 4–8 d beatings. Several frequencies belonging to the 7.7 c d^{-1} group are harmonics or could be the result of simple combinations. In fact, no frequencies in the 7.7 c d^{-1} groups seem to be independent. A detailed phase analysis is presented in Sect. 7.

For this early Be-type star, we observed a double-peaked Hα emission and moderate shell features (see Paper I), but spectroscopy was performed three and a half years after the CoRoT observations.

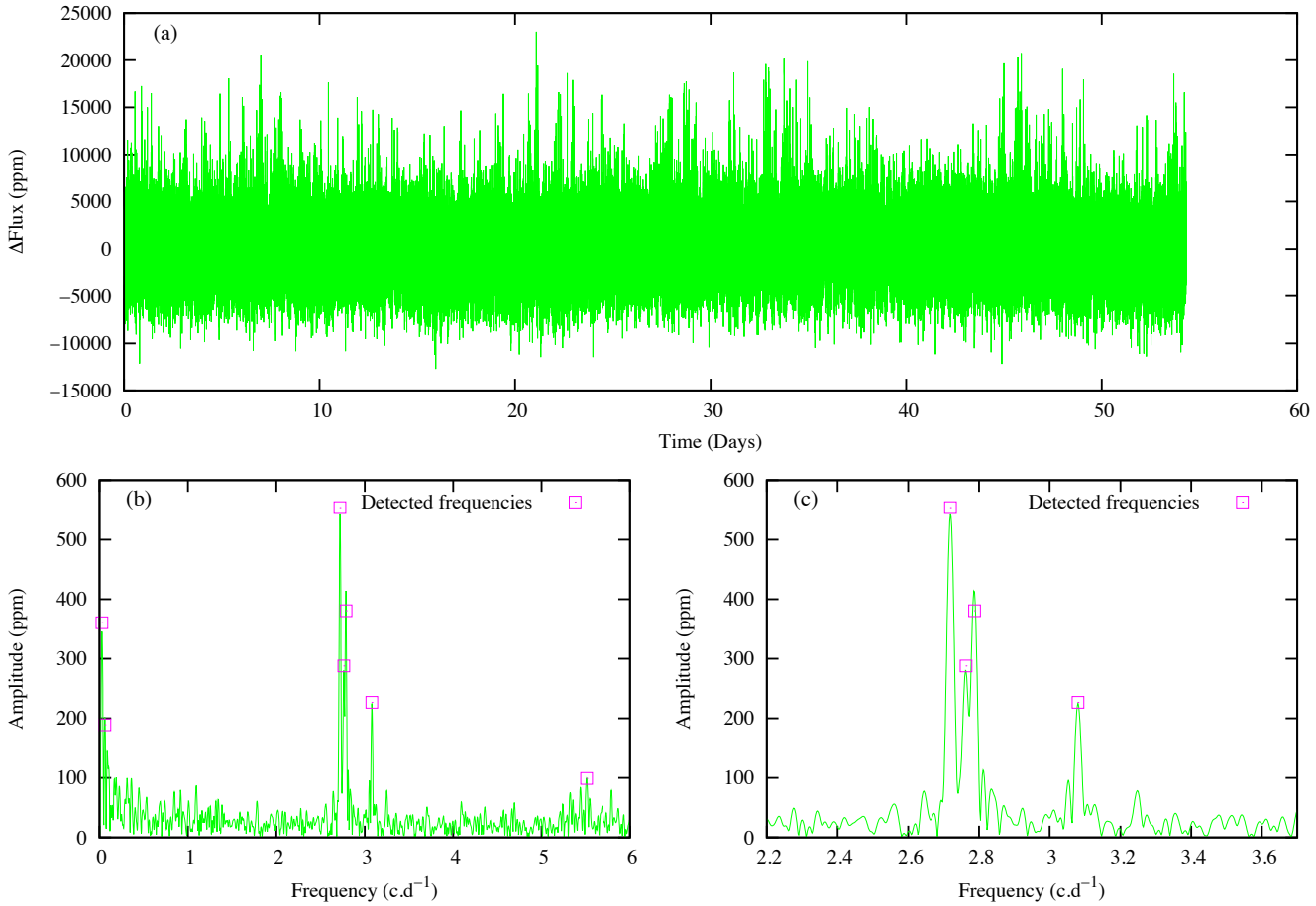

Fig. B.7. Frequency analysis of the Be star CoRoT 102847615 (star No 20) observed in the IR1 (green). *Panel a*: rectified light curve; *panel b*: DFT of the rectified light curve; and *panel c*: DFT zoomed on the second frequency group located at 2.7 c d^{-1}.